Harnessing intestinal tryptophan catabolism to relieve atherosclerosis in mice

Mouna Chajadine, Ludivine Laurans, Tobias Radecke, Nirmala Mouttoulingam, Rida Al-Rifai, Emilie Bacquer, Clara Delaroque, Héloïse Rytter, Marius Bredon, Camille Knosp, et al.

Harnessing intestinal tryptophan catabolism to relieve atherosclerosis in mice

Tryptophan, IDO, intestine, atherosclerosis

Mouna Chajadine[1], Ludivine Laurans[1*], Tobias Radecke[1*], Nirmala Mouttoulingam[1], Rida Al-Rifai[1], Emilie Bacquer[1], Clara Delaroque[2,3], Héloïse Rytter[2,3], Marius Bredon[4,5], Camille Knosp[1], José Vilar[1], Coralie Fontaine[6], Nadine Suffee[1], Marie Vandestienne[1], Bruno Esposito[1], Julien Dairou[7], Jean Marie Launay[8], Jacques Callebert[8], Alain Tedgui[1], Hafid Ait-Oufella[1], Harry Sokol[4,5,9], Benoit Chassaing[2,3], Soraya Taleb[1]

[1] Université Paris Cité, Inserm, PARCC, F-75015 Paris, France

[2] Microbiome-Host interactions, Institut Pasteur, Université Paris Cité, INSERM U1306, Paris, France

[3] INSERM U1016, Team "*Mucosal microbiota in chronic inflammatory diseases*", CNRS UMR10 8104, Université Paris Cité, Paris, France.

[4] Sorbonne Université, INSERM, Centre de Recherche Saint-Antoine, CRSA, AP-HP, Saint Antoine Hospital, Gastroenterology Department, F-75012 Paris, France.

[5] Paris Centre for Microbiome Medicine (PaCeMM) FHU, Paris, France.

[6] Inserm U1297, Institut des Maladies Métaboliques et Cardiovasculaires, Université de Toulouse, BP 84225, 31 432 Toulouse cedex 04, France.

[7] Université Paris cité, CNRS, Laboratoire de Chimie et de Biochimie Pharmacologiques et Toxicologiques, F-75006 Paris, France. 45 rue des Saints Pères, 75006 Paris, France

[8] Assistance Publique Hôpitaux de Paris, Service de Biochimie and INSERM U942, Hôpital Lariboisière, Paris, France

[9] Université Paris-Saclay, INRAe, AgroParisTech, Micalis institute, Jouy-en-Josas, France Université Paris-Saclay, INRAe, AgroParisTech, Micalis institute, Jouy-en-Josas, France

* Authors contributed equally to the work

Correspondence to: Dr. Soraya Taleb, PhD, at Inserm 970, 56 rue Leblanc 75015 Paris France. E-Mail: soraya.taleb@inserm.fr

Abstract

Tryptophan (Trp) is an essential amino acid, whose metabolism is a key gatekeeper of intestinal homeostasis. Yet, its systemic effects, particularly on atherosclerosis, remain unknown. Here we show that high-fat diet (HFD) increases the activity of intestinal indoleamine 2, 3-dioxygenase 1 (IDO), which shifts Trp metabolism from the production of microbiota-derived indole metabolites towards kynurenine production. Under HFD, the specific deletion of IDO in intestinal epithelial cells leads to intestinal inflammation, impaired intestinal barrier, augmented lesional T lymphocytes and atherosclerosis. This is associated with an increase in serotonin production and a decrease in indole metabolites, thus hijacking Trp for the serotonin pathway. Inhibition of intestinal serotonin production or supplementation with indole derivatives alleviates plaque inflammation and atherosclerosis. In summary, we uncover a pivotal role of intestinal IDO in the fine-tuning of Trp metabolism with systemic effects on atherosclerosis, paving the way for new therapeutic strategies to relieve gut-associated inflammatory diseases.

Introduction

The gastrointestinal tract has become recognized as a central organ in linking diet and cardiovascular diseases (CVDs), including atherosclerosis[1]. Particularly, the gut microbiota has been identified as a potential mediator that could impact atherosclerosis[2]. Although experimental and clinical data point to a critical role of intestinal inflammation in increased risk of CVD, little is known about the mechanisms whereby the intestine might specifically contribute to atherosclerosis. Particularly, diet-induced disruption of gut homeostasis might cause systemic deleterious conditions leading to atherosclerosis.

Tryptophan (Trp) is one of the essential amino acids provided by the diet, whose metabolism appears as a key metabolic gatekeeper of intestinal homeostasis. Trp is involved in various physiological processes and contributes to the maintenance of intestinal and systemic homeostasis in health and disease[3-5]. In mice, dietary lack of Trp leads to impaired intestinal immunity and gut microbiota dysbiosis, which causes intestinal inflammation and diarrhea[6]. In humans, patients with inflammatory bowel disease (IBD) exhibit disturbed tryptophan metabolism on both host and microbiota sides[7,8]. However, despite the importance of intestinal Trp metabolism in gut homeostasis along with the ascertainment that intestinal inflammation is associated with CVDs, the systemic impact of impaired gut Trp metabolism on atherosclerosis is still unclear.

Under homeostatic conditions, intestinal Trp catabolism follows three pathways[9], which consist in the Kynurenine (Kyn) pathway, mainly acting in intestinal epithelial cells (IECs) via the enzyme indoleamine 2, 3-dioxygenase 1, IDO (~95 % of Trp); the gut microbiota pathway of direct transformation of Trp into indole metabolites (~5 % of Trp); and the serotonin or 5-hydroxytryptamine (5-HT) pathway in enterochromaffin cells (ECs) via Trp hydroxylase 1 (TPH1) (~1-2 % of Trp), which accounts for the majority (~90 %) of whole body 5-HT production.

Previous studies reported either proatherogenic[10,11] or atheroprotective effects[12] of IDO. In particular, prior work by our group has shown that the global invalidation of IDO dampened atherosclerosis under high-cholesterol diet (HCD) feeding [12]. This pro-atherogenic effect was attributed to increased IDO expression in myeloid cells, involving the Kyn pathway, especially kynurenic acid[12]. In a subsequent study, we revealed a critical role for IDO in the fine-tuning of intestinal Trp metabolism under conditions of obesogenic high-fat diet (HFD), with major consequences on metabolic syndrome[13]. However, the specific role of intestinal IDO in cardiometabolic diseases, including atherosclerosis, is still unknown. Moreover, although recent studies highlighted the local effects of Trp-derived metabolites in intestinal homeostasis[9], their systemic impacts on atherosclerosis is poorly known. In this work, we demonstrate that HFD increases intestinal IDO activity, while decreasing the production of indole metabolites. Functional studies of Trp catabolic pathways reveal a protective role of intestinal IDO and indole metabolites, in contrast to the detrimental role of serotonin in atherosclerosis.

Results

HFD has a major effect on intestinal Trp catabolism in a mouse model of atherosclerosis

First, we assessed the effect of diet on intestinal Trp catabolic pathways (Kyn, 5-HT and indole pathways) using low-density lipoprotein receptor-deficient (*Ldlr*$^{-/-}$) mice, as a validated model of atherosclerosis. In particular, we examined the effect of HCD, a pro-atherogenic diet, as well as the effect of HFD, which has previously been shown to increase intestinal IDO activity in C57Bl/6 mice[13]. For this purpose, *Ldlr*$^{-/-}$ mice were fed with either a normal chow diet (NCD) and the purified diets HFD, HCD, or the combination of HFD+HCD for 13 weeks (**Supp. Fig. 1A**). As shown in **Fig. 1A**, intestinal Trp levels decrease along with a marked increase in Kyn levels, indicating a substantial increase in intestinal IDO activity (as assessed by Kyn/Trp ratio), under HFD conditions (HFD or HFD+HCD) compared to NCD or HCD (**Fig. 1A**). In agreement with previous reports[13,14], indole levels decreased under HFD conditions (with or without HCD) compared to HCD alone (**Fig. 1B**). Intestinal 5-HT levels also decreased in HFD conditions (HFD or HFD+HCD) compared to NCD or HCD (**Fig. 1C**). These data indicate that HFD, but not HCD, had a major effect on intestinal Trp metabolism through promoting the Kyn pathway to the detriment of the pathways of indole and 5-HT.

Next, we investigated the mechanisms underlying the observed increase in intestinal IDO activity under HFD. Short-chain fatty acids (SCFAs), such as acetate and butyrate, are the end products of the fermentation of dietary fibers by the anaerobic intestinal microbiota[15]. Recently, it was shown that butyrate, one of the SCFAs, negatively regulated IDO expression in IECs[16], suggesting a potential role of dietary fibers-induced bacterial SCFA metabolites in the regulation of Trp metabolism. In agreement with previous reports[17], mice fed HFD (containing a low level of fibers)[18] but not HCD, exhibited a decrease in acetate and butyrate levels in feces (**Supp. Fig. 1B**). Interestingly, the supplementation with soluble fibers like FOS (fructo-oligosaccharids) to *Ldlr*$^{-/-}$ mice fed HFD increased SCFA production, including acetate and butyrate (**Supp. Fig. 1C**), and led to a significant decrease in fecal Kyn levels without significant differences in fecal Trp levels (**Fig. 1D** and **Supp. Fig. 1D**), further suggesting the importance of fibers-mediated SCFA production in the regulation of the intestinal IDO activity. Taken together, these data indicate that feeding mice with HFD, which contains low levels of fibers, led to reduced SCFA production, including butyrate, a negative regulator of IEC IDO[16], which could explain, at least in part, the observed increase in intestinal IDO activity under this condition.

IDO expressed in IECs has a protective role in atherosclerosis under HFD

We next explored the role of intestinal IDO in atherosclerosis. For this purpose, mice devoid of IDO in IECs (*Ido-1*$^{flox/flox}$ *villin-cre*) were generated by crossing *loxP*-flanked *Ido-1* mice (*Ido-1*$^{flox/flox}$) with mice expressing Cre recombinase under the control of the murine villin promoter (*villin-cre*+/-). Then, we crossed *Ido-1*$^{flox/flox}$ *Villin-cre* (IEC IDOKO) mice with *Ldlr*$^{-/-}$ mice. Male *Ldlr*$^{-/-}$ IEC IDOKO and

littermate control mice (*Ldlr*$^{-/-}$ IEC IDO) were fed for 8 weeks with either NCD or HFD combined with HCD (HFD+HCD) to induce intestinal IDO activity and atherosclerosis, respectively. The absence of IDO in IECs led to a substantial decrease in *Ido-1 mRNA* expression in small intestines compared to controls (**Supp. Fig. 1E**) despite increased *Ido-1 mRNA* in the small intestine FACS-sorted CD45+ cells (**Supp. Fig. 1F**), underscoring the importance of IDO expression in IECs in intestinal Trp metabolism. Moreover, as shown above, *Ldlr*$^{-/-}$ IEC IDO mice fed HFD+HCD had increased intestinal IDO activity (as assessed by Kyn/Trp ratio) compared to *Ldlr*$^{-/-}$ IEC IDO mice fed NCD (**Fig. 1E**). In addition, IDO activity (Kyn/Trp) in small intestines was dampened in absence of IDO in IECs (**Fig. 1E**). This was also true in blood, as shown by increased plasma Kyn/Trp ratio in HFD+HCD compared to NCD, and marked decrease in plasma Kyn/Trp ratio in *Ldlr*$^{-/-}$ IEC IDOKO mice fed HFD+HCD at a level similar as in *Ldlr*$^{-}$ IEC IDOKO mice fed NCD (**Fig. 1F**), emphasizing the prominence of IEC IDO activity under HFD to the systemic Trp metabolism. Of note, Kyn/Trp ratio was much higher in the small intestines than in the colons (**Supp. Fig. 1G**), indicating the importance of the small intestine in the Kyn pathway. Remarkably, male *Ldlr*$^{-/-}$ IEC IDOKO mice fed HFD+HCD exhibited an increase in plaque size in the aortic sinus compared to the littermate *Ldlr*$^{-/-}$ IEC IDO mice fed HFD+HCD without any changes in plasma cholesterol levels (**Fig. 1G-H**), indicating that IEC IDO exerts a protective role against atherosclerosis under HFD.

Then, we sought to know whether this protective effect prevailed over a longer period of HFD+HCD feeding, in advanced atherosclerosis. Thus, male *Ldlr*$^{-}$ IEC IDOKO mice and their littermate controls were fed HFD+HCD for 13 weeks. As shown in **Supp. Fig. 2 A-D**, no major differences in mouse body weight, and metabolic parameters including insulin tolerance test (ITT), oral glucose tolerance test (OGTT), and insulin-resistance index (HOMA-IR) were observed between the two groups. Moreover, we found no significant differences in plasma cholesterol and plaque size (in the aortic sinus) between the two groups of mice, after 13 weeks of HFD+HCD (**Supp. Fig. 2E** and **F**). The absence of effects after a long period of HFD+HCD feeding in males was likely due to the significant decrease in *Ido-1* gene expression in the small intestines of control mice at 13 weeks compared to 8 weeks (**Supp. Fig. 2G**).

Then, we examined plaque size in females at short (8 weeks) and long period (13 weeks) of HFD+HCD. At 8 weeks of HFD+HCD, the absence of IDO in IECs did not significantly impact plaque size (in the aortic sinus) and plasma cholesterol levels, despite a significant decrease in *Ido-1 mRNA* in the small intestines (**Supp. Fig. 3A-C**). We then analyzed atherosclerotic plaques after 13 weeks of HFD+HCD. Remarkably, female mice with IDO deletion in IECs had increased plaque size in the aortic sinus without significant changes in plasma cholesterol levels (**Fig. 1I-J**). The increase in plaque size was also observed in the thoracic aorta (**Supp. Fig. 3D**). Interestingly, *Ido-1* mRNA was markedly increased in female control mice at 13 weeks compared to 8 weeks of HFD+HCD feeding (**Supp. Fig. 3E**). Moreover, *Ido-1 mRNA* was higher in the intestine of female compared to male control mice after 13

weeks of HFD+HCD (**Supp. Fig. 3F**), which most likely explain why the impact of intestinal IDO on plaque size in female mice was observed in advanced but not in early atherosclerosis. Of note, a decrease in gene expression of estrogen receptors (*esr1* and *esr2 mRNA*), as well as that of their target gene *greb1*[19], was observed in the small intestines of females. On the contrary, increased expression of these genes were found in males after 13 weeks of HFD+HCD (**Supp. Fig. 3G-H**). Moreover, an inverse correlation between *Ido-1 mRNA* and *esr2 mRNA* was observed in the small intestines of both males and females after 13 weeks of HFD+HCD (**Supp. Fig. 3I**), suggesting a differential sex hormone regulation of IDO expression within the gut.

In agreement with a major effect of HFD in inducing intestinal IDO activity, both male and female IEC IDO KO mice fed with only HCD did not display any significant differences in plaque size in the aortic sinus and plasma cholesterol levels despite a marked decrease in *Ido-1 mRNA* in IEC IDOKO (**Supp. Fig. 4**), further pointing to the importance of HFD in intestinal IDO-mediated effects on atherosclerosis.

Taken together, these findings demonstrate that under HFD condition, IDO expressed in IECs protects against atherosclerosis in both males and females, in a sex- and time-dependent manner.

Intestinal IDO decreases local and systemic inflammation

Then, we sought to assess the mechanisms that could account for the pro-atherogenic effects of intestinal IDO deficiency. Gut inflammation is known to be associated with increased susceptibility to CVD[1]. This may be due to alterations of the intestinal barrier, leading to enhanced permeability and translocation of microbial molecules, such as lipopolysaccharides (LPS), to the bloodstream, resulting in sustained peripheral inflammatory responses[20]. Interestingly, after 8 weeks of HFD+HCD feeding, male *Ldlr*$^{-/-}$ IEC IDO KO mice displayed a range of features of intestinal inflammation including elevated levels of fecal lipocalin-2 (Lcn2), a sensitive marker for gut inflammation[21], as well as increased pathohistological scores of colonic sections, compared to littermate controls (**Fig. 2A-B**). In agreement with this observation, we detected a decrease in the average distance between the closest bacteria and the epithelium surface in intestinal IDO-deficient mice (**Fig. 2C**) indicative of microbiota encroachment known to be associated with chronic intestinal inflammation[22]. Moreover, this was associated with increased intestinal expression of inflammatory factors such as tumor necrosis factor (TNF)α and interferon (IFN)γ as well as the chemokine and chemokine receptors-encoding genes XCL1, CXCR6, and CCR10 (**Supp. Fig. 5A-B**). Also, flow cytometry analysis of the small intestine lamina propria showed higher numbers of T lymphocytes including $CD4^+$ and $CD8^+$ cells (**Fig. 2D** and **Supp. Fig. 6A**), without significant changes in T helper (Th) polarization (expressed as % of CD4): no differences in Th1-specific T box transcription factor (T-bet), Th17-specific RAR-related orphan receptor (ROR)-γt, or T regulatory cells (Treg)-specific forkhead box P3 (Foxp3) expression (**Supp. Fig. 6B-C**). In addition, we found decreased expression of the tight junction occludin-1 gene (**Supp. Fig. 6D**), as well as elevated levels of serum IgG antibodies to LPS (**Fig. 2E**), suggesting increased intestinal permeability.

Consistently, female *Ldlr*$^{-/-}$IEC IDOKO mice fed HFD+HCD for 13 weeks displayed increased colon pathohistological scoring (**Supp. Fig. 7A**), as well as serum FITC-dextran 4,000 Da levels following oral gavage (**Fig. 2F**), compared to controls, providing further evidence for increased intestinal permeability in the absence of intestinal IDO. Moreover, blood lymphocyte numbers, including CD4+, CD8+, and B lymphocyte CD19+ cells, were increased in male IEC IDOKO mice, as assessed by flow cytometry analysis (**Supp. Fig. 7B**).

Collectively, these data suggest an increase in gut inflammation and alteration in intestinal barrier in the absence of intestinal IDO, which may cause systemic inflammation.

Then, we wanted to examine systemic inflammation, particularly within the atherosclerotic plaques. Analysis of plaques in male *Ldlr*$^{-/-}$ IEC IDOKO mice after 8 weeks of HFD+HCD revealed marked pro-inflammatory phenotype, as assessed by increased accumulation of CD3^{+} T cells (**Fig. 2G**) and large necrotic cores (**Supp. Fig. 7C**), compared to control mice. The increase in necrotic core size was also observed in female *Ldlr*$^{-/-}$ IEC IDOKO mice after 13 weeks of HFD+HCD (**Supp. Fig. 7D**). No differences in MOMA2^{+} macrophages were observed between the 2 groups in male mice (**Supp. Fig. 7E**).

To further evaluate whether increased T cells, known to promote atherosclerosis[23], was involved in the pro-atherogenic phenotype observed in IEC IDOKO mice, we generated a mouse model of atherosclerosis deficient for both intestinal IDO and lymphocytes (*Ldlr*$^{-/-}$*Rag1*$^{-/-}$IEC IDOKO mice) and compared them to *Ldlr*$^{-/-}$*Rag1*$^{-/-}$IEC IDO littermate mice. As shown in **Fig. 2H-I**, lymphocyte deficiency abrogated the pro-atherogenic effects observed in the absence of intestinal IDO without significant changes in plasma cholesterol levels, suggesting a major role for lymphocytes in this process. Taken together our data indicate that the absence of intestinal IDO promotes gut and plaque inflammation.

Intestinal 5-HT exerts a pro-atherogenic role

IDO is known to catabolize Trp into Kyn, which is the common metabolite upstream of the Kyn-derived metabolites. First, we sought to examine whether a decrease in Kyn levels observed in *Ldlr*$^{-/-}$IEC IDO KO was responsible for the observed phenotype. For this purpose, we supplemented *Ldlr*$^{-/-}$IEC IDO KO mice with Kyn (**Supp. Fig. 8A**) during the 8 weeks of HFD+HCD feeding. As shown in **Supp. Fig. 8B**, there was no correlation between fecal Kyn levels and plaque size, suggesting that the main pathway responsible for the observed phenotype was unlikely dependent on Kyn or Kyn-derived metabolites.

We then investigated the other Trp-dependent pathways, particularly 5-HT, which was previously shown to exert a deleterious role in several inflammatory diseases such as myocardial infarction[24] and colitis[25]. Intestinal 5-HT levels were not significantly changed in control mice fed 8 weeks of HFD+HCD, compared to mice fed NCD (**Supp. Fig. 8C**). To examine whether intestinal 5-HT was involved in atherosclerosis, we specifically inhibited TPH1, which is responsible for 5-HT production

within the gut (~90% of total serotonin[26]). *Ldlr*$^{-/-}$ mice fed HFD+HCD for 8 weeks treated with TPH1 inhibitor (LP533401) exhibited a marked decrease in 5-HT production in the small intestine (**Fig. 3A**) as well as in the blood (**Supp. Fig. 8D**). The inhibition of TPH1 was associated with an increase in indole production, as assessed by a higher fecal IAA and indole production, without any significant changes in IDO activity in the small intestine and plasma, as assessed by Kyn/Trp ratio (**Supp. Fig. 8E-G**). This was accompanied by an enhanced intestinal expression of anti-microbial peptides, regenerating islet-derived (Reg)3g, Reg3b as well as occludin-1 genes (**Supp. Fig. 8H-I**). Remarkably, blockade of intestinal 5-HT production was associated with an important reduction in plaque size in the aortic sinus (**Fig. 3B**) and in the thoracic aorta (**Supp. Fig. 8J**), without any changes in plasma cholesterol levels (**Supp. Fig. 8K**). Moreover, atherosclerotic plaques within the aortic sinus of TPH1 inhibitor-treated mice, contained fewer inflammatory cells including macrophages MOMA-2+ (**Fig. 3C**) and CD3+ T cells (**Fig. 3D**).

5-HT supplementation in HCD-fed male *Ldlr*$^{-/-}$ mice increased intestinal permeability, as assessed by augmented serum FITC-dextran 4KDa after oral gavage, and enhanced atherosclerosis, without any significant changes in plasma cholesterol levels between the 2 groups (**Supp. Fig. 9A-D**). Serum FITC-dextran and blood 5-HT levels were positively correlated with plaque size (**Supp. Fig. 9E-F**), suggesting a pro-atherogenic role of 5-HT.

Taken together, these results indicate that intestinal 5-HT exerts pro-inflammatory and pro-atherogenic effects.

Considering the observed pro-atherogenic role of intestinal 5-HT, we hypothesized that the possible increase in 5-HT in the absence of intestinal IDO may explain the pro-atherogenic phenotype of IEC IDOKO mice. We therefore examined intestinal 5-HT levels in male *Ldlr*$^{-/-}$ IEC IDOKO mice and littermate controls after 8 weeks of HFD+HCD. As expected, considering the availability of Trp for the other catabolic pathways, the absence of IDO in IECs led to a significant increase in 5-HT production (**Supp. Fig. 10A**). Interestingly, we found a correlation between 5-HT levels within the small intestine and plaque size in these mice (**Supp. Fig. 10B**). Then we sought to investigate whether increased plaque size in the absence of intestinal IDO was due to the observed increase in 5-HT production. To this end, we inhibited TPH1 in both male *Ldlr*$^{-/-}$ IEC IDOKO and *Ldlr*$^{-/-}$ IEC IDO mice fed HFD+HCD for 8 weeks. In agreement with the above results, TPH1 inhibition in both *Ldlr*$^{-/-}$ IEC IDO and *Ldlr*$^{-/-}$ IEC IDO KO mice led to a significant decrease in plaque size in the aortic sinus (**Fig. 3E**), without any significant changes in plasma cholesterol levels (**Supp. Fig. 10C**). Moreover, TPH1 inhibition led to a marked decrease in intestinal inflammation in IEC IDOKO mice, as assessed by a low colon histological scoring (**Fig. 3F**) and fecal Lcn2 levels (**Fig. 3G**). In agreement with the 5-HT pro-atherogenic role, we observed a significant correlation between blood 5-HT levels and plaque size in the aortic sinus (**Supp. Fig. 10D**). Although TPH1 inhibition significantly reduced plaque size in *Ldlr*$^{-/-}$ IEC IDO KO mice,

there was still a trend towards larger plaque size in *Ldlr*$^{-/-}$ IEC IDO KO mice treated with TPH1 inhibitor compared to littermate controls treated with TPH1 inhibitor (**Fig. 3E**), suggesting the involvement of also other mechanisms in the pro-atherogenic phenotype associated with IDO deficiency in IECs.

Trp-dependent microbiota modulation impacts atherosclerosis

Accumulating evidence showed that intestinal cells along with immune cells interact with gut microbiota to determine disease outcomes[27]. We therefore hypothesized that intestinal IDO activity might shape gut microbiota, and promote systemic inflammation and atherosclerosis. We first explored the bacterial fecal composition of the microbiota by the use of 16S rDNA sequencing of male *Ldlr*$^{-/-}$ IEC IDOKO and *Ldlr*$^{-/-}$ IEC IDO mice fed either HFD+HCD or NCD for 8 weeks. Principal coordinates analysis (PCoA) based on microbiota composition revealed significant differences between the groups of mice (**Supp. Fig. 11A**). In agreement with the deleterious effects of HFD on microbiota[28], the alpha-diversity analysis showed decreased diversity and richness under HFD+HCD compared to NCD, but no significant differences were observed according to the mice genotypes (**Supp. Fig. 11B**). At family levels, there were differences in relative abundance between groups (**Supp. Fig. 11C**). Fecal SCFA measurements in these groups showed only a decrease in fecal acetate levels in *Ldlr*$^{-/-}$ IEC IDOKO mice compared to littermate controls fed NCD (**Supp. Fig. 11D**). Under HFD+HCD condition, the levels of acetate decreased, but no significant difference was observed between the genotypes (**Supp. Fig. 11D**).

To address the importance of the microbiota, we depleted gut microbiota in *Ldlr*$^{-/-}$ IEC IDOKO and *Ldlr*$^{-/-}$ IEC IDO male mice fed HFD+HCD using a broad-spectrum antibiotic cocktail (ATB) supplemented in the drinking water. In agreement with previous studies[29], depletion of microbiota with ATB aggravated atherosclerosis due to enhanced plasma cholesterol levels. Moreover, ATB treatment abrogated the differences in plaque size without significant differences in plasma cholesterol, as well as gut inflammation as assessed by Lcn-2 levels, in male *Ldlr*$^{-/-}$ IEC IDO and *Ldlr*$^{-/-}$ IEC IDOKO mice fed HFD+HCD (**Fig. 4A-B** and **Supp. Fig. 12A**). Then, we wanted to test whether microbiota exchange between the two mouse genotypes might impact atherosclerosis. To this end, HFD+HCD-fed *Ldlr*$^{-/-}$ IEC IDO and *Ldlr*$^{-/-}$ IEC IDO KO mice were co-housed after weaning and compared to mice housed in cages separated according to the genotype. As shown in **Fig. 4C**, atherosclerosis plaque size in the aortic sinus of co-housed animals (whether *Ldlr*$^{-/-}$ IEC IDO or *Ldlr*$^{-/-}$ IEC IDO KO) was similar to those of *Ldlr*$^{-/-}$ IEC IDO KO mice housed in separate cages without significant changes in plasma cholesterol levels between the groups (**Supp. Fig. 12B**), suggesting a dominant pro-atherogenic effect of microbiota from *Ldlr*$^{-/-}$ IEC IDO KO mice. Then, as Trp is catabolized through microbiota-generated indole metabolites, we assessed whether the absence of IDO in IECs might alter indole production. However, unexpectedly considering the availability of Trp for the indole pathway in IEC IDOKO, lack of IDO in IECs led to a decrease in indole production, as assessed by low levels of fecal IAA (**Supp. Fig. 12C**). Trp is metabolized by gut bacteria into indole derivatives that activate aryl hydrocarbon receptor (AhR)[7]. We

then measured AhR agonists (such as IAA, IAld, and tryptamine) in feces of *Ldlr*$^{-/-}$ IEC IDO and *Ldlr*$^{-/-}$ IEC IDO KO mice separated by genotype, and in feces of mice co-housed after weaning, as well as in mice separated by genotype but treated with ATB. As shown in **Supp. Fig. 12D**, a decrease in AhR agonists (IAA, IAld, and tryptamine) was observed in *Ldlr*$^{-/-}$ IEC IDO KO compared to *Ldlr*$^{-/}$ IEC IDO mice, whereas this difference was abrogated in the cohoused mice. As expected given the specific production of indole derivatives by bacteria, AhR agonists (IAA, IAld, and tryptamine) markedly decreased in *Ldlr*$^{-/-}$ IEC IDO KO and *Ldlr*$^{-/-}$ IEC IDO mice treated with ATB (**Supp. Fig. 12D**). Noteworthy, among indole-producing bacteria[30], *Parabacteroides distasonis* relative abundance decreased in IEC IDO KO mice, and showed a positive correlation with fecal IAA levels and an inverse correlation with plaque size in control and *Ldlr*$^{-/-}$ IEC IDOKO mice fed HFD+HCD (**Supp. Fig. 12E-G**).

To investigate the physiological importance of impaired microbiota AhR activity, 6-formylindolo(3,2-b)carbazole (Ficz), an AhR agonist, was administered to HCD-fed female *Ldlr*$^{-/-}$ mice. Ficz treatment decreased colonic histological scoring (**Fig. 4D**) and alleviated atherosclerosis in the aortic sinus without any significant changes in plasma cholesterol levels (**Fig. 4E-F**), compared to untreated counterparts. This was associated with a decrease in CD3^{+} T cell accumulation within plaques (**Fig. 4G**), without significant changes in macrophage MOMA-2^{+} surface area (**Supp. Fig. 13A**). Moreover, to test the effects of indoles in atherosclerosis, we supplemented bacterial AhR agonists (a mixture of IAA, IPA, and tryptamine) to HCD-fed female *Ldlr*$^{-/-}$ mice for 8 weeks. Indole supplementation led to significant increase in the fecal levels of these indole derivatives without any significant changes in intestinal 5-HT or intestinal IDO activity (Kyn/Trp) (**Fig. 5A** and **Supp. Fig. 13B**). Indole supplementation was also associated with decreased leukocyte (CD45+) numbers in the intestine, particularly macrophages (CD64+), T (CD4+, CD8+) cells, and B (CD19+) cells (**Fig. 5B** and **Supp. Fig. 13C**). This was accompanied by a significant decrease in plaque size in the aortic sinus without significant changes in plasma cholesterol levels (**Fig. 5C-D**). The decrease in atherosclerosis in indole-supplemented group was also observed in the thoracic aorta (**Fig. 5E**). This was associated with a decrease in lesional macrophages MOMA2^{+} (**Fig. 5F**). Assessment of Th polarization, including Th1 (T-bet+), Th17 (ROR-γt+), and Treg (Foxp3+) subsets in the small intestines, Peyer's Patches (PP), mesenteric lymph nodes (MLNs), and spleens, showed only a significant increase in Th17 in PPs from indole-treated mice compared to controls (**Supp. Fig. 14 and 15**).

Taken together, these results point to the importance of microbiota, particularly bacteria-produced indoles, and AhR-mediated effects in atherosclerosis.

Discussion

Trp is one of the nine essential amino acids from dietary origin and whose metabolism has major effects on host functions[9]. IDO is the main pathway for degrading Trp in the extrahepatic compartments[31]. Although IDO has previously been reported to be highly expressed in the gastrointestinal tract[32], together with the ascertainment of the importance Trp metabolism for intestinal homeostasis[4], the specific role of intestinal IDO has not yet been explored. During inflammation, IDO is classically known to be up-regulated in myeloid cells by pro-inflammatory stimuli, such as LPS and interferon (IFN)-γ[33]. IDO is an upstream enzyme that is involved in the generation of Kyn and thereafter, following a cascade of different enzymatic reactions, Kyn-derived metabolites that exert either protective or deleterious effects[34]. As a protective role, IDO through Kyn metabolite, has been described as an immunosuppressive enzyme that inhibits effector T-cell function and favors the differentiation of Tregs[35]. This seems to be highly relevant during infection and pregnancy settings[36]. However, in our study, the absence of IDO in IEC did not significantly impact intestinal Treg polarization, which may indicate that this would not be the primary mechanism. Accordingly, Kyn supplementation in intestinal IDO-deficient mice did not significantly impact atherosclerotic plaque size.

The biological effects of IDO are not limited to the regulation of the immune response. IDO activity has been shown to contribute to arterial vessel relaxation and to the control of blood pressure in septic shock[37]. IDO activity was also shown to play a critical role in aneurysm [38,39] as well as in obesity[13] and acute myocardial infarction [40].

In the last decades, a number of experimental studies have been conducted to elucidate the role of IDO in inflammatory intestinal diseases, but contradictory results have been reported [41]. The discrepancies regarding the role of IDO in IBD might be explained by differences in mouse models and experimental settings used to induce colitis. In atherosclerosis, the findings of previous studies using global deletion of IDO have been controversial, showing both proatherogenic[10,11] or atheroprotective effects[12]. Our prior work has shown that under HCD condition IDO expressed in myeloid cells exerted a pro-atherogenic role through kynurenic acid[12]. Yet, it is noteworthy that under HCD condition IDO is weakly induced in the gut, as shown in the present study, which suggests that the observed phenotype of mice fed HCD with global deficiency of IDO was independent of IDO expression in the gut.

IDO seems to play a versatile role that might be due to the tissue-specific effects of this enzyme, suggesting that its function is tailored to the tissue/organ and the microenvironment in different pathological settings. Understanding the role of intestinal IDO is particularly important since the Trp metabolism in the gut is specific insofar as serotonin and microbiota-produced indoles are mainly produced in the gut[9]. Herein, we showed that the specific deletion of IDO in IECs led to a marked decrease in its activity in the small intestine, indicating that the expression of IDO in IECs is crucial for its activity in the gastrointestinal tract. Intestinal IDO deficiency resulted in augmented intestinal and peripheral inflammation that likely accounted for increased atherosclerosis. This was associated with a

high number of lymphocyte accumulation within the atheromatous plaques. Moreover, the proatherogenic role due to intestinal IDO deficiency was highly dependent on lymphocytes as the phenotype was abrogated in lymphocyte-deficient mice.

The Kyn, indole, and 5-HT pathways are interrelated in such a way that they depend on the use of Trp[9]. This makes it difficult to dissect the functional impact of each pathway, as the change of one catabolic pathway impacts the others. Therefore, as expected, the absence of IDO in intestinal cells led to an increase in 5-HT production. However unexpectedly, IEC IDOKO mice showed decreased indole production, while increased production was expected since more Trp was available for this pathway as a result of Kyn pathway blockade. The most likely explanation for this observation is that the lack of IDO in intestinal cells decreased indole-produced bacteria and/or promoted the expression of IDO in gut leukocytes, which ultimately hijacked Trp. In agreement with this hypothesis, we observed an increase in IDO expression in leukocytes isolated from the intestines of IEC IDO KO mice. We also observed a decrease in the relative abundance of one bacteria involved in indole production[30] *Parabacteroides distasonis*, which abundance positively correlated with fecal IAA levels and negatively with plaque size. Although these observations could account for decreased indole production in IEC IDOKO mice, the precise mechanisms responsible for the changes in microbiota and thus indole production remain to be further investigated. Moreover, whether the observed decrease in indole levels in IEC IDO KO was directly involved in the observed increase in atherosclerosis remains to be further examined.

IDO expression within the small intestines during atherosclerosis was different according to the gender, suggesting sex hormone regulation of IDO expression within the gut. In particular, there was an inverse significant correlation between the gene expression of IDO and estrogen receptor 2 in the small intestines, suggesting a negative regulation of IDO expression in the gut through this receptor, which is in agreement with a previous study in cancer cells[42]. However, as there are no estrogen response elements on the *Ido1* promoter sequence, we believe that the effect of estrogens on *Ido1* expression in the gut is indirect, which required further studies to decipher the mechanisms behind how estrogens could modulate intestinal IDO-mediated effects on atherosclerosis.

The IEC IDO-dependent anti-atherogenic effect was revealed in conditions of HFD combined with HCD, but not in conditions of HCD alone, which can be accounted for by the fact that intestinal IDO activity was markedly induced by HFD, but not by HCD. HFD-mediated upregulation of intestinal IDO most likely resulted from HFD-driven decrease in the production of SCFA, especially butyrate that has been reported to down-regulate *Ido1* expression in IECs[16]. Consistently, supplementation of HFD with soluble fibers, which increased butyrate levels, down-regulated IDO activity, as shown by decreased Kyn levels in this condition.

The HFD-mediated increase in intestinal IDO activity might participate in a negative feedback loop to limit inflammatory responses caused by HFD.

HFD has many other pathogenic effects. Particularly, we found that HFD alleviated indole production, in agreement with previous studies[13,14]. Microbiota-derived indole metabolites promote intestinal barrier

integrity and immune cell homeostasis, which has been shown to play a protective role in obesity[13,14], and IBD[43]. The protective roles of indole metabolites in maintaining intestinal barrier integrity and immune cell homeostasis seem, at least in part, to be dependent on the activation of AhR and the production of interleukin (IL)-22[3,7]. The transcription factor, AhR a well-known receptor for indole metabolites (such as IAA, IPA, and tryptamine), has been reported to promote intestinal homeostasis and suppress inflammation[44]. Recently, one of the indole metabolites, IPA, has been shown to protect against atherosclerosis[45]. In agreement with these observations, we found that the supplementation with Ficz, an AhR agonist as well as indole metabolites relieved intestinal inflammation and decreased atherosclerosis.

5-HT is another important Trp-derived metabolite that plays key roles in gut function. Although serotonin is considered as an important central physiologic mediator of intestinal function by regulating gut motility, permeability and other functions, accumulating evidence point to its potent inflammatory effects [46]. The increase in 5-HT acts as a pro-inflammatory factor within the gut, as evidenced by studies showing that blocking 5-HT production with LP533401, a small molecule inhibitor of TPH1, an enzyme responsible for the synthesis of gut-derived serotonin, reduced inflammation in colitis models, without affecting the brain serotonin content[46]. The inflammatory role of 5-HT in the gut seems likely related to nuclear factor-kappa B (NF-κB) induction[47].

5-HT levels were also associated with CVD and thought to exert a deleterious role[46], although its role in atherosclerosis has been poorly investigated.

We found that daily injection of LP533401 resulted in a marked decrease in 5-HT levels in both the gut and blood, compared to vehicle-treated mice. TPH1 inhibition reduced atherosclerosis and alleviated intestinal and plaque inflammation. The protective role of TPH1 inhibition was also observed in IEC IDOKO mice as evidenced by our results showing the decrease in gut and plaque inflammation as well as atherosclerosis in this mouse model. Moreover, 5-HT supplementation led to increase in intestinal permeability and atherosclerosis, confirming the pro-atherogenic role of 5-HT.

In conclusion, our data uncover the pivotal role of intestinal Trp-dependent pathways in gut inflammation and, as a result, in atherosclerosis development, thereby contributing to a better understanding of the link between the gut and the periphery, and unveiling this metabolic pathway as a potential therapeutic target.

Methods

Mice.

All experiments were conducted according to the ethical committee for animal experimentation (University of Paris Cité, CEEA 34) and the National Charter on the ethics of animal experimentation from the French Minister of Higher Education and Research under the reference MESR no. 01373.01. All mice were bred in specific pathogen-free laboratory animal facilities under standard conditions with temperatures of 21–23 °C, 40–60% humidity and 12 h light/dark cycles. Animals were provided with food and water ad libitum. Both male and female mice at age of 8 weeks were used in this study. We implemented reduction and refinement principles to minimize harm to the animals. Procedures were used to minimize pain, suffering, and distress for the mice, ensuring their welfare is prioritized. This includes improving housing conditions, using less invasive techniques, and providing effective analgesia and anesthesia. Before euthanasia by cervical dislocation, animals were anesthetized with isoflurane (3% in oxygen).
Ldlr$^{-/-}$ (JAX:002207), *Rag1*$^{-/-}$ (JAX:002216), *Villin-cre*$^{+/-}$ (JAX:004586) mice were bought from the Jackson Laboratory and bred in our facility. *Rag1*$^{-/-}$ mice were crossed with *ldlr*$^{-/-}$ mice to obtain *Rag1*$^{-/-}$ *ldlr*$^{-/-}$ mice. *Ido-1*$^{flox/flox}$ mice were kindly given by Marc Veldhoen (Babraham Institute Cambridge). *Ido-1*$^{flox/flox}$ mice were crossed with *Villin-cre*$^{+/-}$mice. Then the resulting mice were crossed with *Ldlr*$^{-/-}$ to obtain *ldlr*$^{-/-}$ *Ido-1*$^{flox/flox}$*villin-cre* mice. *ldlr*$^{-/-}$ *Ido-1*$^{flox/flox}$*villin-cre*+/- and littermate *ldlr*$^{-/-}$ *Ido-1*$^{flox/flox}$*villin-cre-/-* control mice were used in some experiments. *Rag1*$^{-/-}$ *ldlr*$^{-/-}$ mice were crossed with *ldlr*$^{-/}$ *Ido-1*$^{flox/flox}$*villin-cre* mice to obtain *Rag1*$^{-/-}$ *ldlr*$^{-/-}$ *Ido-1*$^{flox/flox}$*villin-cre* mice. *Rag1*$^{-/-}$ *ldlr*$^{-/-}$ *Ido-1*$^{flox/flox}$*villin-cre*+/- mice and littermate *Rag1*$^{-/-}$ *ldlr*$^{-/-}$ *Ido-1*$^{flox/flox}$*villin-cre-/-* control mice were used in some experiments. All mice were on C57Bl/6 background and were backcrossed for more than 10 generations. In general, mice (n=5/cage) were separated by genotype at weaning until the sacrifice. In co-housing experiments, 4 mice (n=2 per genotype) were mixed in the same cages from the weaning until the sacrifice.

Mice were fed with either a normal chow diet (NCD) (A03, SAFE, France) or subjected to high-fat diet (HFD) containing 60% FAT (E15742-347, SSNIFF, Germany) or a high-cholesterol diet (HCD) containing 1.25 % cholesterol (E15106-347, SSNIFF, Germany) or a combination of both HFD+HCD diet (SSNIFF, Germany) (composition shown in **Supp. Fig.1A**). A specific diet was started at 7 weeks of age and continued for 13 weeks or less with ad libitum access to water and food. In some experiments, FOS (Fructooligosaccharides), as a source of soluble dietary fibers was diluted in drinking water (7.5%). Gut microbiota was depleted using a combination of oral antibiotics (metronidazole 1g/L, amoxicillin 0.5g/L, vancomycin 0.5g/L, neomycin 1g/L) dissolved in drinking water with sucralose (4g/L)[48]. In other experiments, kynurenine or indole derivatives (IAA, IPA, and tryptamine) or the 5-HT precursor, L-5-hydroxytryptophane (5-HTP) (2 mg/ml diluted in drinking water, Sigma-Aldrich) supplementation to *ldlr*$^{-/-}$ or *ldlr*$^{-/-}$ *Ido-1*$^{flox/flox}$*villin-cre* mice was performed for 8 weeks of HFD+HCD or HCD. A group of mice was injected with the 6-formylindolo(3,2-b)carbazole (Ficz; 1 µg/mouse, one time per week, Santa Cruz Biotechnology, USA) or vehicle along the 8 weeks of HCD. Other groups of mice were daily injected with TPH1 inhibitor LP533401 (25 mg/kg, Dalton Pharma Services, Canada) or an equal volume of vehicle along the 8 weeks of HFD+HCD feeding period. All mice used in these experiments were bred and housed in a specific pathogen-free barrier facility (the health certificate is provided in the **Supp. Table 1**). Animal experiments were performed according to the European directive (2010/63/UE) and to the institutional guidelines approved by the local ethics committee of the French authorities, the 'Comité d'Ethique en Experimentation Animale' (CEEA) under the following number APAFIS #33148-2021080517361889.

***In vivo* Studies.**
For oral glucose tolerance test (OGTT), mice were fasted overnight prior to an oral administration of 1 g/kg glucose. Blood was sampled from the tail vein at 0, 5, 15, 30, 60, 90 and 120 min in order to assay glucose concentration (OneTouch Ultra glucometer, LifeScan Europe). At 0, 15, 30, 60 min tail vein blood was collected, plasma samples were stored at -20°C until they were analyzed for insulin concentration (Crystal Chem Inc., Downers Grove, USA). Insulin tolerance test (ITT) was performed in

mice food deprived for 5 h prior to an intraperitonial injection of 1 U/kg insulin. Blood was sampled from the tail vein at 0, 5, 15, 30, 60 and 90 min in order to assay glucose concentration.

***In vivo* intestinal permeability.**
Permeability *in vivo* was assessed using fluorescein isothiocyanate-conjugated dextran (FITC–dextran 3000–5000 Da, Sigma–Aldrich) tracer[7]. Briefly, at the endpoint 0.6 mg/g body weight of FITC–dextran dissolved in PBS was administered to mice by oral gavage. To measure the presence of FITC–dextran in blood, 3.5 h after the gavage blood samples were recovered from the retro-orbital venous plexus and kept in dark at 4°C until analysis. Serum has separated by centrifugation (5000 g, 30 minutes, 4°C) and plasma FITC levels were determined using a fluorescence microplate reader (excitation 485 nm and emission 530 nm).

Biochemical measurements.
Blood glucose level was measured using a glucometer (OneTouch Ultra, LifeScan Europe). Plasma insulin (Crystal Chem Inc., Downers Grove, USA) was determined by enzyme-linked immunosorbent assay (ELISA) (R&D Systems). HOMA-IR in mice was calculated using the equation ((fasting glucose concentration x fasting insulin concentration)/405) [49].

Fecal lipocalin-2 measurements.
Frozen fecal samples were reconstituted in phosphate-buffered saline (PBS) containing 0.1% Tween 20 (100 mg/mL) and vortexed for 20 minutes to get a homogenous fecal suspension, which was then centrifuged at 18000 g and 4°C for 10 minutes. Lipocalin-2 concentrations were measured in the supernatants using Duoset murine lipocalin-2 ELISA kit (R&D Systems, Minneapolis, MN) [21].

Serum LPS-specific immunoglobulins.
Lipopolysaccharide (LPS)-specific IgG levels were quantified by ELISA. Microtiter plates were coated overnight with purified *E. coli* LPS (1 µg/well from *E. coli* 0128: B12, Sigma, Catalog No. 2887). Serum samples diluted 1:200 were then applied. After incubation and washing, wells were incubated with anti-mouse IgG-HRP. Quantification was performed using the colorimetric peroxidase substrate tetramethylbenzidine and optical density (OD) was read at 650 nm with an ELISA plate reader. Data are reported as OD corrected by subtracting background (determined by readings in samples lacking serum).

Histology.
The entire mouse colon was excised, and segments of the proximal colon (1 cm) were fixed in buffered 4% formalin, paraffin embedded, cut into 4-µm sections, and stained with hematoxylin/eosin/safranin (HES). The histological severity of colitis was graded in a "blinded" fashion. The tissue samples were evaluated for the amount and depth of inflammation with a range of 0 to 3 and the amount of crypt damage or regeneration with a range of 0 to 3, as previously established[50].

Localization of bacteria by FISH.
Fluorescent *in situ* hybridization (FISH) was performed[51], in order to analyze bacteria localization at the surface of the intestinal mucosa. Briefly, colonic tissues (proximal colon, 2nd cm from the cecum) containing fecal material were placed in methanol-Carnoy's fixative solution (60% methanol, 30% chloroform, 10% glacial acetic acid) for a minimum of 3 h at room temperature. Tissue were then washed in methanol 2 × 30 min, ethanol 2 × 15 min, ethanol/xylene (1:1) 15 min and xylene 2 × 15 min, followed by embedding in Paraffin with a vertical orientation. Five µm sections were performed and dewax by preheating at 60°C for 10 min, followed by xylene 60°C for 10 min, xylene for 10 min and 99.5% ethanol for 10 minutes. Hybridization step was performed at 50°C overnight with EUB338 probe (5'-GCTGCCTCCCGTAGGAGT-3', with a 5' labeling using Alexa 647) diluted to a final concentration of 10 µg/mL in hybridization buffer (20 mM Tris–HCl, pH 7.4, 0.9 M NaCl, 0.1% Sodium Dodecyl Sulfate (SDS), 20% formamide). After washing 10 min in wash buffer (20 mM Tris–HCl, pH 7.4, 0.9 M NaCl) and 3 × 10 min in PBS, PAP pen (Sigma, St. Louis, MO) was used to mark around the section and block solution (5% fetal bovine serum in PBS) was added for 30 min at 4°C. Mucin-2 primary antibody (rabbit H-300, Santa Cruz Biotechnology) was diluted 1:1500 in block solution and apply overnight at 4°C.

After washing 3 × 10 min in PBS, block solution containing anti-rabbit Alexa 488 secondary antibody diluted 1:1500, Phalloidin-Tetramethylrhodamine B isothiocyanate (Sigma, St. Louis, MO) at 1µg/mL and Hoechst 33258 (Sigma, St. Louis, MO) at 10µg/mL was applied to the section for 2h. After washing 3 × 10 min in PBS slides were mounted using Prolong anti-fade mounting media (Life Technologies). Observations were performed with a Zeiss LSM 700 confocal microscope with software Zen 2011 version 7.1. This software was used to determine the distance between bacteria and epithelial cell monolayer.

Extent and plaque composition of atherosclerotic lesions.
Mice were anesthetized with isoflurane before sacrifice. Plasma cholesterol were measured using a commercial cholesterol assay kit (DiaSys Diagnostic Systems GmbH). The heart and aorta, including the brachiocephalic artery, were taken off, fixed in 4% paraformaldehyde for 2 hours. Lipids were detected using Oil red O coloration[52]. Lesion extent in the thoracic aorta represents the percentage of Oil red O staining. For immunostaining, we used antibodies raised against MOMA-2 (MAB1852, Merck Milllipore®) and CD3 (A0452, Dako®) to detect macrophages and T cells respectively[53]. Masson's trichrome staining was performed to visualize necrotic cores[52]. Quantification within atherosclerotic lesions was performed in cross-sectional areas throughout the whole aortic sinus, which represents ~6-8 sections per mouse, and appropriate negative controls were used. Morphometric studies using Histolab software (Microvision), or ImageJ (NIH) software.

Quantitative Real time PCR and NanoString technology.
Intestines were lysed in detergent buffer RLT and then subjected to RNA extraction and reverse transcription (Qiagen) or NanoString technology. Quantitative real-time PCR was performed on an ABI PRISM 7700 (Applied Biosystems) in triplicates. Cycle threshold for Gapdh (primers: Gapdh-R, 5'-CGTCCCGTAGACAAAATGGTGAA-3'; *Gapdh*-L, 5'-GCCGTGAGTGGAGTCATACTGGAACA-3') was used to normalize gene expression. Primers for *Reg3g*-R 5′-TTCCTGTCCTCCATGATCAAAA-3′ and *Reg3g*-L 5′-CATCCACCTCTGTTGGGTTCA-3′; *Reg3b*-R 5′-ATGCTGCTCTCCTGCCTGATG-3′ and *Reg3b*-L 5′-CTAATGCGTGCGGAGGGTATATTC-3; *Occludin*-R 5'-AAGGTTTCCGTCTGTCATAATCTC-3' and *Occludin*-L 5'-TGGCTGCTGCTGATGAATATAATA 3'; *TNF-α*-R 5'-CGTGGGCTACAGGCTTGTCAG 3' and *TNF-α*-L 5'-GATGGGGGGCTTCCAGAACT 3', *esr1*-R 5'- CTCCCGCCTTCTACAGGTCTAA-3' and *esr1*-L 5'-GACAGTCTCTCTCGGCCATTCT-3', *esr2*-R 5'-GCCCTGTTACTAGTCCAAGC-3' and *esr2*-L 5'-CAGGACCAGACACCGTAATG-3, *greb1*-R 5'-TCATTATCTGTGCCTGCCGGA-3' and *greb1*-L 5'-CACTTTGCCAGTGACCAGCTC-3'. PCR conditions were 10 min at 95°C; 35 cycles of 95°C for 15 s, 60°C for 20 s and 72°C for 20 s and a final extension at 72°C for 20 s. The NanoString Mouse Immunology Panel was used to profile gene expression of immunology-related genes. Briefly, RNA samples (50 ng) were hybridized with the NanoString probe sets. Then, Hybridized samples were processed on the nCounter Analysis System, which digitally counts the barcoded probe signals. Data was exported to nSolver Analysis Software for normalization and analysis.

Metabolite quantifications.
Measurement of short chain fatty acids (SCFA) including acetate and butyrate in feces was performed, as previously described[54]. Briefly, a stock solution of SCFA metabolites (Sigma Aldrich, France) was prepared and serially diluted to get 10 calibration solutions. A working solution of internal standards was prepared in 0.15 M NaOH to get the following final concentrations: 75 mmol/L of D3-acetate and 2.5 mmol/L of 13C-butyrate (Sigma Aldrich). Stool samples were weighed (~50 mg), dissolved in 200 µL of sodium hydroxide solution at 0.15 M (NaOH, Sigma Aldrich). Twenty microliters of the internal standard solution were added to stool samples and calibration solutions. Each sample was then acidified with 5 µL of hydroxide chloride 37% (Sigma Aldrich, France) and then extracted with 1.7 mL of diethyl ether (Biosolve, France). Samples were stirred gently for 1 hour and then centrifuged 2 min (3000 g, 4°C). The organic layers were transferred into 1.5 ml glass vials and SCFAs were derivatized with 20 µL of tert-butyldimethylsilyl imidazole (Sigma Aldrich, France). Samples were heated at 60°C for 30 minutes before analysis using an Agilent Technologies gas chromatography system (model 7890A-5975C, France). The temperature program started at 50 °C for 1 min, ramped to 90°C at 5°C/min, then up to 300 °C at 70°C/min.

L-Tryptophan (Trp) and L-Kynurenine (Kyn), and serotonin or 5-hydroxytryptamine (5-HT) levels were measured via liquid chromatography using a coulometric electrode array (ESA Coultronics, ESA Laboratories, Chelsford, MA, USA)[55]. Quantifications were performed by referencing calibration curves obtained with internal standards.
Metabolites were extracted from the fecal pellets using a methanol/chloroform extraction method [56]with minor modifications. Cold methanol/chloroform (2:1, v/v; 1.5 ml) was added to a preweighed cecal or fecal sample and homogenized on ice. The sample tube was centrifuged at 15,000g for 10 minutes at 4°C, and the supernatant was transferred to a new sample tube through a 70-mm cell strainer. Ice-cold water (0.6 ml) was added, and the sample tube was vortexed and centrifuged (15,000g, 5 minutes, 4°C) to obtain phase separation. The upper and lower phases were separately collected in fresh sample tubes with a syringe, taking care not to disturb the interface. The polar (upper) phase (500 ml) was evaporated to dryness in a Savant SpeedVac concentrator (Thermo Scientific, Asheville, NC), and then was reconstituted in 50 ml of methanol/water (1:1, v/v). Extracted metabolites were stored at -80°C until analysis. Indole-3-acetic (IAA), Indole-3-propionic acid (IPA), Indole-3-aldehyde (IAld), indole, and tryptamine were quantified via liquid chromatography coupled to mass spectrometry (LC-MS) and/or via liquid chromatography coupled to a fluorescence detector (LC-Fluo) by using a Shimadzu Prominence. The LC system is equipped with a binary solvent delivery manager and sample manager (Shimadzu, Kyoto, Japan) and that was coupled to a triple quadrupole (TQ-MS) mass spectrometer equipped with an electrospray interface (ESI) for LC-MS or with a fluorescence detector (RF20Ax, Shimadzu) for LC-Fluo. The fluorescence detection was carried out simultaneously at three different excitation wavelengths: 280, 344 and 309 nm and the emission wavelength was set at 330 or 398 nm. Compounds (IAld, IAA, IPA, and tryptamine) were identified by comparing with the retention time of reference standards in our in-house library. For LC-MS the quantification was done on Multiple reaction monitoring (MRM) mode and MRM transitions for IAA, IPA, and indole are used as follows: 173>129; 190>130; 118>91. The quantification was done by integration of the peak absorbance area, employing a calibration curve established with various known concentrations of indole derivatives. The measurements were performed in triplicate for each sample.

Intestine digestion, flow cytometry and cell sorting.
Cells from the small intestine lamina propria were isolated as previously described[57]. Briefly, after removing payer patches and fat the small intestine was cut longitudinal open and washed in 4 changes of Roswell Park Memorial Institute (RPMI). Next, samples were incubated under rotation for 20 min at 37°C in RPMI containing 5 mM Ethylenediaminetetraacetic acid (EDTA), 1 mM Dithiothreitol (DTT), and 5 % fetal calf serum (FCS) to remove epithelial cells. Samples were then washed 3 times in PBS and transferred to the digestion solution (RPMI containing 0.1 mg/ml Liberase TL (Roche) and 0.5 mg/ml DNase I (Roche)) and incubated for 30 min at 37°C under rotation. The digested tissue was filtered through a 70 µm cell strainer followed by a 40/80 % Percoll density gradient centrifugation. Then, the isolated cells were counted and used for flow cytometry staining.
For cell surface staining the following antibodies were used: 2.5 µg/ml Fluorescein isothiocyanate (FITC) conjugated CD45 (BD Biosciences Ref: 553079. Clone: 30-F11), 2.5 µg/ml Allophycocyanin (APC)/Fire 750 conjugated CD3 (Biolegend Ref: 100362. Clone: 145-2C11), 1.25 µg/ml Brilliant Violet™ (BV) 605 conjugated CD8a (Biolegend Ref: 100744. Clone 53-6.7), 0.625 µg/ml Alexa Fluor700 conjugated CD4 (Biolegend Ref: 100536. Clone RM4-5), 0.625 µg/ml PerCP-Cyanine 5.5 conjugated CD19 (Biolegend Ref: 115534. Clone 6D5), Zombie aqua (Bio-legend Ref: 423102), 0.625 µg/ml BV510 conjugated CD11b (Biolegend Ref: 101263. Clone M1/70), 0.625 µg/ml BV510 conjugated CD11c (Biolegend Ref: 117338. Clone N418). Intranuclear staining was performed using 2.5 µg/ml phycoerythrin (PE) conjugated T-bet (Biolegend Ref: 644810. Clone: 4B10), 0.625 µg/ml PE-Cyanine7 conjugated FoxP3 (eBioscience Ref: 25-5773-80. Clone: FJK-16s), 0.1 µg/ml BV-421 conjugated GATA-3 (Biolegend Ref: 653814. Clone: 16E10A23) and 0.3125 µg/ml APC conjugated ROR-γt (Invitrogen Ref: 17-6981-82. Clone: B2D). Samples were acquired using a flow cytometer (LSR Fortessa, Becton Dickinson) and data was analyzed using FlowJo software (Tree-Star, OR, USA). Cell doublets were excluded using forward (FSC-A vs. FSC-H) and side (SSC-A vs. SSC-W) scatter. Live

CD45+ cells were sorted from the digested lamina propria of the small intestine by using a FACS Aria II (BD Biosciences).

16S rDNA gene sequencing and analysis.
16S rDNA gene sequencing of fecal DNA samples was performed as previously described[7]. Briefly, the V3-V4 region (16S (sense) 5′-TACGGRAGGCAGCAG-3′ and (antisense) 5′-CTACCNGGGTATCTAAT-3′) was amplified and sequencing was done using an Illumina MiSeq platform (GenoScreen, Lille, France). Raw paired-end reads were subjected to the following process: (1) quality-filtering using the PRINSEQ-lite PERL script38 by truncating the bases from the 3′ end that did not exhibit a quality <30 based on the Phred algorithm; (2) searching and removing both forward and reverse primer sequences using CutAdapt, with no mismatches allowed in the primer sequences. Sequences for which perfect forward and reverse primers were not found were eliminated. Analysis was performed using the Qiime2 pipeline (version 2020.8.0) in R version 4.2.2[58]. Sequencing errors were corrected with Dada2[59] using custom parameters (--p-trunc-len-f 230 --p-trunc-len-r 220). Taxonomic classification of resulted ASVs was performed using Silva trained database (v138-99)[60] based on scikit-lern's naïve Bayes algorithm. Results were deep analysed with the Phyloseq package (version 1.34.0)[61] as for the analysis of taxonomic and alpha diversity. Statistical analyses were performed using rstatix[62] (version 0.7) and figures were plotted using the ggplot2 package (version 3.3.5)[63]. Principal coordinate analyses (PCoA) were carried out with Vegan package (version 2.5-7)[64] on the Bray-Curtis dissimilarity matrices constructed from the relative abundance of ASVs. Communities that emerged were verified using a PERMANOVA test with adonis2 function using 999 permutations, and the confidence interval were plotted at 95% and 97% confidence limits, using the standard deviation method.

Statistical analysis.
Graphs and statistical analyses were performed using Prism software (Graphpad). Values are expressed as means ± s.e.m. Differences between values were examined using the two-tailed Mann-Whitney test. Normal distribution was assessed by Kolmogorov-Smirnov test. One-way analysis of variance was used to compare 3 or more independent experimental groups. The analysis was performed by Brown-Forsythe ANOVA test followed by Tukey's multiple comparison test, as appropriate. Significance of data that did not respect normality were assessed using Kruskal-Wallis, followed by post-Hoc Dunn's test. Values were considered significant at $P<0.05$.

Data availability

The authors declare that the data supporting the findings of this study are available within the paper and its supplementary information files. All the raw data generated in this study are provided in the Source Data file. Microbiota 16s RNA data are accessible with the following links https://www-ncbi-nlm-nih-gov.proxy.insermbiblio.inist.fr/sra/PRJNA996874 and https://www.ebi.ac.uk/ena/browser/view/PRJNA996874. Raw data of the metabolites analyzed by mass spectrometry are accessible with the following link http://www.peptideatlas.org/PASS/PASS05869.

References

1 Cainzos-Achirica, M. *et al.* Inflammatory Bowel Disease and Atherosclerotic Cardiovascular Disease: JACC Review Topic of the Week. *J Am Coll Cardiol* **76**, 2895-2905 (2020). https://doi.org:10.1016/j.jacc.2020.10.027

2 Witkowski, M., Weeks, T. L. & Hazen, S. L. Gut Microbiota and Cardiovascular Disease. *Circ Res* **127**, 553-570 (2020). https://doi.org:10.1161/circresaha.120.316242

3 Zelante, T. *et al.* Tryptophan catabolites from microbiota engage aryl hydrocarbon receptor and balance mucosal reactivity via interleukin-22. *Immunity* **39**, 372-385 (2013). https://doi.org:10.1016/j.immuni.2013.08.003

4 Gao, J. *et al.* Impact of the Gut Microbiota on Intestinal Immunity Mediated by Tryptophan Metabolism. *Frontiers in cellular and infection microbiology* **8**, 13 (2018). https://doi.org:10.3389/fcimb.2018.00013

5 Agus, A., Planchais, J. & Sokol, H. Gut Microbiota Regulation of Tryptophan Metabolism in Health and Disease. *Cell Host Microbe* **23**, 716-724 (2018). https://doi.org:10.1016/j.chom.2018.05.003

6 Hashimoto, T. *et al.* ACE2 links amino acid malnutrition to microbial ecology and intestinal inflammation. *Nature* **487**, 477-481 (2012). https://doi.org:10.1038/nature11228

7 Lamas, B. *et al.* CARD9 impacts colitis by altering gut microbiota metabolism of tryptophan into aryl hydrocarbon receptor ligands. *Nat Med* **22**, 598-605 (2016). https://doi.org:10.1038/nm.4102

8 Michaudel, C. *et al.* Rewiring the altered tryptophan metabolism as a novel therapeutic strategy in inflammatory bowel diseases. *Gut* **72**, 1296-1307 (2023). https://doi.org:10.1136/gutjnl-2022-327337

9 Taleb, S. Tryptophan Dietary Impacts Gut Barrier and Metabolic Diseases. *Frontiers in immunology* **10**, 2113 (2019). https://doi.org:10.3389/fimmu.2019.02113

10 Cole, J. E. *et al.* Indoleamine 2,3-dioxygenase-1 is protective in atherosclerosis and its metabolites provide new opportunities for drug development. *Proc Natl Acad Sci U S A* **112**, 13033-13038 (2015). https://doi.org:10.1073/pnas.1517820112

11 Polyzos, K. A. *et al.* Inhibition of indoleamine 2,3-dioxygenase promotes vascular inflammation and increases atherosclerosis in Apoe-/- mice. *Cardiovasc Res* **106**, 295-302 (2015). https://doi.org:10.1093/cvr/cvv100

12 Metghalchi, S. *et al.* Indoleamine 2,3-Dioxygenase Fine-Tunes Immune Homeostasis in Atherosclerosis and Colitis through Repression of Interleukin-10 Production. *Cell metabolism* **22**, 460-471 (2015). https://doi.org:10.1016/j.cmet.2015.07.004

13 Laurans, L. *et al.* Genetic deficiency of indoleamine 2,3-dioxygenase promotes gut microbiota-mediated metabolic health. *Nat Med* **24**, 1113-1120 (2018). https://doi.org:10.1038/s41591-018-0060-4

14 Natividad, J. M. *et al.* Impaired Aryl Hydrocarbon Receptor Ligand Production by the Gut Microbiota Is a Key Factor in Metabolic Syndrome. *Cell metabolism* **28**, 737-749 e734 (2018). https://doi.org:10.1016/j.cmet.2018.07.001

15 Schroeder, B. O. & Backhed, F. Signals from the gut microbiota to distant organs in physiology and disease. *Nat Med* **22**, 1079-1089 (2016). https://doi.org:10.1038/nm.4185

16 Martin-Gallausiaux, C. *et al.* Butyrate Produced by Commensal Bacteria Down-Regulates Indolamine 2,3-Dioxygenase 1 (IDO-1) Expression via a Dual Mechanism in Human Intestinal Epithelial Cells. *Frontiers in immunology* **9**, 2838 (2018). https://doi.org:10.3389/fimmu.2018.02838

17 Murphy, E. F. *et al.* Composition and energy harvesting capacity of the gut microbiota: relationship to diet, obesity and time in mouse models. *Gut* **59**, 1635-1642 (2010). https://doi.org:10.1136/gut.2010.215665

18 Morrison, K. E., Jasarevic, E., Howard, C. D. & Bale, T. L. It's the fiber, not the fat: significant effects of dietary challenge on the gut microbiome. *Microbiome* **8**, 15 (2020). https://doi.org:10.1186/s40168-020-0791-6

19 Deschênes, J., Bourdeau, V., White, J. H. & Mader, S. Regulation of GREB1 transcription by estrogen receptor alpha through a multipartite enhancer spread over 20 kb of upstream flanking sequences. *J Biol Chem* **282**, 17335-17339 (2007). https://doi.org:10.1074/jbc.C700030200

20 Cani, P. D. *et al.* Metabolic endotoxemia initiates obesity and insulin resistance. *Diabetes* **56**, 1761-1772 (2007). https://doi.org:10.2337/db06-1491

21 Chassaing, B. *et al.* Fecal lipocalin 2, a sensitive and broadly dynamic non-invasive biomarker for intestinal inflammation. *PLoS One* **7**, e44328 (2012). https://doi.org:10.1371/journal.pone.0044328

22 Tran, H. Q., Ley, R. E., Gewirtz, A. T. & Chassaing, B. Flagellin-elicited adaptive immunity suppresses flagellated microbiota and vaccinates against chronic inflammatory diseases. *Nat Commun* **10**, 5650 (2019). https://doi.org:10.1038/s41467-019-13538-y

23 Taleb, S. Inflammation in atherosclerosis. *Arch Cardiovasc Dis* **109**, 708-715 (2016). https://doi.org:10.1016/j.acvd.2016.04.002

24 Mauler, M. *et al.* Platelet Serotonin Aggravates Myocardial Ischemia/Reperfusion Injury via Neutrophil Degranulation. *Circulation* **139**, 918-931 (2019). https://doi.org:10.1161/circulationaha.118.033942

25 Ghia, J. E. *et al.* Serotonin has a key role in pathogenesis of experimental colitis. *Gastroenterology* **137**, 1649-1660 (2009). https://doi.org:10.1053/j.gastro.2009.08.041

26 Walther, D. J. *et al.* Synthesis of serotonin by a second tryptophan hydroxylase isoform. *Science* **299**, 76 (2003). https://doi.org:10.1126/science.1078197

27 Belkaid, Y. & Hand, T. W. Role of the microbiota in immunity and inflammation. *Cell* **157**, 121-141 (2014). https://doi.org:10.1016/j.cell.2014.03.011

28 Murphy, E. A., Velazquez, K. T. & Herbert, K. M. Influence of high-fat diet on gut microbiota: a driving force for chronic disease risk. *Current opinion in clinical nutrition and metabolic care* **18**, 515-520 (2015). https://doi.org:10.1097/mco.0000000000000209

29 Villette, R. *et al.* Unraveling Host-Gut Microbiota Dialogue and Its Impact on Cholesterol Levels. *Frontiers in pharmacology* **11**, 278 (2020). https://doi.org:10.3389/fphar.2020.00278

30 Roager, H. M. & Licht, T. R. Microbial tryptophan catabolites in health and disease. *Nat Commun* **9**, 3294 (2018). https://doi.org:10.1038/s41467-018-05470-4

31 Ball, H. J., Jusof, F. F., Bakmiwewa, S. M., Hunt, N. H. & Yuasa, H. J. Tryptophan-catabolizing enzymes - party of three. *Frontiers in immunology* **5**, 485 (2014). https://doi.org:10.3389/fimmu.2014.00485

32 Dai, X. & Zhu, B. T. Indoleamine 2,3-dioxygenase tissue distribution and cellular localization in mice: implications for its biological functions. *J Histochem Cytochem* **58**, 17-28 (2010). https://doi.org:jhc.2009.953604 [pii]10.1369/jhc.2009.953604

33 Chon, S. Y., Hassanain, H. H. & Gupta, S. L. Cooperative role of interferon regulatory factor 1 and p91 (STAT1) response elements in interferon-gamma-inducible expression of human indoleamine 2,3-dioxygenase gene. *J Biol Chem* **271**, 17247-17252 (1996).

34 Gheorghe, C. E. *et al.* Focus on the essentials: tryptophan metabolism and the microbiome-gut-brain axis. *Curr Opin Pharmacol* **48**, 137-145 (2019). https://doi.org:10.1016/j.coph.2019.08.004

35 Mellor, A. L. & Munn, D. H. IDO expression by dendritic cells: tolerance and tryptophan catabolism. *Nat Rev Immunol* **4**, 762-774 (2004). https://doi.org:10.1038/nri1457nri1457 [pii]

36 Mellor, A. L., Lemos, H. & Huang, L. Indoleamine 2,3-Dioxygenase and Tolerance: Where Are We Now? *Frontiers in immunology* **8**, 1360 (2017). https://doi.org:10.3389/fimmu.2017.01360

37 Wang, Y. *et al.* Kynurenine is an endothelium-derived relaxing factor produced during inflammation. *Nat Med* **16**, 279-285 (2010). https://doi.org:nm.2092 [pii]10.1038/nm.2092

38 Wang, Q. *et al.* Tryptophan-Derived 3-Hydroxyanthranilic Acid Contributes to Angiotensin II-Induced Abdominal Aortic Aneurysm Formation in Mice In Vivo. *Circulation* **136**, 2271-2283 (2017). https://doi.org:10.1161/CIRCULATIONAHA.117.030972

39 Metghalchi, S. *et al.* Indoleamine 2 3-dioxygenase knockout limits angiotensin II-induced aneurysm in low density lipoprotein receptor-deficient mice fed with high fat diet. *PLoS One* **13**, e0193737 (2018). https://doi.org:10.1371/journal.pone.0193737

40 Melhem, N. J. *et al.* Endothelial Cell Indoleamine 2, 3-Dioxygenase 1 Alters Cardiac Function After Myocardial Infarction Through Kynurenine. *Circulation* **143**, 566-580 (2021). https://doi.org:10.1161/circulationaha.120.050301

41 Acovic, A. *et al.* Role of indoleamine 2,3-dioxygenase in pathology of the gastrointestinal tract. *Therapeutic advances in gastroenterology* **11**, 1756284818815334 (2018). https://doi.org:10.1177/1756284818815334

42 Noonepalle, S. K. *et al.* Promoter Methylation Modulates Indoleamine 2,3-Dioxygenase 1 Induction by Activated T Cells in Human Breast Cancers. *Cancer Immunol Res* **5**, 330-344 (2017). https://doi.org:10.1158/2326-6066.Cir-16-0182

43 Agus, A., Clément, K. & Sokol, H. Gut microbiota-derived metabolites as central regulators in metabolic disorders. *Gut* **70**, 1174-1182 (2021). https://doi.org:10.1136/gutjnl-2020-323071

44 Schiering, C. *et al.* Feedback control of AHR signalling regulates intestinal immunity. *Nature* **542**, 242-245 (2017). https://doi.org:10.1038/nature21080

45 Xue, H. *et al.* Gut Microbially Produced Indole-3-Propionic Acid Inhibits Atherosclerosis by Promoting Reverse Cholesterol Transport and Its Deficiency Is Causally Related to Atherosclerotic Cardiovascular Disease. *Circ Res* **131**, 404-420 (2022). https://doi.org:10.1161/circresaha.122.321253

46 Bader, M. Inhibition of serotonin synthesis: A novel therapeutic paradigm. *Pharmacol Ther* **205**, 107423 (2020). https://doi.org:10.1016/j.pharmthera.2019.107423

47 Ghia, J. E. *et al.* Serotonin has a key role in pathogenesis of experimental colitis. *Gastroenterology* **137**, 1649-1660 (2009). https://doi.org:10.1053/j.gastro.2009.08.041

48 Sonnenberg, G. F. & Artis, D. Innate lymphoid cell interactions with microbiota: implications for intestinal health and disease. *Immunity* **37**, 601-610 (2012). https://doi.org:10.1016/j.immuni.2012.10.003

49 Berglund, E. D. *et al.* Glucose metabolism in vivo in four commonly used inbred mouse strains. *Diabetes* **57**, 1790-1799 (2008). https://doi.org:10.2337/db07-1615

50 Barnich, N. *et al.* Beneficial Effects of Natural Mineral Waters on Intestinal Inflammation and the Mucosa-Associated Microbiota. *Int J Mol Sci* **22** (2021). https://doi.org:10.3390/ijms22094336

51 Johansson, M. E. & Hansson, G. C. Preservation of mucus in histological sections, immunostaining of mucins in fixed tissue, and localization of bacteria with FISH. *Methods Mol Biol* **842**, 229-235 (2012). https://doi.org:10.1007/978-1-61779-513-8_13

52 Taleb, S. *et al.* Loss of SOCS3 expression in T cells reveals a regulatory role for interleukin-17 in atherosclerosis. *J Exp Med* **206**, 2067-2077 (2009). https://doi.org:jem.20090545 [pii]10.1084/jem.20090545

53 Mallat, Z. *et al.* Induction of a regulatory T cell type 1 response reduces the development of atherosclerosis in apolipoprotein E-knockout mice. *Circulation* **108**, 1232-1237 (2003).

54 Ferchaud-Roucher, V., Pouteau, E., Piloquet, H., Zair, Y. & Krempf, M. Colonic fermentation from lactulose inhibits lipolysis in overweight subjects. *American journal of physiology. Endocrinology and metabolism* **289**, E716-720 (2005). https://doi.org:10.1152/ajpendo.00430.2004

55 Maneglier, B. *et al.* Simultaneous measurement of kynurenine and tryptophan in human plasma and supernatants of cultured human cells by HPLC with coulometric detection. *Clin Chem* **50**, 2166-2168 (2004). https://doi.org:10.1373/clinchem.2004.037465
56 Sellick, C. A. *et al.* Evaluation of extraction processes for intracellular metabolite profiling of mammalian cells: matching extraction approaches to cell type and metabolite targets. *Metabolomics* **6**, 427-438 (2010). https://doi.org:10.1007/s11306-010-0216-9
57 Kim, E., Tran, M., Sun, Y. & Huh, J. R. Isolation and analyses of lamina propria lymphocytes from mouse intestines. *STAR Protoc* **3**, 101366 (2022). https://doi.org:10.1016/j.xpro.2022.101366
58 Bolyen, E. *et al.* Reproducible, interactive, scalable and extensible microbiome data science using QIIME 2. *Nat Biotechnol* **37**, 852-857 (2019). https://doi.org:10.1038/s41587-019-0209-9
59 Callahan, B., Proctor, D., Relman, D., Fukuyama, J. & Holmes, S. Reproducible Research Workflow in R for the Analysis of Personalized Human Microbiome Data. *Pacific Symposium on Biocomputing. Pacific Symposium on Biocomputing* **21**, 183-194 (2016).
60 Quast, C. *et al.* The SILVA ribosomal RNA gene database project: improved data processing and web-based tools. *Nucleic Acids Res* **41**, D590-596 (2013). https://doi.org:10.1093/nar/gks1219
61 McMurdie, P. J. & Holmes, S. phyloseq: an R package for reproducible interactive analysis and graphics of microbiome census data. *PLoS One* **8**, e61217 (2013). https://doi.org:10.1371/journal.pone.0061217
62 Kassambara, A. *rstatix: Pipe-friendly framework for basic statistical tests. R package version 0.7. 0*, <https://rpkgs.datanovia.com/rstatix/> (2021).
63 Wickham H (2007) Reshaping data with the reshape package. J Stat Soft 21(12). http://www.jstatsoft.org/v21/i12/paper.
64 Oksanen, J. vegan: Community Ecology Package. R Package Version 2.4-5. (2017).

Acknowledgements

This work was supported by Inserm, Agence Nationale de la Recherche (ANR-22CE14-0014-01 to S.T.), Fondation pour la Recherche Médicale (FRM) (to H.A.O. and S.T.), Federation Française de Cardiologie (FFC) (to S.T.), and Fondation De France (FDF) (to S.T.). S.T. received an award from FRM/Institut Danone. N. M. and M.C. are the recipients of a scholarship from FDF for their thesis. M.C. is the recipient of a scholarship from Nouvelle Societé Française d'Athérosclerose (NSFA) for the 4th year of her thesis. T.R. received a scholarship from DFG (Walter Benjamin program). We thank members of our animal and histology Facilities. We are thankful to the Genomics Platform of Translational Research Department, Institut Curie, PSL Research University for sharing their expertise and helping us with Nanostring analyse.

Author contributions statement

M.C. was involved in experimental design, conducted most experiments and analyzed data. L.L., T.R., N.M., R.A.R., E.B., N. S., M.V., and B.E helped in some experiments. J.V. provided some technical helps. C.F. discussed estrogen effects. J.D., J-M.L., and J.C. measured Trp and Trp-derived metabolites. C. K. performed cell sorting**.** A.T., and H.A.O. discussed results. M.B. and H.S. performed and interpreted gut microbiota analysis, and discussed results. C.D., H.R., B.C. performed histological scoring, FISH experiments, and helped in some experiments, interpreted and discussed the results. S.T. designed the study, analyzed and interpreted the data, and wrote the manuscript.

Competing interest statement

The authors declare no competing interests.

Figure Legends

Figure 1: Induction of IEC IDO by HFD has a protective role in atherosclerosis. A. Tryptophan (Trp), Kynurenine (Kyn) levels, and related Kyn/Trp ratio (%) in the small intestine extracts (n=5 mice/group), **B.** plasma indole levels in the portal vein, **C.** 5-hydroxytryptamine (5-HT) in the small intestine extracts of male *Ldlr*$^{-/-}$ mice fed either normal chow diet (NCD), high-fat diet (HFD), or high-cholesterol diet (HCD) or the combination of both HFD+HCD for 13 weeks (n=5 mice/group). **D.** Kyn levels in feces of *Ldlr*$^{-/-}$ mice fed HFD supplemented or not with FOS for 13 weeks (n=5 mice/group). **E-F.** Kyn/Trp ratio (%) in the small intestine extracts and plasma in male *Ldlr*$^{-/-}$ IEC IDO KO and littermate control *Ldlr*$^{-/-}$ IEC IDO mice (n=5 mice/group), after 8 weeks of HFD+HCD or NCD feeding period. NCD represents the control group without atherosclerosis development. **G.** Plasma cholesterol, **H.** representative pictures, and quantifications of plaque size in the aortic sinus in male *Ldlr*$^{-/-}$ IEC IDO KO (n=12 mice) and littermate control *Ldlr*$^{-/-}$ IEC IDO (n=12 mice) fed HFD+HCD for 8 weeks; scale bar 200µm. **I.** Plasma cholesterol, **J.** representative pictures and quantifications of plaque size in the aortic sinus in female *Ldlr*$^{-/-}$ IEC IDO KO (n=9 mice), and littermate controls *Ldlr*$^{-/-}$ IEC IDO (n=9 mice) fed HFD+HCD for 13 weeks; scale bar 200µm. Individual data are presented as scattered dot plots, with the mean and s.e.m. The p values were determined using Brown-Forsythe one-way ANOVA test followed by Tukey's multiple comparison test. Source data are provided as a Source Data file.

Figure 2: Deficiency of IDO in intestinal epithelial cells (IECs) increases intestinal and plaque inflammation. A. fecal lipocalin 2 (Lcn2) levels scoring in male *Ldlr*$^{-/-}$ IEC IDO KO (n=10 mice) and littermate control *Ldlr*$^{-/-}$ IEC IDO (n=9 mice). **B.** colon pathohistological scoring in male *Ldlr*$^{-/-}$ IEC IDO KO and littermate control *Ldlr*$^{-/-}$ IEC IDO mice (n=10 mice/group), after 8 weeks of high-fat and high-cholesterol diet (HFD+HCD) feeding period; scale bar 100µm. **C.** Representative confocal microscopy pictures of microbiota localization: Mucin 2 (green), actin (purple), bacteria (red), and nuclei (blue) and quantifications of mean distances of the closest bacteria (in red) to colonic IEC per condition over three high-powered fields per mouse (IEC IDO n=10 mice, IEC IDOKO n=7 mice); scale bar 100µm. **D.** data were acquired by flow cytometry for Uniform Manifold Approximation and Projection (UMAP) of lymphocytes in the lamina propria of the small intestines. **E.** plasma anti-LPS IgG by ELISA, arbitrary units (arb. units). The results are from male *Ldlr*$^{-/-}$ IEC IDO KO (n=11 mice) and littermate control *Ldlr*$^{-/-}$ IEC IDO mice (n=13 mice) fed HFD+HCD for 8 weeks. **F.** Detection by ELISA of FITC-dextran in serum of female *Ldlr*$^{-/-}$ IEC IDO KO (n=8 mice) and littermate control *Ldlr*$^{-/-}$ IEC IDO (n=9 mice) fed HFD+HCD for 13 weeks. **G.** Representative photomicrographs and quantitative analysis of lesional T cells (CD3+ in red) accumulation in the aortic sinus of male *Ldlr*$^{-/-}$ IEC IDO KO (n=9 mice) and littermate control *Ldlr*$^{-/-}$ IEC IDO (n=10 mice), after 8 weeks of HFD+HCD feeding period; scale bar 100µm. **H.** plasma cholesterol, **I.** representative pictures, and quantifications of plaque size in the aortic sinus in male *Ldlr*$^{-/-}$*Rag1*$^{-/-}$ IEC IDO KO (n=9 mice) and littermate control *Ldlr*$^{-/-}$*Rag1*$^{-/-}$ IEC IDO (n=11 mice) fed HFD+HCD for 8 weeks; scale bar 200µm. Individual data are presented as scattered dot plots,

with the mean and s.e.m. The p values were determined using the two-tailed Mann-Whitney test. Source data are provided as a Source Data file.

Figure 3: Intestinal 5-hydroxytryptamine (5-HT) exhibits pro-inflammatory and pro-atherogenic effects. A. 5-HT levels in small intestine extracts (n=5 mice/group), **B.** plaque quantification in the aortic sinus and representative images of male *Ldlr*$^{-/-}$ treated with Tryptophan Hydroxylase 1 (TPH1) inhibitor (LP533401, n=6 mice) or vehicle (n=8 mice) and fed HFD+HCD for 8 weeks; scale bar 200µm. **C-D.** representative images and quantifications of macrophages (MOMA-2+ in red) and lymphocytes (CD3+ in red) accumulation in the aortic sinus (*Ldlr*$^{-/-}$ Vehicle n=8, *Ldlr*$^{-/-}$ LP533401 n=6); scale bar 100µm. **E.** representative pictures and quantifications of plaque size in the aortic sinus male *Ldlr*$^{-/-}$ IEC IDO KO and littermate control *Ldlr*$^{-/-}$ IEC IDO mice treated with either LP533401 or vehicle and fed HFD+HCD for 8 weeks (IEC IDO Vehicle n=11 mice, IEC IDO KO Vehicle n=7 mice, IEC IDO LP533401 n=11 mice, IEC IDO KO LP533401 n=9 mice); scale bar 200µm. **F.** Colon pathohistological scoring (IEC IDO Vehicle n=5 mice, IEC IDO KO Vehicle n=10 mice, IEC IDO LP533401 n=5 mice, IEC IDO KO LP533401 n=10 mice). **G.** lipocalin-2 (Lcn2) levels in feces (IEC IDO Vehicle n=5 mice, IEC IDO KO Vehicle n=7 mice, IEC IDO LP533401 n=5 mice, IEC IDO KO LP533401 n=10 mice). Individual data are presented as scattered dot plots, with the mean and s.e.m. The p values were determined using the two-tailed Mann-Whitney test for A-D, Kruskal-Wallis, followed by post-Hoc Dunn's test for F, and one-way ANOVA test followed by Tukey's multiple comparison test for E and G. Source data are provided as a Source Data file.

Figure 4: Trp-dependent microbiota effects impact atherosclerosis. A. Plasma cholesterol, **B.** representative pictures and quantifications of plaques in the aortic sinus of male *Ldlr*$^{-/-}$ IEC IDO KO and littermate control *Ldlr*$^{-/-}$ IEC IDO mice treated with antibiotics (ATB) during the 8 weeks of high-fat and high-cholesterol diet (HFD+HCD) feeding period (IEC IDO ATB n=12 mice, IEC IDO KO ATB n=11 mice); scale bar 200µm. **C.** plaque quantification in the aortic sinus of male *Ldlr*$^{-/-}$ IEC IDO KO and littermate control *Ldlr*$^{-/-}$ IEC IDO mice either separated by the genotype or mixed (co-housing) in the same cages from the weaning. The mice were fed HFD+HCD for 8 weeks (IEC IDO n=8 mice, IEC IDO KO n=7 mice, IEC IDO co-housing n=8 mice, and IEC IDO KO co-housing n=8 mice). **D.** colon pathohistological scoring; scale bar 100µm, **E.** plasma cholesterol levels, **F.** representative pictures and quantifications of plaque size in the aortic sinus; scale bar 200µm, **G.** representative pictures and quantifications of lymphocytes (CD3+ in red) accumulation within plaques in the aortic sinus of male *Ldlr*$^{-/-}$mice treated with 6-Formylindolo(3,2-b)carbazole (Ficz) or vehicle; scale bar 100µm (n=8 mice/group) during the 8 weeks of HCD feeding period. Individual data are presented as scattered dot plots, with the mean and s.e.m. The p values were determined using the two-tailed Mann-Whitney test. Source data are provided as a Source Data file.

Figure 5: Indole derivatives alleviate inflammation and atherosclerosis. A. indole derivatives (sum of IAA, IPA, and tryptamine) levels supplemented or not in female *Ldlr*$^{-/-}$ mice fed a high-cholesterol diet (HCD) for 8 weeks (n=10 mice/group). **B.** data were acquired by flow cytometry for Uniform Manifold Approximation and Projection (UMAP) of leukocytes in the lamina propria of small intestines. Unbiased multi-dimensional analysis by X-shift revealed several different clusters. **C**. plasma cholesterol levels, **D.** representative pictures and plaque size quantification in the aortic sinus; scale bar 200µm, **E.** representative images and lipid quantification with en-face staining in the thoracic aorta (n=10 mice/group); scale bar 2mm, **F.** representative photomicrographs and quantitative analysis of lesional macrophages (MOMA2+ in red) accumulation in the aortic sinus of female *Ldlr*$^{-/-}$ mice fed HCD for 8 weeks (*Ldlr*$^{-/-}$ Vehicle n=9 mice, *Ldlr*$^{-/-}$ Indole n=10 mice) ; scale bar 100µm. Individual data are presented as scattered dot plots, with the mean and s.e.m. The p values were determined using the two-tailed Mann-Whitney test. Source data are provided as a Source Data file.

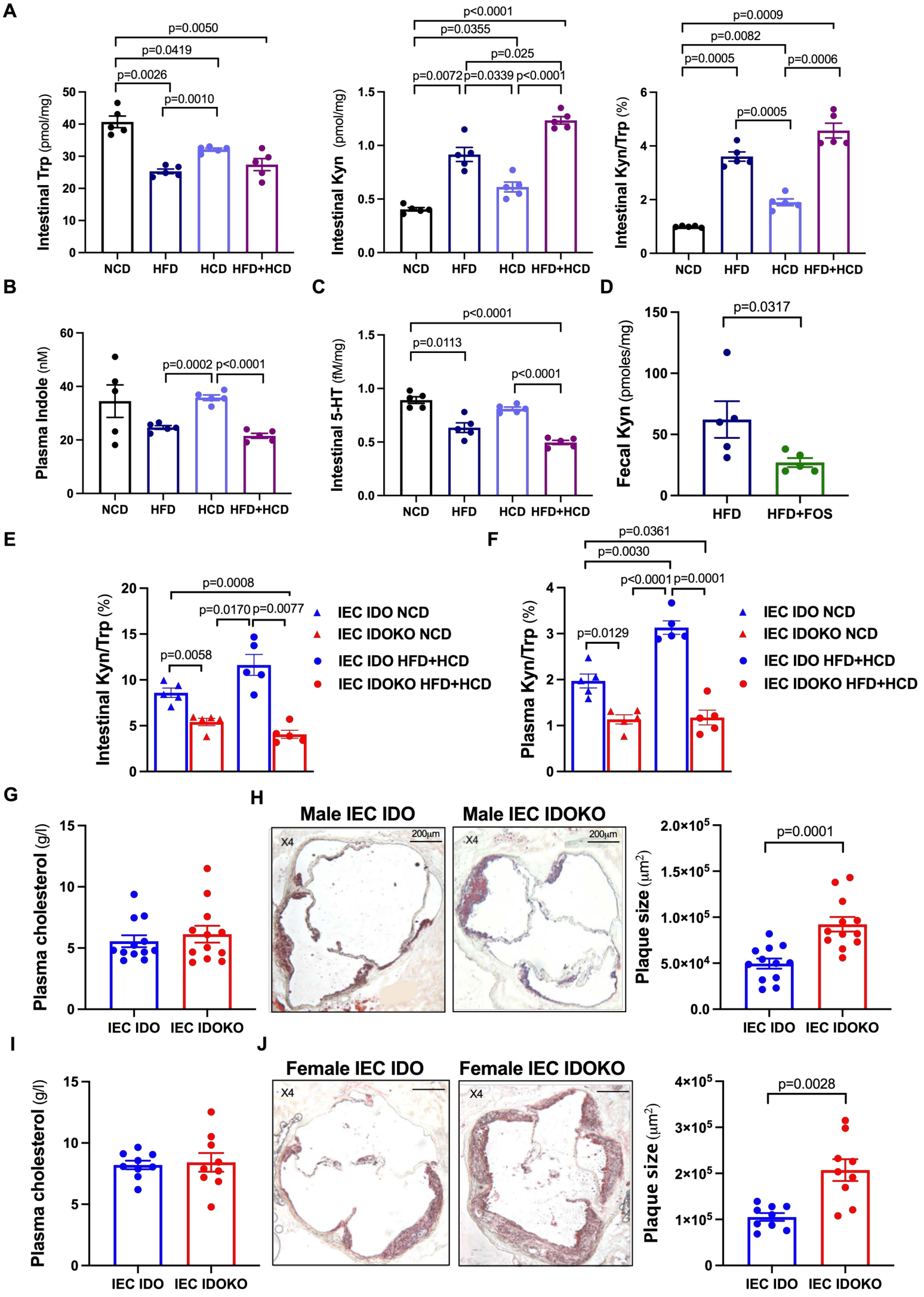
A
Intestinal Trp (pmol/mg)
p=0.0050
p=0.0419
p=0.0026
p=0.0010
NCD HFD HCD HFD+HCD
Intestinal Kyn (pmol/mg)
p<0.0001
p=0.0355
p=0.025
p=0.0072 p=0.0339 p<0.0001
Intestinal Kyn/Trp (%)
p=0.0009
p=0.0082
p=0.0005
p=0.0006
p=0.0005
B
Plasma Indole (nM)
p=0.0002 p<0.0001
C
Intestinal 5-HT (fM/mg)
p<0.0001
p=0.0113
p<0.0001
D
Fecal Kyn (pmoles/mg)
p=0.0317
HFD HFD+FOS
E
Intestinal Kyn/Trp (%)
p=0.0008
p=0.0170 p=0.0077
p=0.0058
IEC IDO NCD
IEC IDOKO NCD
IEC IDO HFD+HCD
IEC IDOKO HFD+HCD
F
Plasma Kyn/Trp (%)
p=0.0361
p=0.0030
p<0.0001 p=0.0001
p=0.0129
G
Plasma cholesterol (g/l)
IEC IDO IEC IDOKO
H
Male IEC IDO
Male IEC IDOKO
X4
200µm
Plaque size (µm²)
p=0.0001
I
Plasma cholesterol (g/l)
IEC IDO IEC IDOKO
J
Female IEC IDO
Female IEC IDOKO
X4
Plaque size (µm²)
p=0.0028

Figure 1

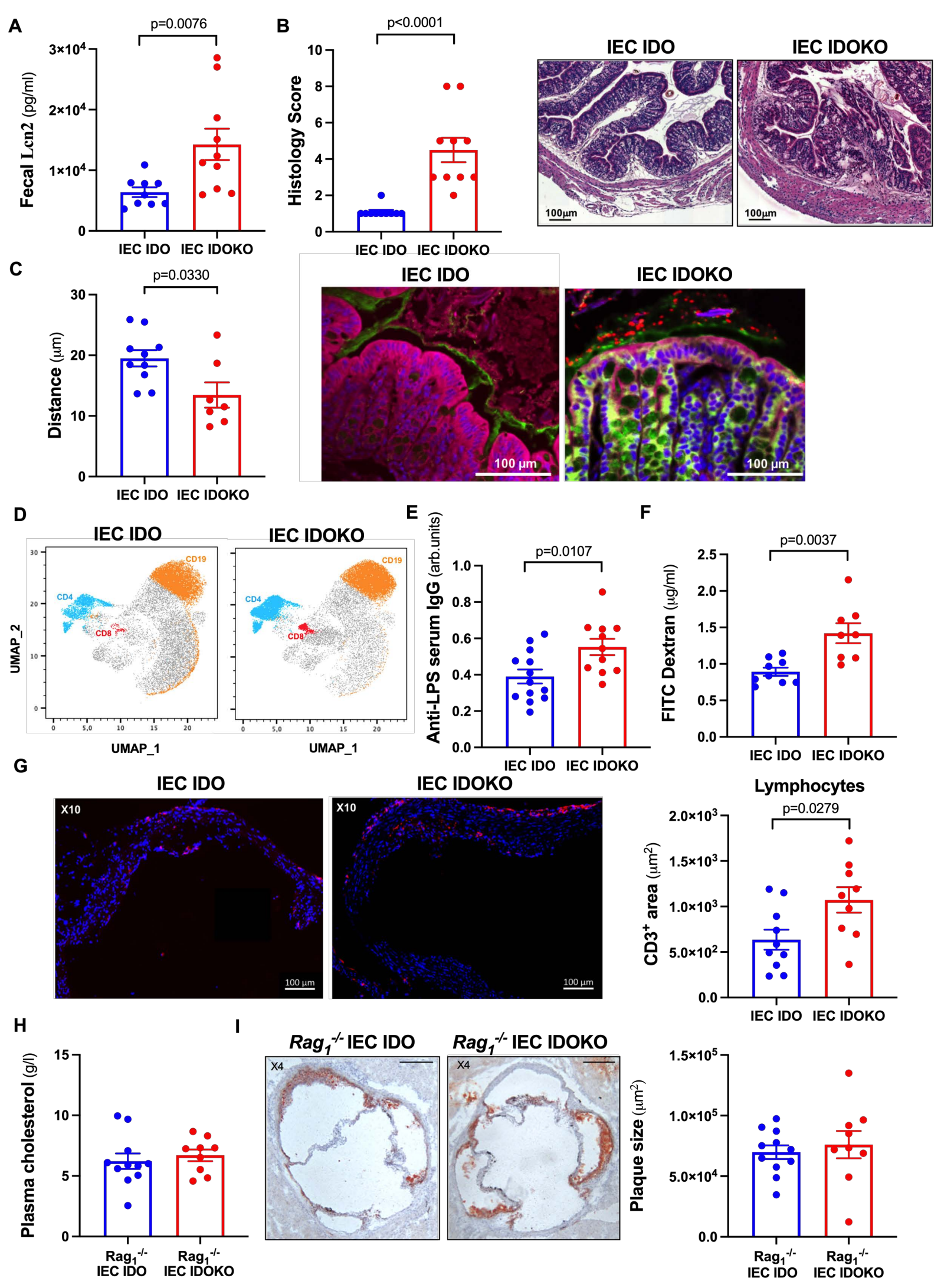
A
p=0.0076
Fecal Lcn2 (pg/ml)
3×10^4
2×10^4
1×10^4
0
IEC IDO
IEC IDOKO
B
p<0.0001
Histology Score
10
8
6
4
2
0
IEC IDO
IEC IDOKO
IEC IDO
IEC IDOKO
100µm
100µm
C
p=0.0330
Distance (µm)
30
20
10
0
IEC IDO
IEC IDOKO
IEC IDO
IEC IDOKO
100 µm
100 µm
D
IEC IDO
IEC IDOKO
CD19
CD4
CD8
UMAP_2
UMAP_1
UMAP_1
E
p=0.0107
Anti-LPS serum IgG (arb.units)
1.0
0.8
0.6
0.4
0.2
0.0
IEC IDO
IEC IDOKO
F
p=0.0037
FITC Dextran (µg/ml)
2.5
2.0
1.5
1.0
0.5
0.0
IEC IDO
IEC IDOKO
G
IEC IDO
IEC IDOKO
X10
X10
100 µm
100 µm
Lymphocytes
p=0.0279
CD3+ area (µm2)
2.0×10^3
1.5×10^3
1.0×10^3
5.0×10^2
0.0
IEC IDO
IEC IDOKO
H
Plasma cholesterol (g/l)
15
10
5
0
Rag1-/- IEC IDO
Rag1-/- IEC IDOKO
I
Rag1-/- IEC IDO
Rag1-/- IEC IDOKO
X4
X4
Plaque size (µm2)
1.5×10^5
1.0×10^5
5.0×10^4
0.0
Rag1-/- IEC IDO
Rag1-/- IEC IDOKO

Figure 2

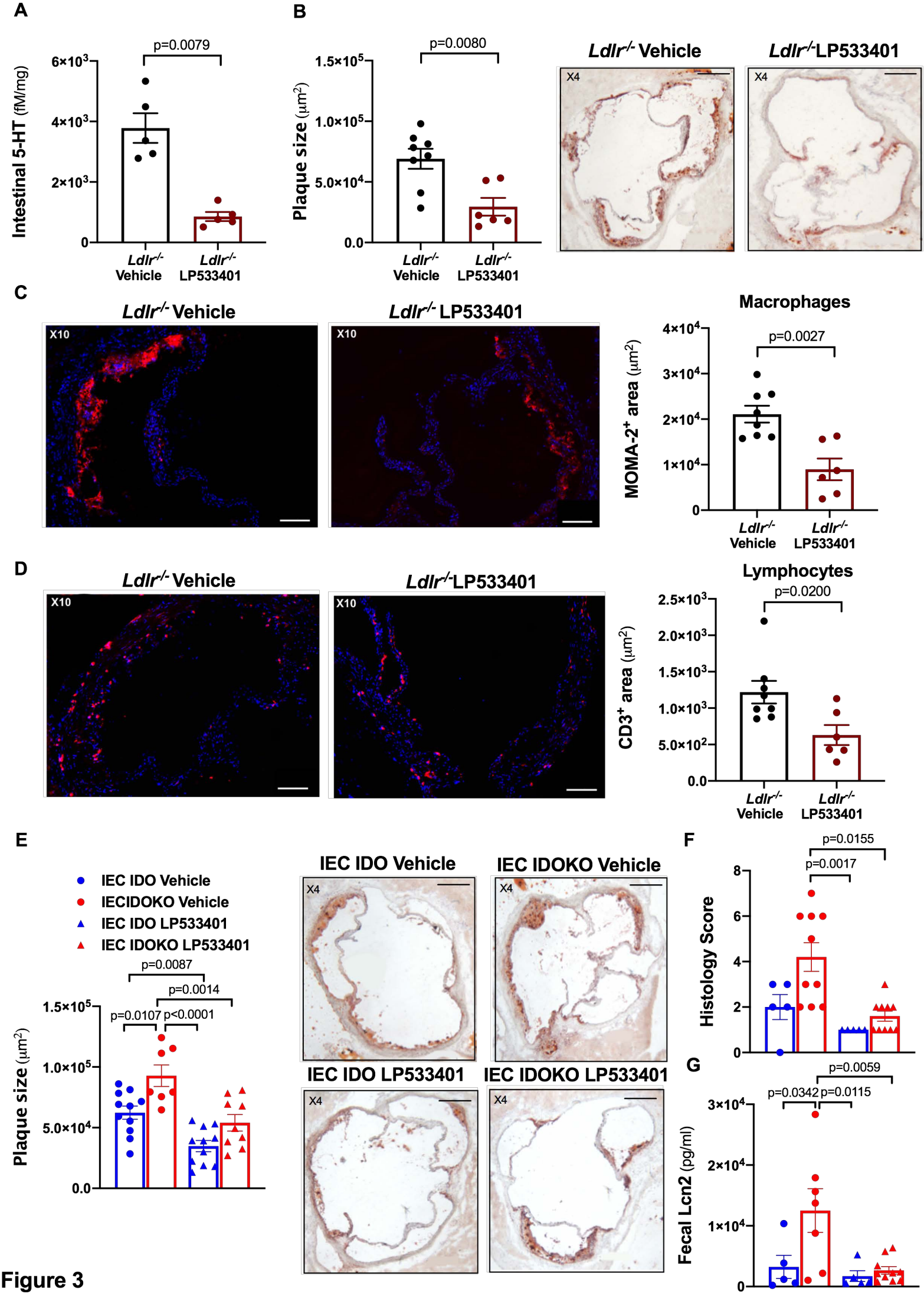
A
Intestinal 5-HT (fM/mg)
p=0.0079
6×10^3
4×10^3
2×10^3
0
Ldlr-/- Vehicle
Ldlr-/- LP533401
B
Plaque size (µm2)
p=0.0080
1.5×10^5
1.0×10^5
5.0×10^4
0.0
Ldlr-/- Vehicle
Ldlr-/- LP533401
Ldlr-/- Vehicle
Ldlr-/-LP533401
X4
C
Ldlr-/- Vehicle
Ldlr-/- LP533401
X10
Macrophages
MOMA-2+ area (µm2)
p=0.0027
4×10^4
3×10^4
2×10^4
1×10^4
0
D
Ldlr-/- Vehicle
Ldlr-/-LP533401
X10
Lymphocytes
CD3+ area (µm2)
p=0.0200
2.5×10^3
2.0×10^3
1.5×10^3
1.0×10^3
5.0×10^2
0.0
E
IEC IDO Vehicle
IECIDOKO Vehicle
IEC IDO LP533401
IEC IDOKO LP533401
p=0.0087
p=0.0014
p=0.0107
p<0.0001
Plaque size (µm2)
1.5×10^5
1.0×10^5
5.0×10^4
0.0
IEC IDO Vehicle
IEC IDOKO Vehicle
IEC IDO LP533401
IEC IDOKO LP533401
X4
F
Histology Score
p=0.0155
p=0.0017
8
6
4
2
0
G
Fecal Lcn2 (pg/ml)
p=0.0059
p=0.0342
p=0.0115
3×10^4
2×10^4
1×10^4
0

Figure 3

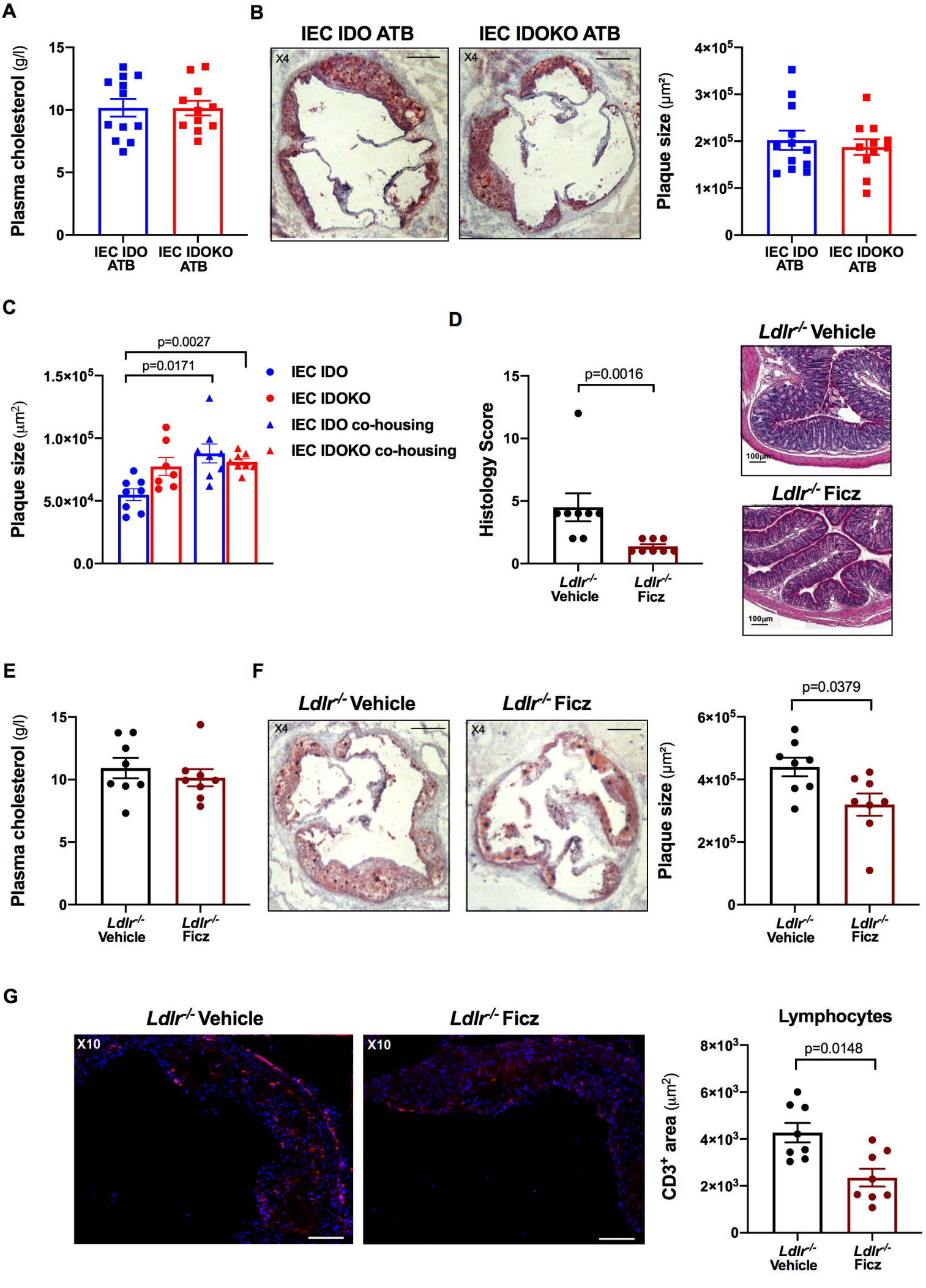
A
Plasma cholesterol (g/l)
15
10
5
0
IEC IDO ATB
IEC IDOKO ATB
B
IEC IDO ATB
IEC IDOKO ATB
X4
X4
Plaque size (µm²)
4×10⁵
3×10⁵
2×10⁵
1×10⁵
0
IEC IDO ATB
IEC IDOKO ATB
C
Plaque size (µm²)
1.5×10⁵
1.0×10⁵
5.0×10⁴
0.0
p=0.0027
p=0.0171
IEC IDO
IEC IDOKO
IEC IDO co-housing
IEC IDOKO co-housing
D
Histology Score
15
10
5
0
p=0.0016
Ldlr-/- Vehicle
Ldlr-/- Ficz
Ldlr-/- Vehicle
100µm
Ldlr-/- Ficz
100µm
E
Plasma cholesterol (g/l)
15
10
5
0
Ldlr-/- Vehicle
Ldlr-/- Ficz
F
Ldlr-/- Vehicle
Ldlr-/- Ficz
X4
X4
Plaque size (µm²)
6×10⁵
4×10⁵
2×10⁵
0
p=0.0379
Ldlr-/- Vehicle
Ldlr-/- Ficz
G
Ldlr-/- Vehicle
Ldlr-/- Ficz
X10
X10
Lymphocytes
CD3+ area (µm²)
8×10³
6×10³
4×10³
2×10³
0
p=0.0148
Ldlr-/- Vehicle
Ldlr-/- Ficz

Figure 4

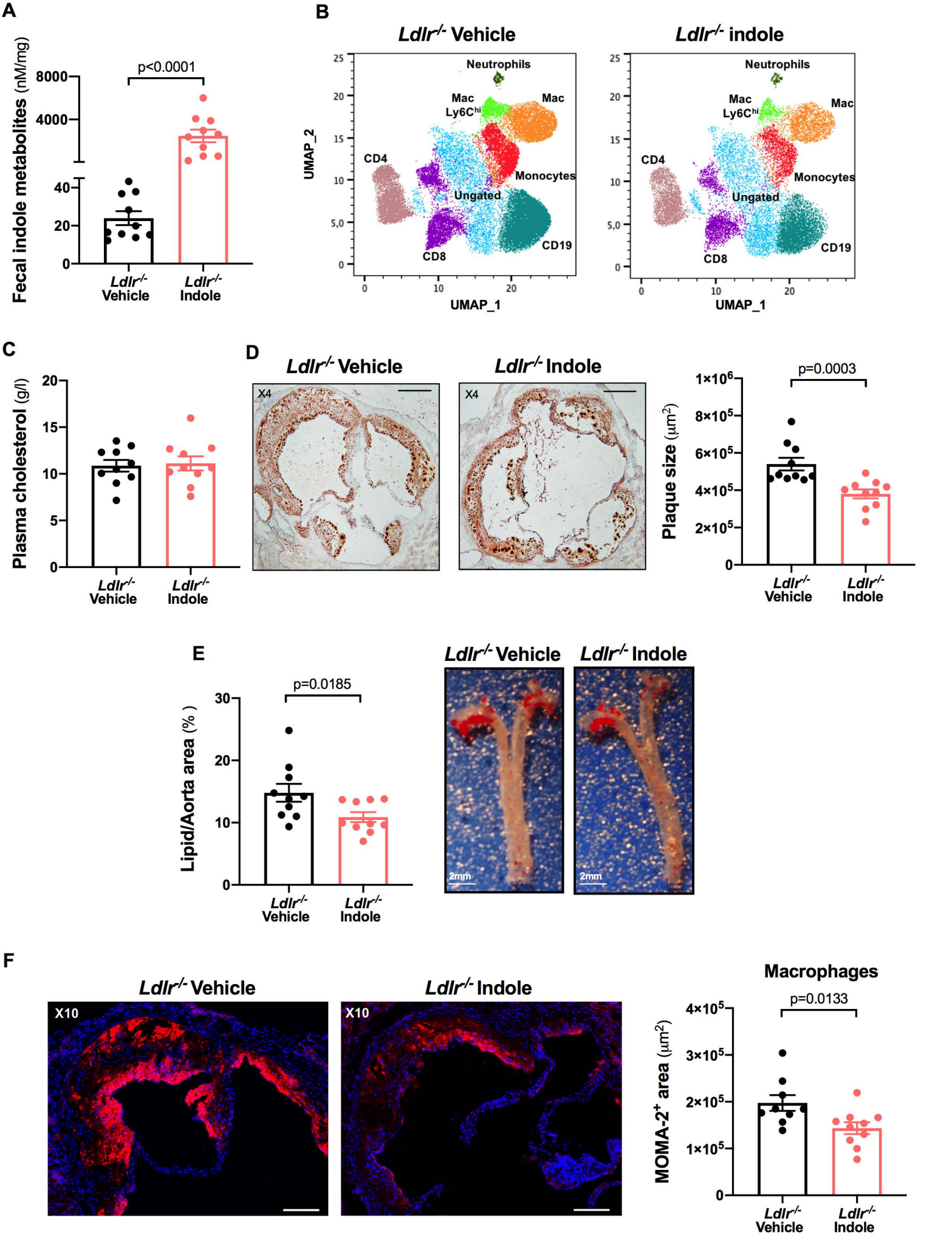
A
Fecal indole metabolites (nM/mg)
p<0.0001
8000
4000
40
20
0
Ldlr-/- Vehicle
Ldlr-/- Indole
B
Ldlr-/- Vehicle
Ldlr-/- indole
Neutrophils
Mac Ly6Chi
Mac
CD4
Monocytes
Ungated
CD8
CD19
UMAP_2
UMAP_1
C
Plasma cholesterol (g/l)
D
Ldlr-/- Vehicle
Ldlr-/- Indole
X4
Plaque size (µm2)
p=0.0003
E
Lipid/Aorta area (%)
p=0.0185
2mm
F
Ldlr-/- Vehicle
Ldlr-/- Indole
X10
Macrophages
MOMA-2+ area (µm2)
p=0.0133

Figure 5

Supplementary Information file

Harnessing intestinal tryptophan catabolism to relieve atherosclerosis in mice

Chajadine *et al.*

Test Date	Species	Submitter	Area	Profile
24 Aug 2023	Mouse	Inserm U970-PARCC	Zone 1-82 T16288	375M

Viruses	Test Methods	Latest Result
Ectromelia virus	Bead	0/1
Lymphocytic choriomeningitis virus	Bead	0/1
Minute virus of mice	Bead	0/1
Mouse adenovirus type 1 (MAd FL)	Bead	0/1
Mouse adenovirus type 2 (MAd K87)	Bead	0/1
Mouse hepatitis virus	Bead	0/1
Mouse norovirus	Bead	0/1
Mouse parvovirus	Bead	0/1
Mouse rotavirus (EDIM)	Bead	0/1
Pneumonia virus of mice	Bead	0/1
Reovirus type 3 (Reo 3)	Bead	0/1
Sendai Virus	Bead	0/1
Theiler's murine encephalomyelitis virus	Bead	0/1
Bacteria, Mycoplasma and Fungi	**Test Methods**	**Latest Result**
Streptobacillus moniliformis	qPCR	0/1
Helicobacter	qPCR	0/1
Citrobacter rodentium	Culture	0/1
Corynebacterium kutscheri	Culture	0/1
Pasteurella pneumotropica	Culture	0/1
Salmonella spp	Culture	0/1
Streptococci Beta-haemolytic (not group D)	Culture	0/1
Streptococcus pneumoniae	Culture	0/1
Clostridium piliforme	Bead	0/1
Mycoplasma pulmonis	Bead	0/1
Parasites	**Test Methods**	**Latest Result**
Ectoparasites	Microscopy	0/1
Endoparasites	Microscopy	0/1
Pathological Lesions	**Test Methods**	**Latest Result**
Pathological Lesions	Necropsy	0/1

Supplementary Table 1: health certificate

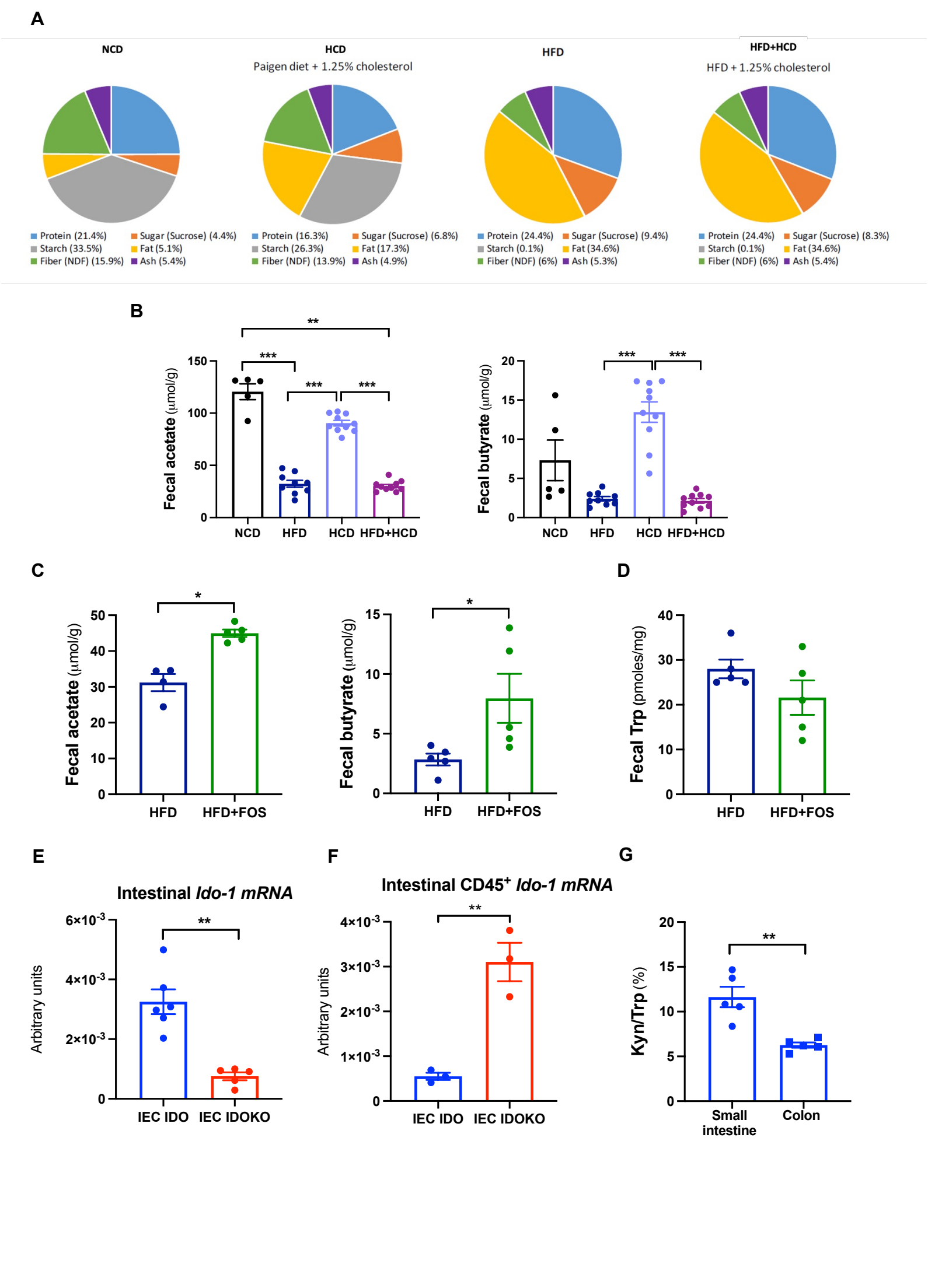
A
NCD
Protein (21.4%)
Sugar (Sucrose) (4.4%)
Starch (33.5%)
Fat (5.1%)
Fiber (NDF) (15.9%)
Ash (5.4%)
HCD
Paigen diet + 1.25% cholesterol
Protein (16.3%)
Sugar (Sucrose) (6.8%)
Starch (26.3%)
Fat (17.3%)
Fiber (NDF) (13.9%)
Ash (4.9%)
HFD
Protein (24.4%)
Sugar (Sucrose) (9.4%)
Starch (0.1%)
Fat (34.6%)
Fiber (NDF) (6%)
Ash (5.3%)
HFD+HCD
HFD + 1.25% cholesterol
Protein (24.4%)
Sugar (Sucrose) (8.3%)
Starch (0.1%)
Fat (34.6%)
Fiber (NDF) (6%)
Ash (5.4%)
B
Fecal acetate (µmol/g)
Fecal butyrate (µmol/g)
NCD
HFD
HCD
HFD+HCD
C
Fecal acetate (µmol/g)
Fecal butyrate (µmol/g)
HFD
HFD+FOS
D
Fecal Trp (pmoles/mg)
E
Intestinal Ido-1 mRNA
Arbitrary units
IEC IDO
IEC IDOKO
F
Intestinal CD45+ Ido-1 mRNA
G
Kyn/Trp (%)
Small intestine
Colon

Supplementary Fig. 1: effects of diet on SCFAs and Trp metabolites. A. diet composition, **B.** acetate and butyrate levels in feces from male *Ldlr*$^{-/-}$ mice fed either normal chow diet (NCD) (n=5 mice), high-fat diet (HFD) (n=9 mice), or high-cholesterol diet (HCD) (n=10 mice) or the combination of both HFD+HCD (n=10 mice) for 13 weeks, **C**. short chain fatty acid (SCFA), acetate and butyrate, **D.** Trp levels in feces from *Ldlr*$^{-/-}$ mice fed HFD for 13 weeks supplemented or not with fructooligosaccharide (FOS) (n=5 mice/group). **E.** *Ido-1 mRNA* in the small intestines of male *Ldlr*$^{-/-}$ IEC IDO KO mice and littermate control *Ldlr*$^{-/-}$ IEC IDO mice fed HFD+HCD for 8 weeks (IEC IDO n=6 mice, IEC IDOKO n=5 mice). **F.** *Ido-1 mRNA* in CD45+ FACS-sorted cells from digested small intestines of male *Ldlr*$^{-/-}$ IEC IDO KO mice and littermate control *Ldlr*$^{-/-}$ IEC IDO mice fed HFD+HCD for 8 weeks (n=3 mice/group, pools of n=7-9 mice independent samples/group). **G**. Kyn/Trp % in the small intestine and colon extracts of *Ldlr*$^{-/-}$ mice at baseline (n=5 mice/group). Individual data are presented as scattered dot plots, with the mean and s.e.m. The p values were determined using Brown-Forsythe ANOVA test followed by Tukey's multiple comparison test for A, the two-tailed Mann-Whitney test for B, C, and two-tailed Unpaired T test for E. Source data are provided as a Source Data file.

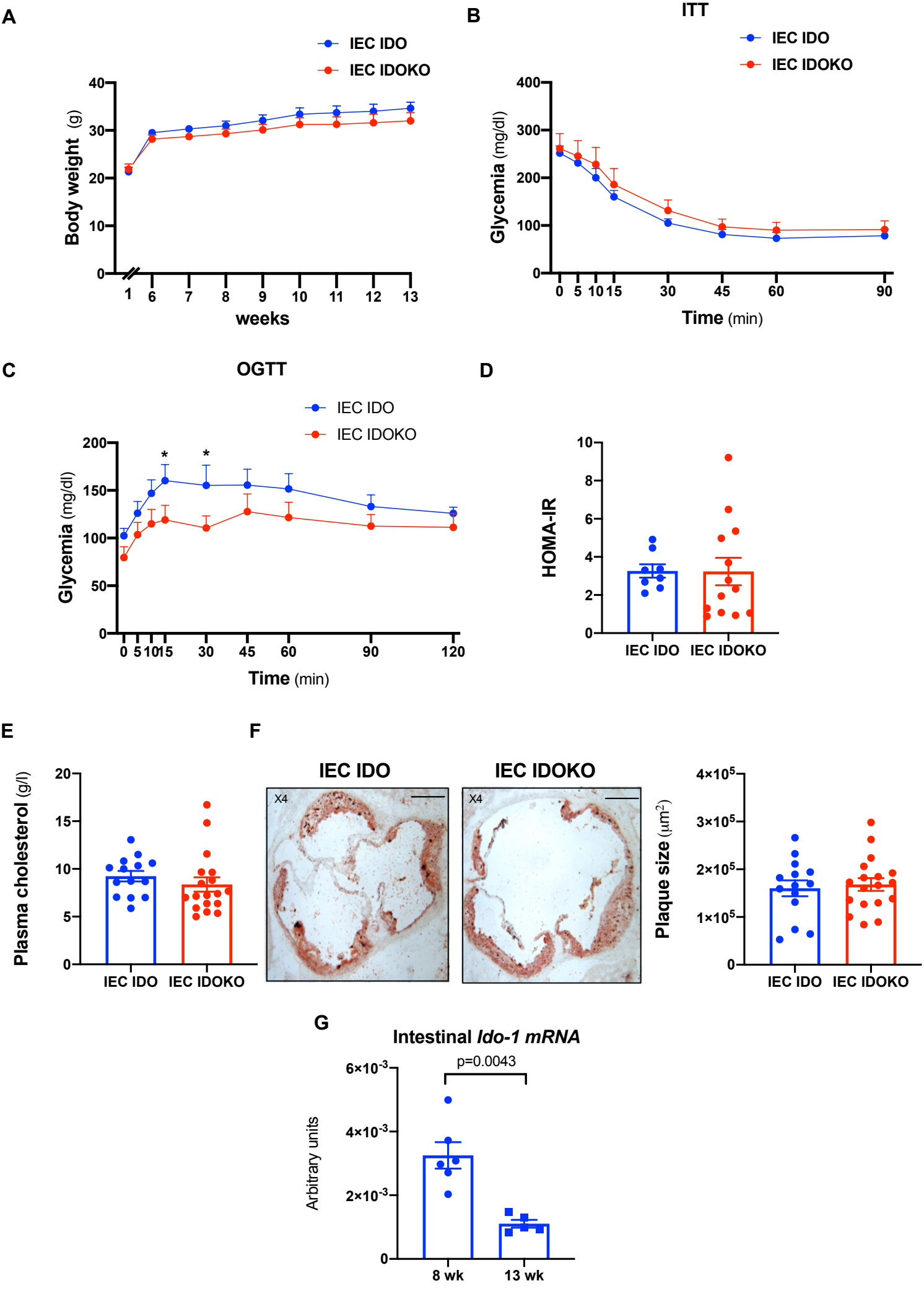
A
IEC IDO
IEC IDOKO
Body weight (g)
weeks
B
ITT
IEC IDO
IEC IDOKO
Glycemia (mg/dl)
Time (min)
C
OGTT
IEC IDO
IEC IDOKO
Glycemia (mg/dl)
Time (min)
D
HOMA-IR
IEC IDO
IEC IDOKO
E
Plasma cholesterol (g/l)
IEC IDO
IEC IDOKO
F
IEC IDO
IEC IDOKO
X4
X4
Plaque size (µm²)
IEC IDO
IEC IDOKO
G
Intestinal Ido-1 mRNA
p=0.0043
Arbitrary units
8 wk
13 wk

Supplementary Fig. 2: effects of intestinal IDO deletion on metabolic parameters and atherosclerosis. A. weight curves, **B.** ITT, **C.** OGTT, and **D.** HOMA-IR in male *Ldlr*$^{-/-}$ IEC IDO KO, and littermate control *Ldlr*$^{-/-}$ IEC IDO mice fed HFD+HCD for 13 weeks (IEC IDO n=8 mice, IEC IDOKO n=13 mice). **E.** plasma cholesterol, **F.** representative pictures and quantifications of plaque size in the aortic sinus of male *Ldlr*$^{-/-}$ IEC IDO KO, and littermate control *Ldlr*$^{-/-}$ IEC IDO mice fed HFD+HCD for 13 weeks (IEC IDO n=14 mice, IEC IDOKO n=18 mice); scale bar 200µm. **G.** *Ido-1 mRNA* in the small intestines of male *Ldlr*$^{-/-}$ mice fed HFD+HCD for 8 or 13 weeks (wk) (8wk n=6 mice, 13wk n=5 mice). Individual data are presented as scattered dot plots, with the mean and s.e.m. The p values were determined using the two-tailed Mann-Whitney test. Source data are provided as a Source Data file.

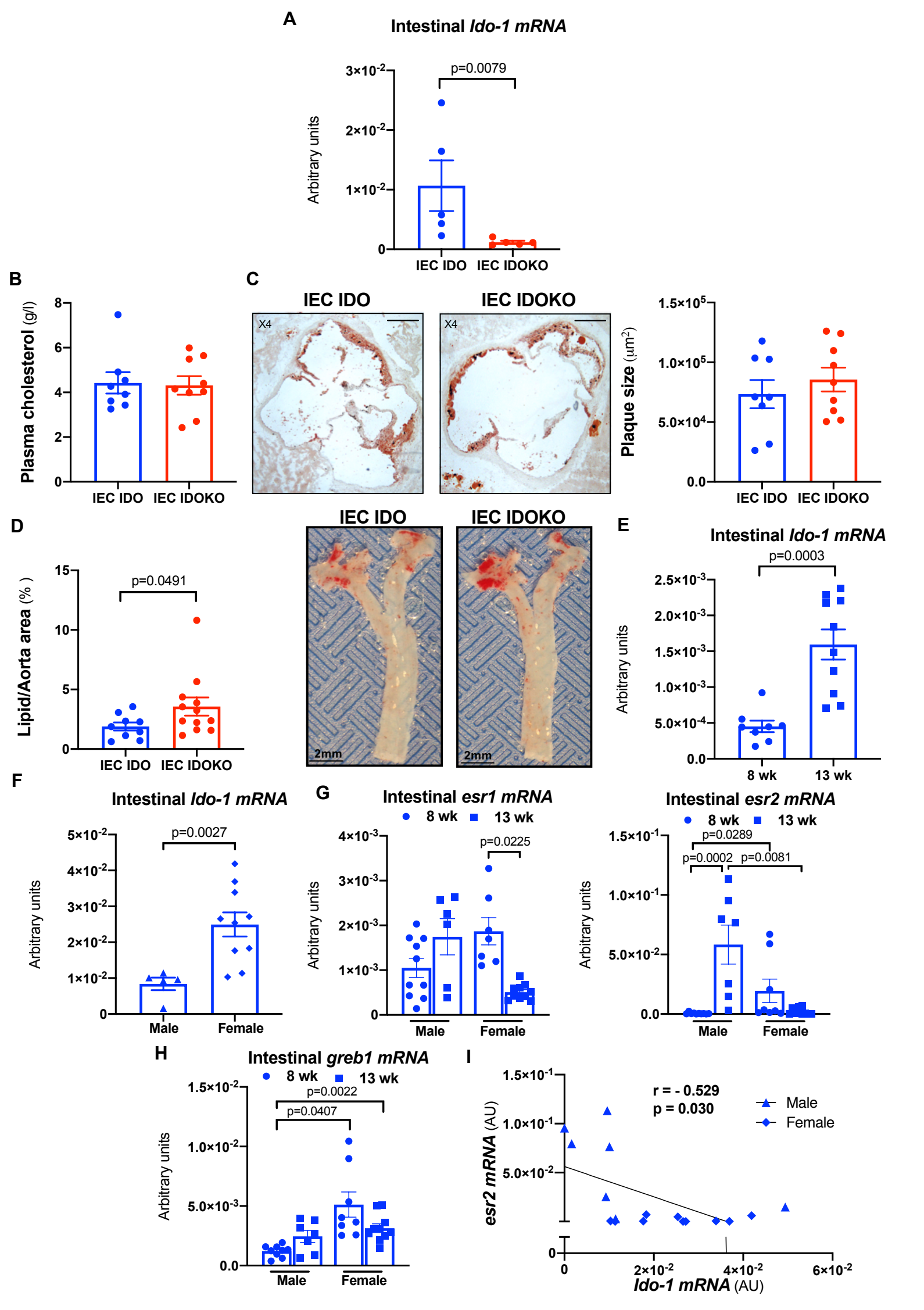
A
Intestinal Ido-1 mRNA
p=0.0079
Arbitrary units
IEC IDO
IEC IDOKO
B
Plasma cholesterol (g/l)
IEC IDO
IEC IDOKO
C
IEC IDO
IEC IDOKO
X4
Plaque size (µm²)
D
Lipid/Aorta area (%)
p=0.0491
2mm
E
Intestinal Ido-1 mRNA
p=0.0003
8 wk
13 wk
F
Intestinal Ido-1 mRNA
p=0.0027
Male
Female
G
Intestinal esr1 mRNA
Intestinal esr2 mRNA
p=0.0225
p=0.0289
p=0.0002
p=0.0081
H
Intestinal greb1 mRNA
p=0.0022
p=0.0407
I
r = - 0.529
p = 0.030
esr2 mRNA (AU)
Ido-1 mRNA (AU)

Supplementary Fig. 3: effects of intestinal IDO deletion on atherosclerosis and assessing IDO expression in males and females. A. *Ido-1 mRNA* in small intestines (n=5 mice/group), **B.** plasma cholesterol, **C.** representative pictures and quantifications of plaque size in the aortic sinus of female *Ldlr*$^{-/-}$ IEC IDO KO, and littermate control *Ldlr*$^{-/-}$ IEC IDO mice fed HFD+HCD for 8 weeks (IEC IDO n=8 mice, IEC IDOKO n=9 mice); scale bar 200µm. **D.** representative photomicrographs and lipid quantification with en-face staining in the thoracic aorta of female *Ldlr*$^{-/-}$ IEC IDO KO, and littermate control *Ldlr*$^{-/-}$ IEC IDO mice fed HFD+HCD for 13 weeks (IEC IDO n=9 mice, IEC IDOKO n=12 mice); scale bar 2mm. **E.** *Ido-1 mRNA* in the small intestines of female *Ldlr*$^{-/-}$ mice fed HFD+HCD for 8 or 13 weeks (8wk n=8 mice, 13wk n=10 mice). **F.** *Ido-1 mRNA* in the small intestines of male and female *Ldlr*$^{-/-}$ mice fed HFD+HCD for 13 weeks (male n=5 mice, female n=10 mice). **G-H.** *esr1, esr2, and greb1 mRNA* in the small intestines of male and female *Ldlr*$^{-/-}$ mice fed HFD+HCD for 8 or 13 weeks (n=6-10 mice/group). **I.** correlation between *esr2 mRNA* and *Ido-1 mRNA* in the small intestines of male and female *Ldlr*$^{-/-}$ mice fed HFD+HCD for 13 weeks (Spearman correlation) (male n=7 mice, female n=10 mice). Individual data are presented as scattered dot plots, with the mean and s.e.m. The p values were determined using the two-tailed Mann-Whitney test for A, D, E, F, and Brown-Forsythe ANOVA test followed by Tukey's multiple comparison test for G (esr1) and H and Kruskal-Wallis, followed by post-Hoc Dunn’s test for G (esr2). Source data are provided as a Source Data file.

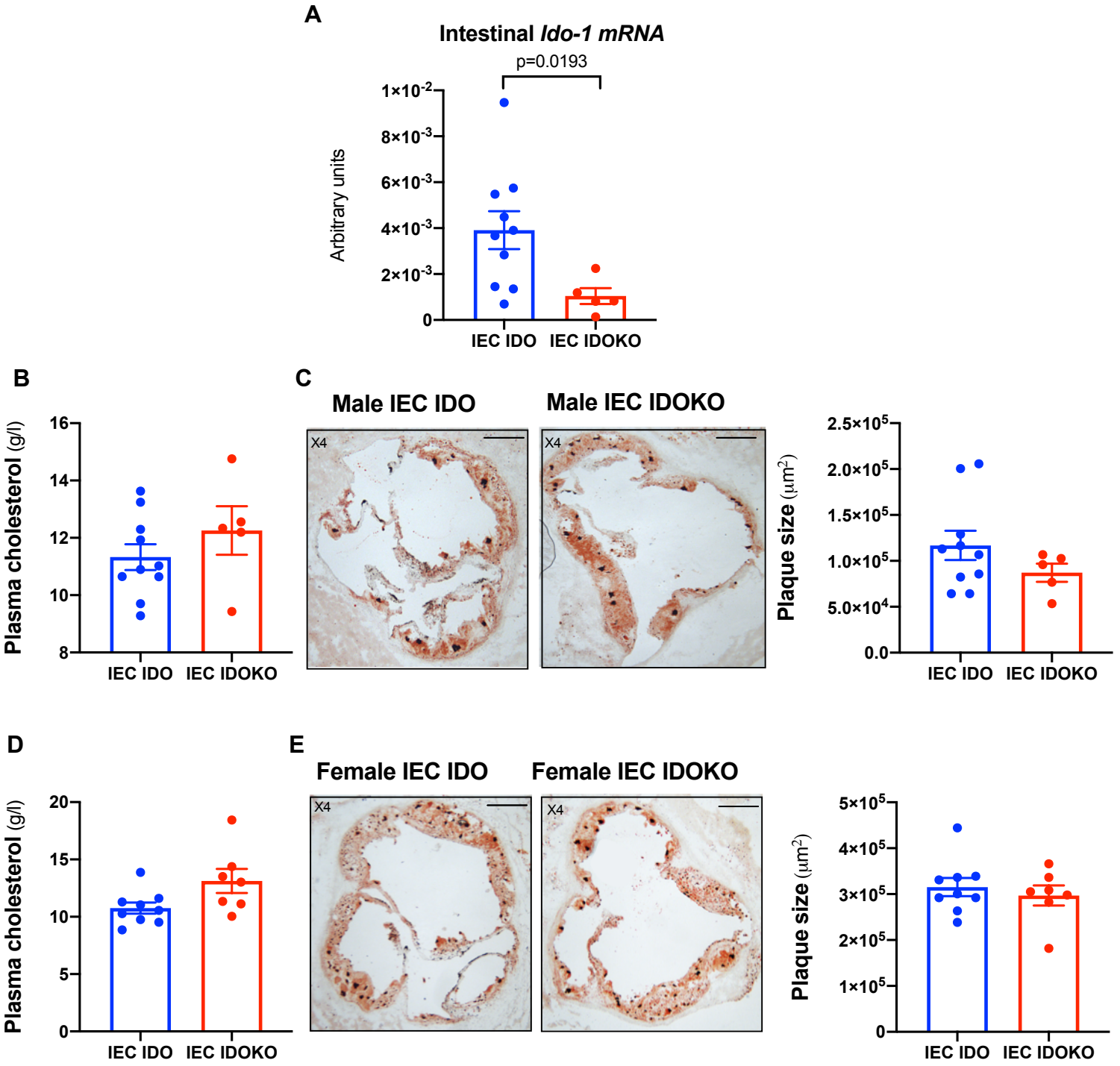
A
Intestinal Ido-1 mRNA
p=0.0193
Arbitrary units
1×10-2
8×10-3
6×10-3
4×10-3
2×10-3
0
IEC IDO
IEC IDOKO
B
Plasma cholesterol (g/l)
16
14
12
10
8
IEC IDO
IEC IDOKO
C
Male IEC IDO
Male IEC IDOKO
X4
X4
Plaque size (µm2)
2.5×105
2.0×105
1.5×105
1.0×105
5.0×104
0.0
IEC IDO
IEC IDOKO
D
Plasma cholesterol (g/l)
20
15
10
5
0
IEC IDO
IEC IDOKO
E
Female IEC IDO
Female IEC IDOKO
X4
X4
Plaque size (µm2)
5×105
4×105
3×105
2×105
1×105
0
IEC IDO
IEC IDOKO

Supplementary Fig.4: effects of intestinal IDO deletion on atherosclerosis under HCD. A. *Ido-1 mRNA* in small intestines, **B.** plasma cholesterol, **C.** representative pictures and quantifications of plaque size in the aortic sinus of male *Ldlr*$^{-/-}$ IEC IDO KO, and littermate control *Ldlr*$^{-/-}$ IEC IDO mice fed a high-cholesterol diet (HCD) for 8 weeks (IEC IDO n=10 mice, IEC IDOKO n=5 mice); scale bar 200µm. **D.** plasma cholesterol, **E.** representative pictures and quantifications of plaque size in the aortic sinus of female *Ldlr*$^{-/-}$ IEC IDO KO, and littermate control *Ldlr*$^{-/-}$ IEC IDO mice fed HCD for 8 weeks (IEC IDO n=9 mice, IEC IDOKO n=7 mice); scale bar 200µm. Individual data are presented as scattered dot plots, with the mean and s.e.m. The p values were determined using the two-tailed Mann-Whitney test. Source data are provided as a Source Data file.

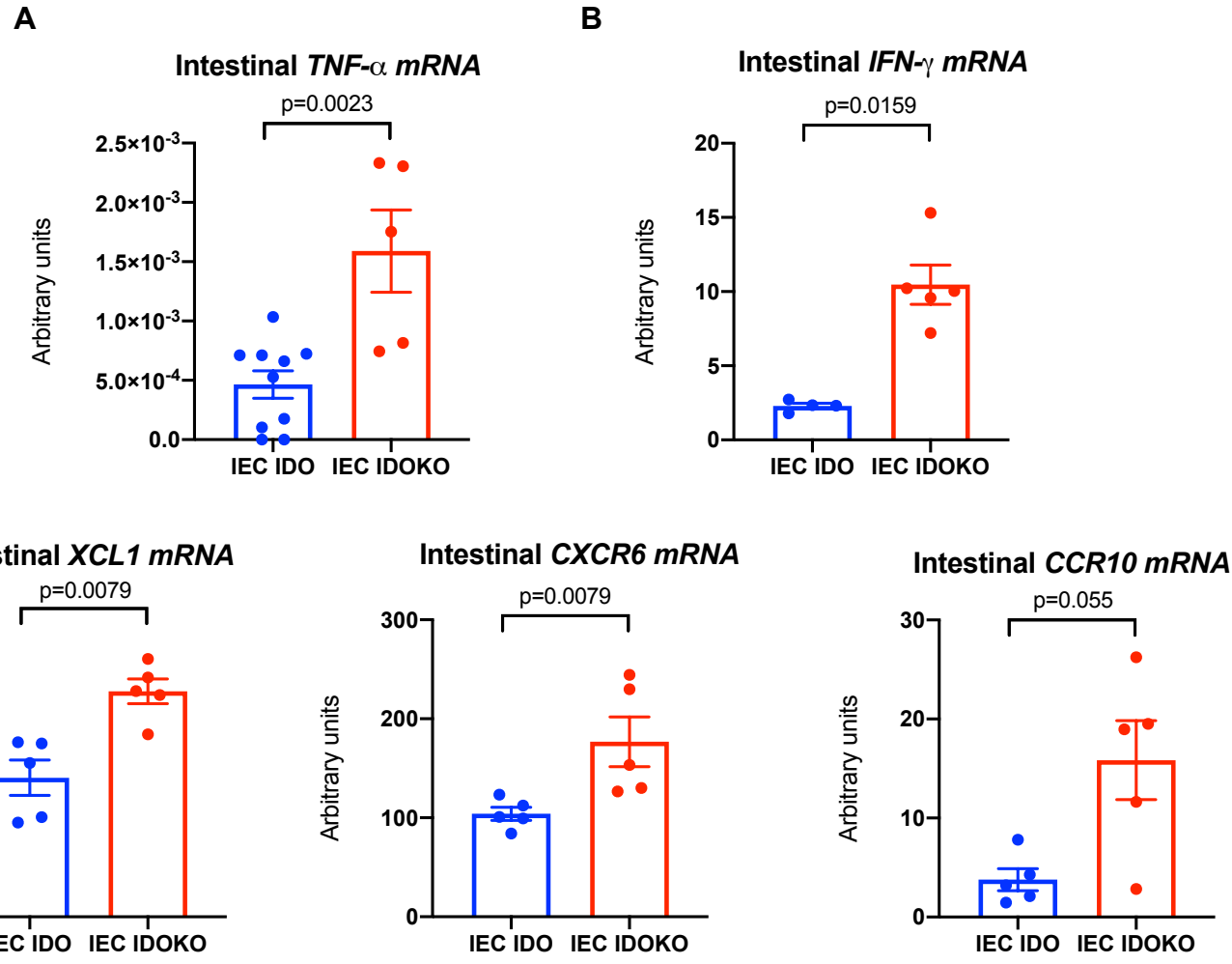
A
Intestinal TNF-α mRNA
p=0.0023
Arbitrary units
2.5×10-3
2.0×10-3
1.5×10-3
1.0×10-3
5.0×10-4
0.0
IEC IDO
IEC IDOKO
B
Intestinal IFN-γ mRNA
p=0.0159
Arbitrary units
20
15
10
5
0
IEC IDO
IEC IDOKO
Intestinal XCL1 mRNA
p=0.0079
Arbitrary units
80
60
40
20
0
IEC IDO
IEC IDOKO
Intestinal CXCR6 mRNA
p=0.0079
Arbitrary units
300
200
100
0
IEC IDO
IEC IDOKO
Intestinal CCR10 mRNA
p=0.055
Arbitrary units
30
20
10
0
IEC IDO
IEC IDOKO

Supplementary Fig. 5: effects of intestinal IDO deletion on inflammation. A. *TNF-α mRNA* by qPCR in the small intestine of male *Ldlr*$^{-/-}$ IEC IDO KO, and littermate control *Ldlr*$^{-/-}$ IEC IDO mice fed HFD+HCD for 8 weeks (IEC IDO n=10 mice, IEC IDOKO n=5 mice). **B.** *Ifn-γ, XCL1, CCR10*, and *CXCR6 mRNA* by nanostring in the small intestine of male *Ldlr*$^{-/-}$ IEC IDO KO, and littermate control *Ldlr*$^{-/-}$ IEC IDO mice fed HFD+HCD for 8 weeks (n=5 mice/group). Individual data are presented as scattered dot plots, with the mean and s.e.m. The p values were determined using the two-tailed Mann-Whitney test. Source data are provided as a Source Data file.

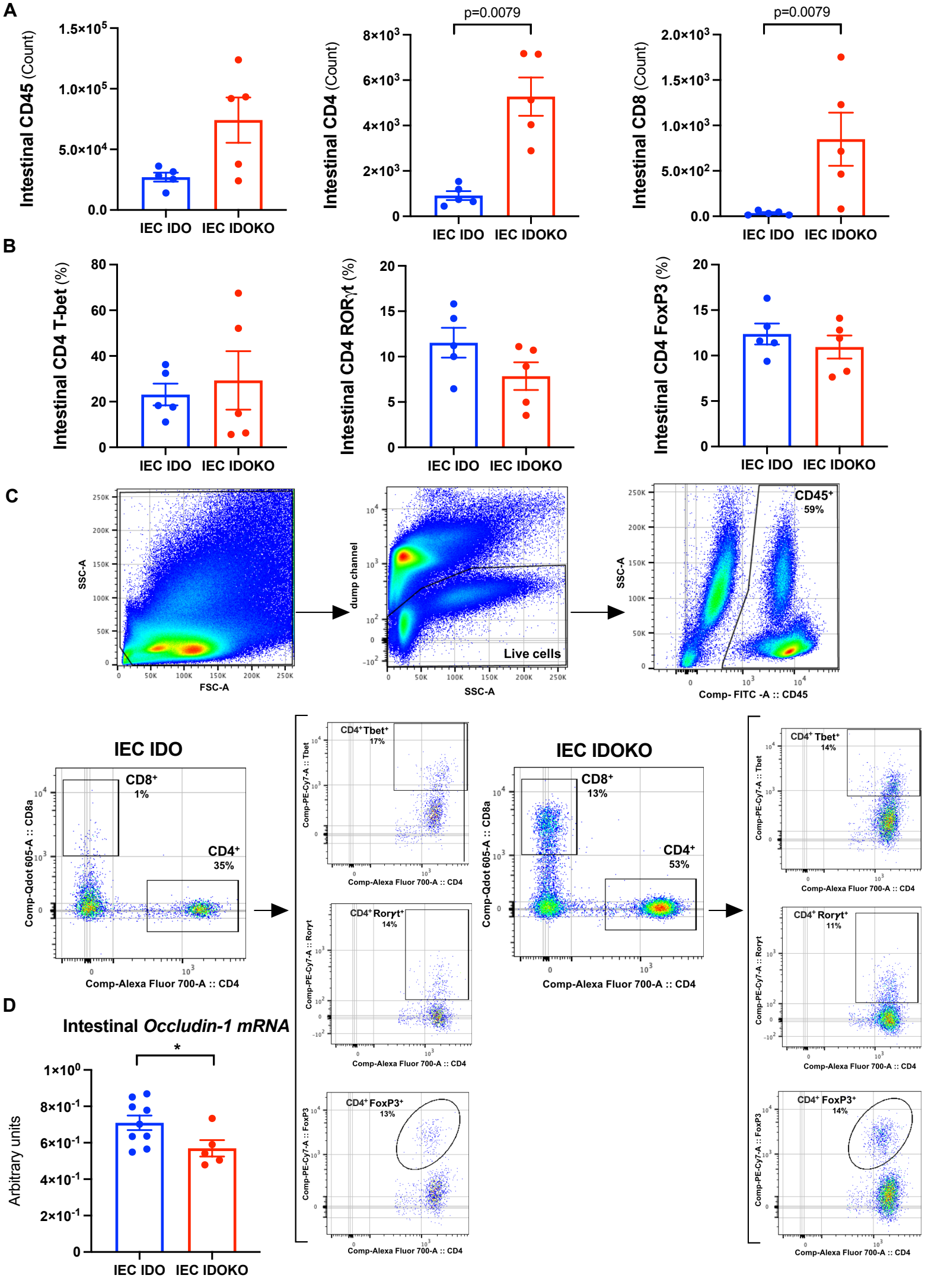
A
Intestinal CD45 (Count)
1.5×10^5
1.0×10^5
5.0×10^4
0.0
IEC IDO
IEC IDOKO
Intestinal CD4 (Count)
p=0.0079
8×10^3
6×10^3
4×10^3
2×10^3
0
Intestinal CD8 (Count)
p=0.0079
2.0×10^3
1.5×10^3
1.0×10^3
5.0×10^2
B
Intestinal CD4 T-bet (%)
80
60
40
20
Intestinal CD4 RORγt (%)
Intestinal CD4 FoxP3 (%)
C
SSC-A
FSC-A
dump channel
Live cells
CD45+
59%
Comp- FITC -A :: CD45
IEC IDO
CD8+
1%
CD4+
35%
Comp-Qdot 605-A :: CD8a
Comp-Alexa Fluor 700-A :: CD4
CD4+ Tbet+
17%
Comp-PE-Cy7-A :: Tbet
CD4+ Rorγt+
14%
Comp-PE-Cy7-A :: Rorγt
CD4+ FoxP3+
13%
Comp-PE-Cy7-A :: FoxP3
IEC IDOKO
CD8+
13%
CD4+
53%
CD4+ Tbet+
14%
CD4+ Rorγt+
11%
CD4+ FoxP3+
14%
D
Intestinal Occludin-1 mRNA
*
Arbitrary units
1×10^0
8×10^-1
6×10^-1
4×10^-1
2×10^-1
0

Supplementary Fig. 6: effects of intestinal IDO deletion on immune cells by flow cytometry. A. flow cytometry analysis of CD45+, CD4+, and CD8+ cells (count) in the lamina propria of the small intestines of male *Ldlr*$^{-/-}$ IEC IDO KO, and littermate control *Ldlr*$^{-/-}$ IEC IDO mice fed HFD+HCD for 8 weeks (n=5 mice/group), **B.** Th subset (%)**, C.** Pseudocolor plot examples show the gating strategy. A dump channel represents dead cells as well as CD11b+ and CD11c+ cells, which were excluded. T cells were gated as single cells dump^{-} CD45^{+} CD4^{+}. The different T cell subsets were identified according to the T-bet, ROR-γt, and FoxP3 expression. **D.** *Occludin-1 mRNA* in the small intestines of male *Ldlr*$^{-/-}$ IEC IDO KO, and littermate control *Ldlr*$^{-/-}$ IEC IDO mice fed HFD+HCD for 8 weeks (IEC IDO n=9 mice, IEC IDOKO n=5 mice). Individual data are presented as scattered dot plots, with the mean and s.e.m. The p values were determined using the two-tailed Mann-Whitney test. Source data are provided as a Source Data file.

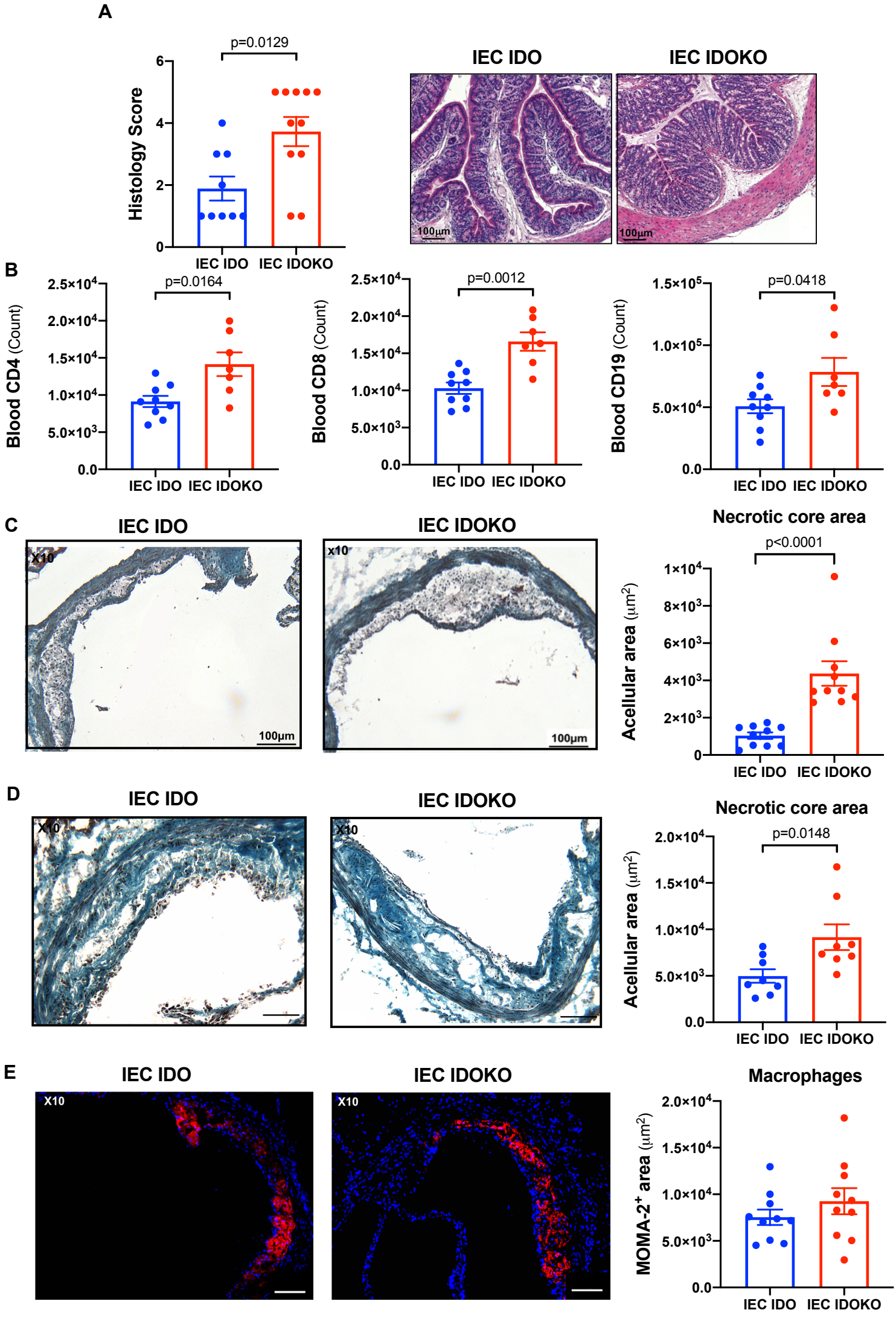
A
p=0.0129
Histology Score
IEC IDO
IEC IDOKO
100µm
B
p=0.0164
Blood CD4 (Count)
p=0.0012
Blood CD8 (Count)
p=0.0418
Blood CD19 (Count)
C
X10
100µm
Necrotic core area
p<0.0001
Acellular area (µm²)
D
p=0.0148
E
Macrophages
MOMA-2⁺ area (µm²)

Supplementary Fig. 7: effects of intestinal IDO deletion on the gut, blood immune cells, and lesional necrotic cores. A. colon pathohistological scoring in female *Ldlr*$^{-/-}$ IEC IDO KO and littermate control *Ldlr*$^{-/-}$ IEC IDO mice fed HFD+HCD for 13 weeks (IEC IDO n=9 mice, IEC IDOKO n=11 mice); scale bar 100µm. **B.** flow cytometry analysis of blood CD4+, CD8+, and CD19+ cells (count) in male *Ldlr*$^{-/-}$ IEC IDO KO, and littermate control *Ldlr*$^{-/-}$ IEC IDO mice fed HFD+HCD for 8 weeks (IEC IDO n=9 mice, IEC IDOKO n=7 mice). **C.** representative pictures and quantifications of necrotic cores visualized by Masson's Trichrome staining in the aortic sinus of male *Ldlr*$^{-/-}$ IEC IDO KO and littermate control *Ldlr*$^{-/-}$ IEC IDO mice fed HFD+HCD for 8 weeks (n=10 mice/group); scale bar 100µm. **D.** representative pictures and quantifications of necrotic cores visualized by Masson's Trichrome staining in the aortic sinus of female *Ldlr*$^{-/-}$ IEC IDO KO and littermate control *Ldlr*$^{-/-}$ IEC IDO mice fed HFD+HCD for 13 weeks (n=8 mice/group); scale bar 100µm. **E.** representative pictures and quantifications of macrophages (MOMA2+ in red) accumulation within plaques in the aortic sinus of male *Ldlr*$^{-/-}$ IEC IDO KO, and littermate control *Ldlr*$^{-/-}$ IEC IDO mice fed HFD+HCD for 8 weeks (n=10 mice/group); scale bar 100µm. Individual data are presented as scattered dot plots, with the mean and s.e.m. The p values were determined using the two-tailed Mann-Whitney test. Source data are provided as a Source Data file.

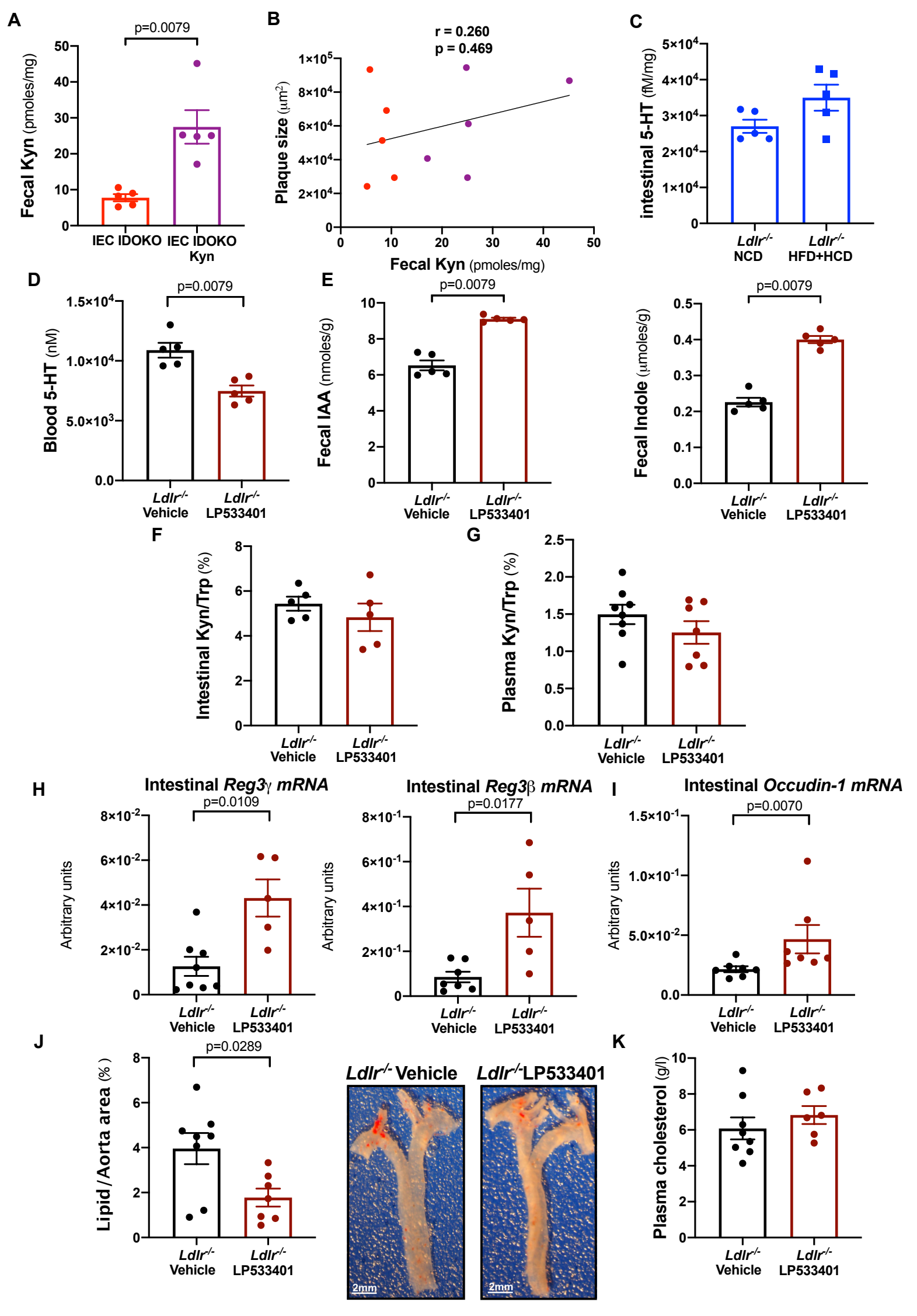
A
p=0.0079
Fecal Kyn (pmoles/mg)
IEC IDOKO
IEC IDOKO Kyn
B
r = 0.260
p = 0.469
Plaque size (µm²)
Fecal Kyn (pmoles/mg)
C
intestinal 5-HT (fM/mg)
Ldlr-/- NCD
Ldlr-/- HFD+HCD
D
p=0.0079
Blood 5-HT (nM)
Ldlr-/- Vehicle
Ldlr-/- LP533401
E
p=0.0079
Fecal IAA (nmoles/g)
Ldlr-/- Vehicle
Ldlr-/- LP533401
p=0.0079
Fecal Indole (µmoles/g)
Ldlr-/- Vehicle
Ldlr-/- LP533401
F
Intestinal Kyn/Trp (%)
Ldlr-/- Vehicle
Ldlr-/- LP533401
G
Plasma Kyn/Trp (%)
Ldlr-/- Vehicle
Ldlr-/- LP533401
H
Intestinal Reg3γ mRNA
p=0.0109
Arbitrary units
Ldlr-/- Vehicle
Ldlr-/- LP533401
Intestinal Reg3β mRNA
p=0.0177
Arbitrary units
Ldlr-/- Vehicle
Ldlr-/- LP533401
I
Intestinal Occudin-1 mRNA
p=0.0070
Arbitrary units
Ldlr-/- Vehicle
Ldlr-/- LP533401
J
p=0.0289
Lipid / Aorta area (%)
Ldlr-/- Vehicle
Ldlr-/- LP533401
Ldlr-/- Vehicle
Ldlr-/- LP533401
2mm
2mm
K
Plasma cholesterol (g/l)
Ldlr-/- Vehicle
Ldlr-/- LP533401

Supplementary Fig. 8: effects of Kyn supplementation and the inhibition of 5-HT production. A. Kynurenine (Kyn) levels in feces of male *Ldlr*$^{-/-}$ IEC IDO KO mice supplemented or not with Kyn and fed high-fat and high-cholesterol diet (HFD+HCD) for 8 weeks (n=5 mice/group), **B.** correlation between plaque size and fecal Kyn in *Ldlr*$^{-/-}$ IEC IDO KO mice supplemented or not with Kyn during the 8 weeks of HFD+HCD (Spearman correlation). **C.** 5-hydroxytryptamine (HT) levels in the small intestine extracts of male *Ldlr*$^{-/-}$ mice fed NCD or HFD+HCD for 8 weeks (n=5 mice/group). **D.** 5-HT levels in blood, **E.** fecal IAA and indole levels, **F.** Kyn/Trp ratio (%) in the small intestine extracts of male *Ldlr*$^{-/-}$ mice treated with LP533401 or vehicle and fed HFD+HCD for 8 weeks (n=5 mice/group). **G.** Kyn/Trp ratio (%) in the plasma of male *Ldlr*$^{-/-}$ mice treated with LP533401 or vehicle and fed HFD+HCD for 8 weeks (*Ldlr*$^{-/-}$ Vehicle n=8 mice, *Ldlr*$^{-/-}$ LP533401 n=7 mice). **H.** *Reg3g, Reg3b mRNA* in the small intestines of male *Ldlr*$^{-/-}$ mice treated or not with LP533401 during the 8 weeks of HFD+HCD (*Ldlr*$^{-/-}$ Vehicle n=8 mice, *Ldlr*$^{-/-}$ LP533401 n=5 mice), **I.** *Occludin-1 mRNA* in the small intestines of male *Ldlr*$^{-/-}$ mice treated or not with LP533401 during the 8 weeks of HFD+HCD (n=7 mice/group). **J.** representative photomicrographs and lipid quantification with en-face staining in the thoracic aorta; scale bar 2mm, **K.** plasma cholesterol levels in male *Ldlr*$^{-/-}$ treated with LP533401 or vehicle and fed HFD+HCD for 8 weeks (*Ldlr*$^{-/-}$ Vehicle n=8 mice, *Ldlr*$^{-/-}$ LP533401 n=7 mice). Individual data are presented as scattered dot plots, with the mean and s.e.m. The p values were determined using the two-tailed Mann-Whitney test. Source data are provided as a Source Data file.

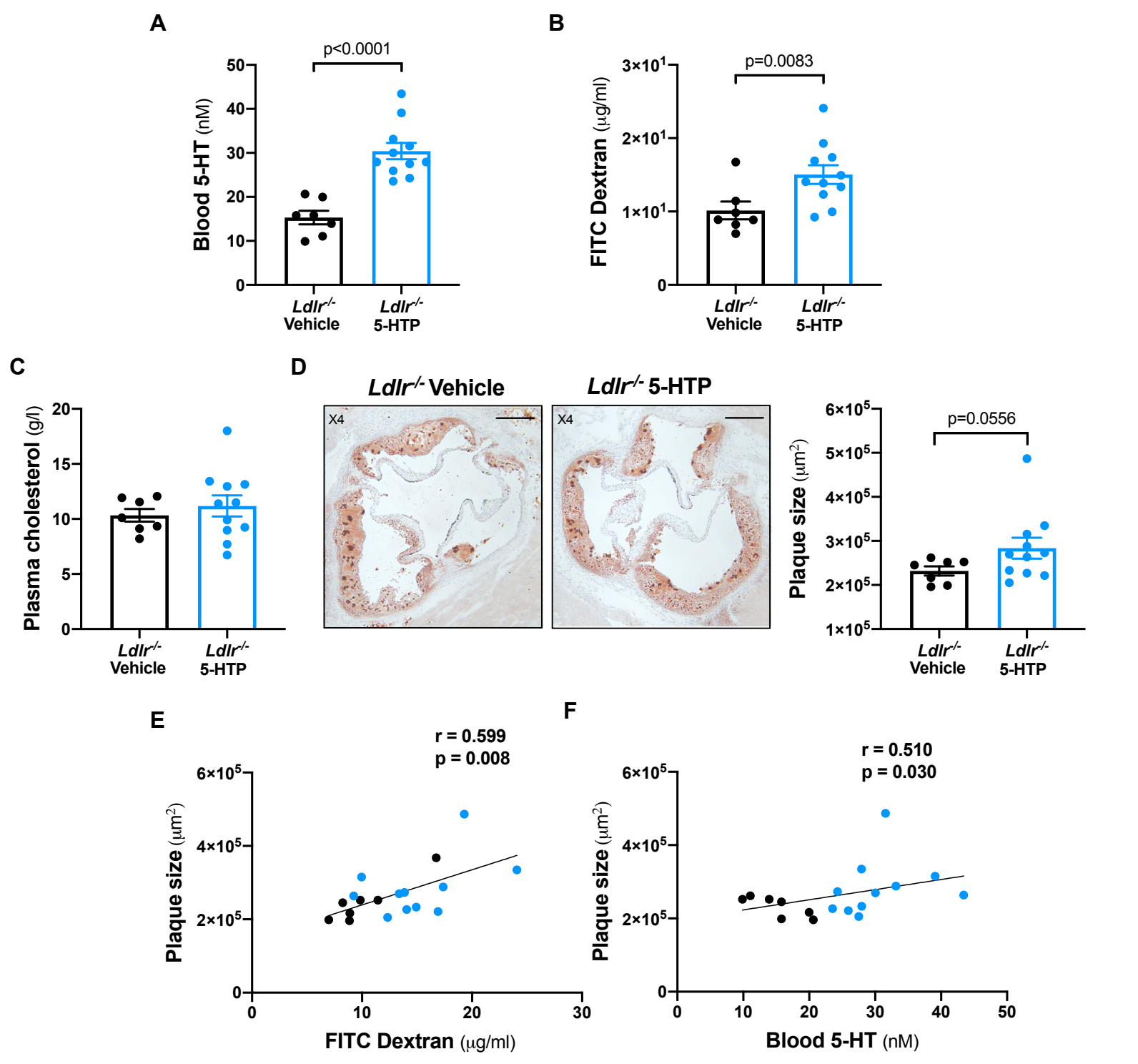
A
p<0.0001
Blood 5-HT (nM)
50
40
30
20
10
0
Ldlr-/- Vehicle
Ldlr-/- 5-HTP
B
p=0.0083
FITC Dextran (µg/ml)
3×10^1
2×10^1
1×10^1
0
Ldlr-/- Vehicle
Ldlr-/- 5-HTP
C
Plasma cholesterol (g/l)
20
15
10
5
0
Ldlr-/- Vehicle
Ldlr-/- 5-HTP
D
Ldlr-/- Vehicle
Ldlr-/- 5-HTP
X4
X4
p=0.0556
Plaque size (µm2)
6×10^5
5×10^5
4×10^5
3×10^5
2×10^5
1×10^5
Ldlr-/- Vehicle
Ldlr-/- 5-HTP
E
r = 0.599
p = 0.008
Plaque size (µm2)
6×10^5
4×10^5
2×10^5
0
0
10
20
30
FITC Dextran (µg/ml)
F
r = 0.510
p = 0.030
Plaque size (µm2)
6×10^5
4×10^5
2×10^5
0
0
10
20
30
40
50
Blood 5-HT (nM)

Supplementary Fig. 9: effects of serotonin supplementation. A. blood 5-hydroxytryptamine (HT) levels, **B.** serum FITC-dextran levels, **C.** plasma cholesterol, **D.** representative images and plaque quantifications in the aortic sinus of male *ldlr*$^{-/-}$ fed high-cholesterol diet (HCD) supplemented or not with 5-hydroxytryptophan (HTP) (*Ldlr*$^{-/-}$ Vehicle n=7 mice, *Ldlr*$^{-/-}$ 5-HTP n=11 mice); scale bar 200µm**. E-F.** correlations between plaque size with serum FITC-dextran and blood 5-HT (Spearman correlation). Individual data are presented as scattered dot plots, with the mean and s.e.m. The p values were determined using the two-tailed Mann-Whitney test. Source data are provided as a Source Data file.

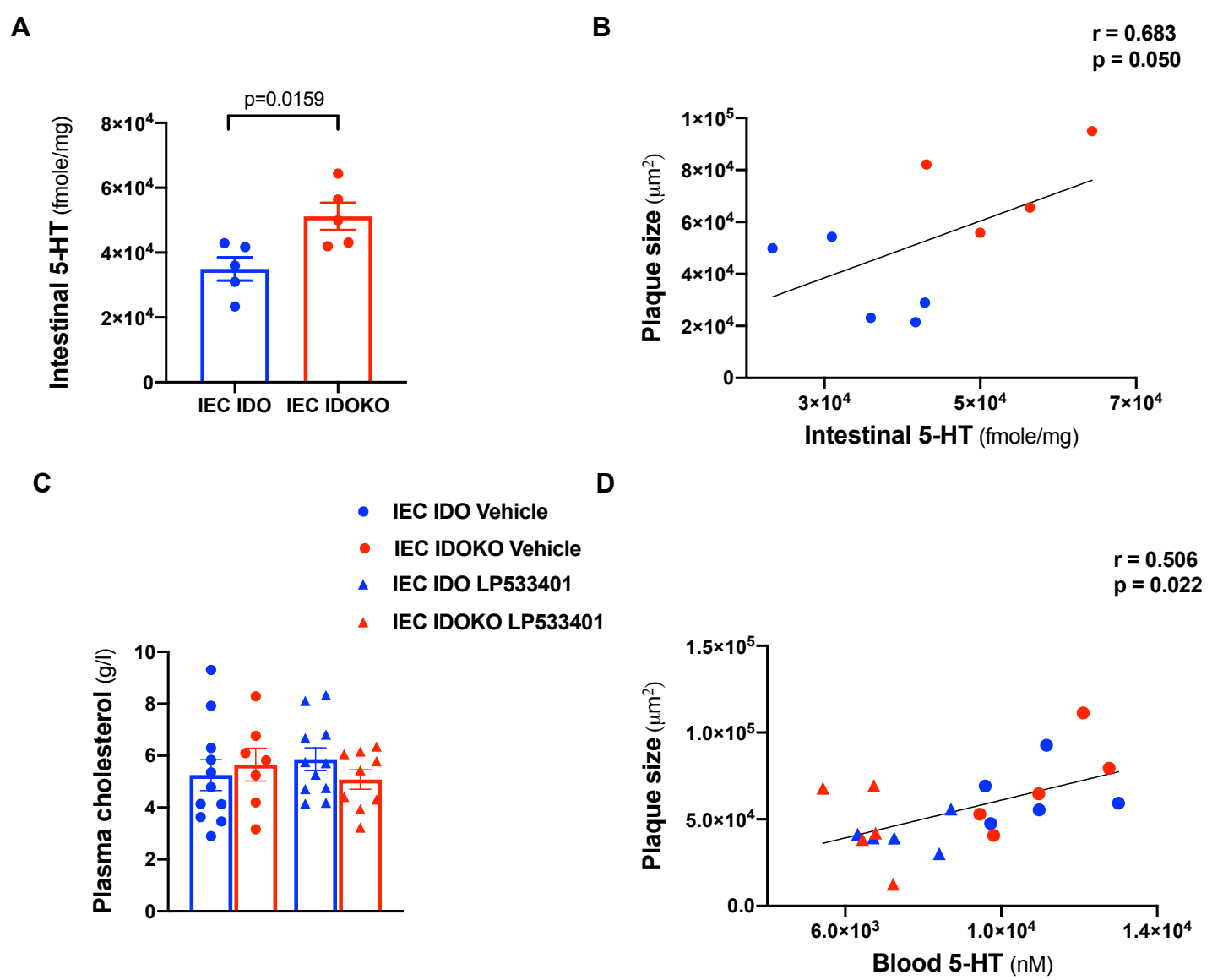
A
p=0.0159
Intestinal 5-HT (fmole/mg)
8×10^4
6×10^4
4×10^4
2×10^4
0
IEC IDO
IEC IDOKO
B
r = 0.683
p = 0.050
Plaque size (µm^2)
1×10^5
8×10^4
6×10^4
4×10^4
2×10^4
0
3×10^4
5×10^4
7×10^4
Intestinal 5-HT (fmole/mg)
C
IEC IDO Vehicle
IEC IDOKO Vehicle
IEC IDO LP533401
IEC IDOKO LP533401
Plasma cholesterol (g/l)
10
8
6
4
2
0
D
r = 0.506
p = 0.022
Plaque size (µm^2)
1.5×10^5
1.0×10^5
5.0×10^4
0.0
6.0×10^3
1.0×10^4
1.4×10^4
Blood 5-HT (nM)

Supplementary Fig. 10: characterization of serotonin production in the model with intestinal IDO deletion. A. 5- (hydroxytryptamine) HT levels in the intestines in male *Ldlr*$^{-/-}$ IEC IDO KO and littermate control *Ldlr*$^{-/-}$ IEC IDO mice fed high-fat and high-cholesterol diet (HFD+HCD) for 8 weeks (n=5 mice/group), **B.** correlation between plaque size and 5-HT levels in the gut (Spearman correlation). **C.** plasma cholesterol levels in male *Ldlr*$^{-/-}$ IEC IDO KO and littermate control *Ldlr*$^{-/-}$ IEC IDO mice treated with LP5333401 or vehicle and fed HFD+HCD for 8 weeks (IEC IDO Vehicle n=11 mice, IEC IDO KO Vehicle n=7 mice, IEC IDO LP533401 n=11 mice, IEC IDO KO LP533401 n=9 mice). **D.** correlation between plaque size and blood 5-HT (Spearman correlation). Individual data are presented as scattered dot plots, with the mean and s.e.m. The p values were determined using the two-tailed Mann-Whitney test for A. Source data are provided as a Source Data file.

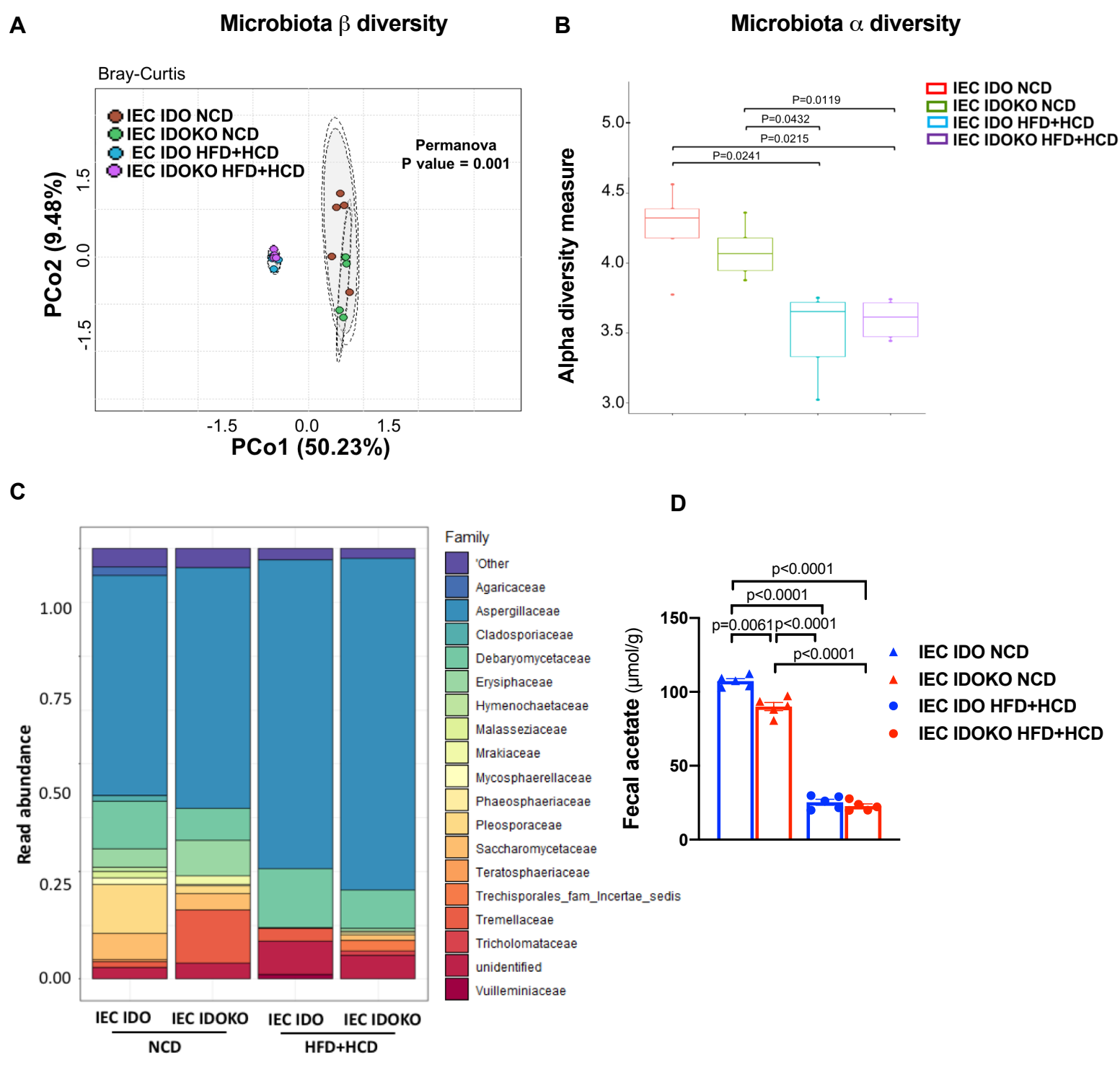
A
Microbiota β diversity
Bray-Curtis
IEC IDO NCD
IEC IDOKO NCD
EC IDO HFD+HCD
IEC IDOKO HFD+HCD
Permanova
P value = 0.001
PCo2 (9.48%)
PCo1 (50.23%)
B
Microbiota α diversity
IEC IDO NCD
IEC IDOKO NCD
IEC IDO HFD+HCD
IEC IDOKO HFD+HCD
P=0.0119
P=0.0432
P=0.0215
P=0.0241
Alpha diversity measure
C
Family
'Other
Agaricaceae
Aspergillaceae
Cladosporiaceae
Debaryomycetaceae
Erysiphaceae
Hymenochaetaceae
Malasseziaceae
Mrakiaceae
Mycosphaerellaceae
Phaeosphaeriaceae
Pleosporaceae
Saccharomycetaceae
Teratosphaeriaceae
Trechisporales_fam_Incertae_sedis
Tremellaceae
Tricholomataceae
unidentified
Vuilleminiaceae
Read abundance
IEC IDO
IEC IDOKO
IEC IDO
IEC IDOKO
NCD
HFD+HCD
D
p<0.0001
p<0.0001
p=0.0061
p<0.0001
p<0.0001
Fecal acetate (µmol/g)
IEC IDO NCD
IEC IDOKO NCD
IEC IDO HFD+HCD
IEC IDOKO HFD+HCD

Supplementary Fig. 11: characterization of gut microbiota in mice expressing or deficient for intestinal IDO. A. PCoA plot based on bacterial 16S rDNA gene relative abundance using the Bray-Curtis dissimilarity in fecal contents of male *Ldlr*$^{-/-}$ IEC IDO KO and littermate control *Ldlr*$^{-/-}$ IEC IDO mice fed with either normal chow diet (NCD) or high-fat and high-cholesterol diet (HFD+HCD) for 8 weeks (n=5 mice/group). Axes correspond to principal coordinate axis 1 (x-axis) and 2 (y-axis). Ellipses were drawn around the centroids of each emerging community (PERMANOVA: F = 6.4231, df = 3, P = 0.001) at 95% (inner) and 97% (outer) confidence intervals. **B.** bacterial diversity based on the Shannon index in the fecal samples (n=5 mice/group). **C.** Barplots at the family level in the fecal samples of male *Ldlr*$^{-/-}$ IEC IDO KO and littermate control *Ldlr*$^{-/-}$ IEC IDO mice fed either NCD or HFD+HCD for 8 weeks (n=5 mice/group). **D.** fecal acetate levels in male *Ldlr*$^{-/-}$ IEC IDO KO and littermate control *Ldlr*$^{-/-}$ IEC IDO mice fed with either NCD or HFD+HCD for 8 weeks (n=5 mice/group). Individual data are presented as scattered dot plots, with the mean and s.e.m. The p values were determined using Brown-Forsythe ANOVA test followed by Tukey's multiple comparison for B and D. Source data are provided as a Source Data file.

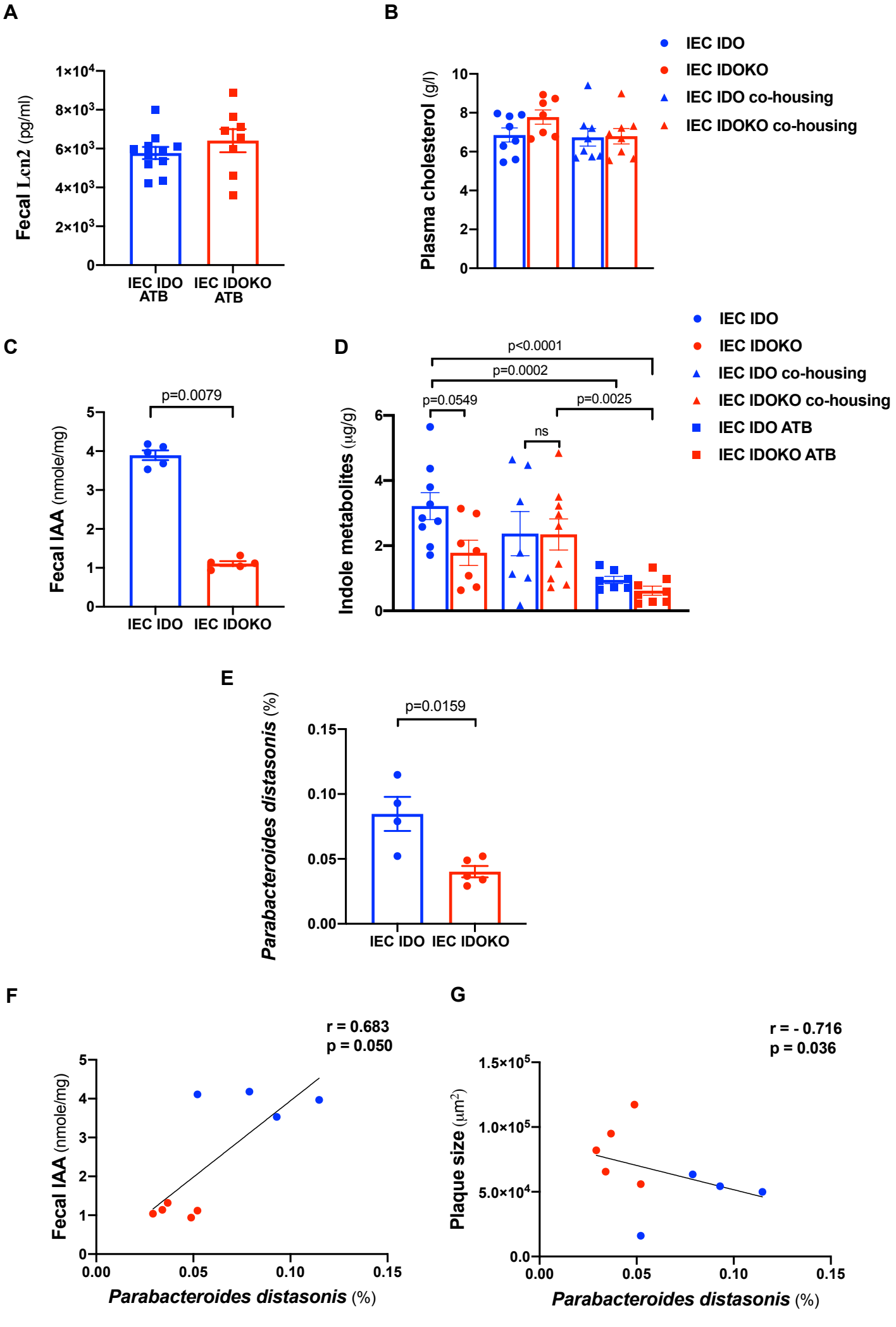
A
Fecal Lcn2 (pg/ml)
1×10^4
8×10^3
6×10^3
4×10^3
2×10^3
0
IEC IDO ATB
IEC IDOKO ATB
B
Plasma cholesterol (g/l)
10
8
6
4
2
0
IEC IDO
IEC IDOKO
IEC IDO co-housing
IEC IDOKO co-housing
C
Fecal IAA (nmole/mg)
p=0.0079
5
4
3
2
1
0
IEC IDO
IEC IDOKO
D
Indole metabolites (µg/g)
p<0.0001
p=0.0002
p=0.0549
p=0.0025
ns
6
4
2
0
IEC IDO
IEC IDOKO
IEC IDO co-housing
IEC IDOKO co-housing
IEC IDO ATB
IEC IDOKO ATB
E
Parabacteroides distasonis (%)
p=0.0159
0.15
0.10
0.05
0.00
IEC IDO
IEC IDOKO
F
r = 0.683
p = 0.050
Fecal IAA (nmole/mg)
5
4
3
2
1
0
0.00
0.05
0.10
0.15
Parabacteroides distasonis (%)
G
r = - 0.716
p = 0.036
Plaque size (µm2)
1.5×10^5
1.0×10^5
5.0×10^4
0.0
0.00
0.05
0.10
0.15
Parabacteroides distasonis (%)

Supplementary Fig. 12: effects of antibiotics and co-housing in mice expressing or deficient for intestinal IDO A. lipocalin-2 (Lcn2) levels in feces of male *Ldlr*$^{-/-}$ IEC IDO KO and littermate control *Ldlr*$^{-/-}$ IEC IDO mice treated with antibiotics (ATB) during the 8 weeks of HFD+HCD feeding period (IEC IDO ATB n=11 mice, IEC IDO KO ATB n=8 mice. **B.** plasma cholesterol levels in male *Ldlr*$^{-/-}$ IEC IDO KO and littermate control *Ldlr*$^{-/-}$ IEC IDO mice either separated by the genotype or mixed (co-housing) in the same cages from the weaning. The mice were fed HFD+HCD for 8 weeks (IEC IDO n=8 mice, IEC IDO KO n=7 mice, IEC IDO co-housing n=8 mice, and IEC IDO KO co-housing n=8 mice). **C.** IAA levels in feces from male *Ldlr*$^{-/-}$ IEC IDO KO and littermate control *Ldlr*$^{-/-}$ IEC IDO mice after 8 weeks of HFD+HCD feeding period (n=5 mice/group). **D.** fecal AhR agonist (IAA, IAld, and tryptamine) levels from male *Ldlr*$^{-/-}$ IEC IDO KO and littermate control *Ldlr*$^{-/-}$ IEC IDO mice after 8 weeks of HFD+HCD feeding period. The mice were either separated according to the genotypes, or mixed (co-housing), or treated with ATB (IEC IDO n=9 mice, IEC IDOKO n=7 mice, IEC IDO co-housing n=7 mice, IEC IDO KO co-housing n=9 mice, IEC IDO ATB n=7 mice, IEC IDO KO ATB n=8 mice). **E.** *Parabacteroides distasonis* relative abundance (%) in feces of male *Ldlr*$^{-/-}$ IEC IDO KO and littermate control *Ldlr*$^{-/-}$ IEC IDO mice fed HFD+HCD for 8 weeks (IEC IDO n=4 mice, IEC IDOKO n=5 mice). **F-G**. correlation between *Parabacteroides distasonis* relative abundance and fecal IAA and plaque size (Spearman correlation). Individual data are presented as scattered dot plots, with the mean and s.e.m. The p values were determined using the two-tailed Mann-Whitney test for C, E, and two-tailed Unpaired T test for D. Source data are provided as a Source Data file.

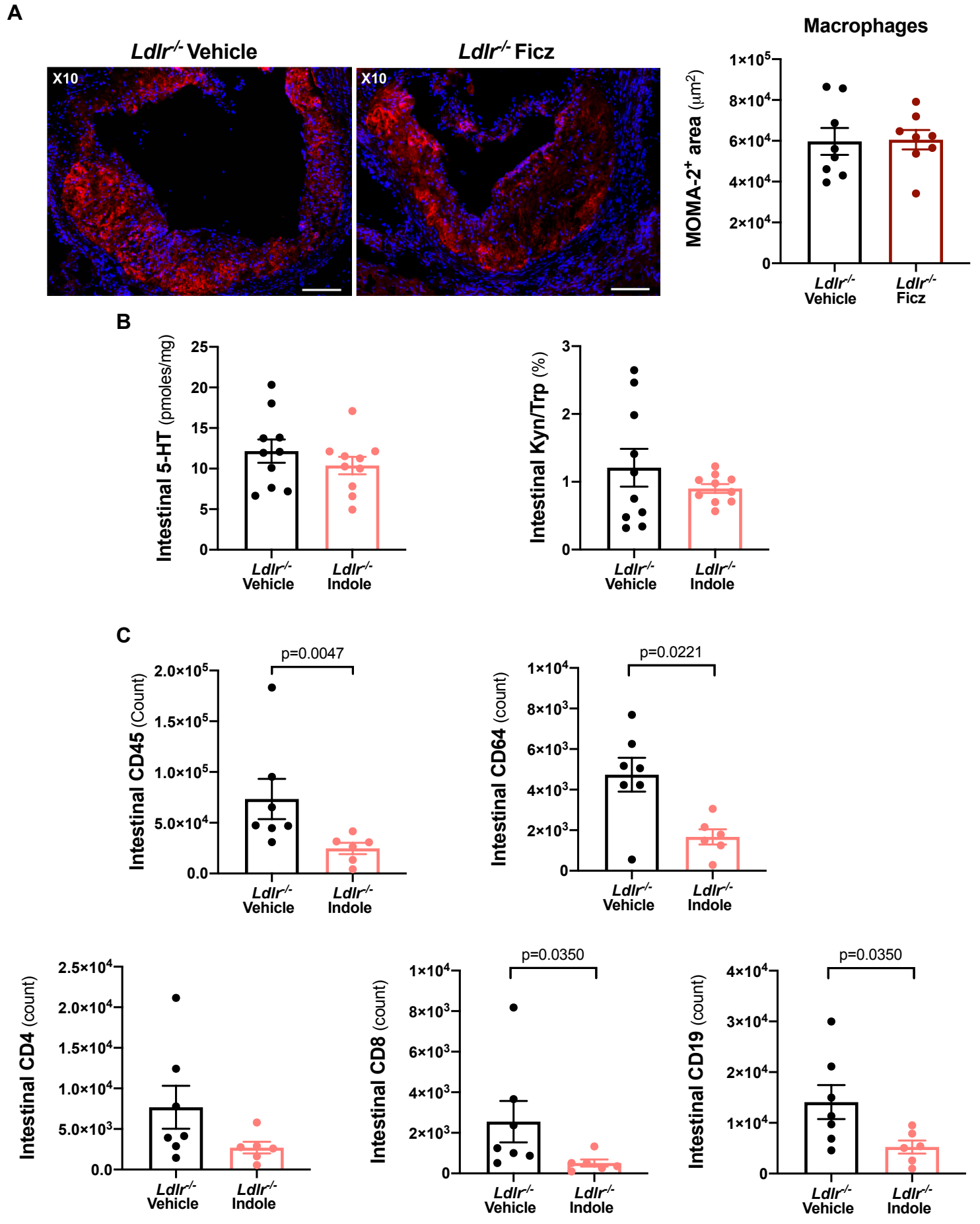
A
Ldlr-/- Vehicle
Ldlr-/- Ficz
X10
X10
Macrophages
MOMA-2+ area (µm2)
1×10^5
8×10^4
6×10^4
4×10^4
2×10^4
0
Ldlr-/- Vehicle
Ldlr-/- Ficz
B
Intestinal 5-HT (pmoles/mg)
25
20
15
10
5
0
Ldlr-/- Vehicle
Ldlr-/- Indole
Intestinal Kyn/Trp (%)
3
2
1
0
Ldlr-/- Vehicle
Ldlr-/- Indole
C
Intestinal CD45 (Count)
p=0.0047
2.0×10^5
1.5×10^5
1.0×10^5
5.0×10^4
0.0
Ldlr-/- Vehicle
Ldlr-/- Indole
Intestinal CD64 (count)
p=0.0221
1×10^4
8×10^3
6×10^3
4×10^3
2×10^3
0
Ldlr-/- Vehicle
Ldlr-/- Indole
Intestinal CD4 (count)
2.5×10^4
2.0×10^4
1.5×10^4
1.0×10^4
5.0×10^3
0.0
Ldlr-/- Vehicle
Ldlr-/- Indole
Intestinal CD8 (count)
p=0.0350
1×10^4
8×10^3
6×10^3
4×10^3
2×10^3
0
Ldlr-/- Vehicle
Ldlr-/- Indole
Intestinal CD19 (count)
p=0.0350
4×10^4
3×10^4
2×10^4
1×10^4
0
Ldlr-/- Vehicle
Ldlr-/- Indole

Supplementary Fig. 13: characterization of the effects of aryl hydrocarbon receptor (AhR) agonists. A. representative pictures and quantifications of macrophages (MOMA2+ in red) accumulation within plaques in the aortic sinus of male *Ldlr*$^{-/-}$mice treated with 6-Formylindolo(3,2-b)carbazole (Ficz) or vehicle (n=8 mice/group) during the 8 weeks of high-cholesterol diet (HCD) feeding period); scale bar 100µm. **B.** 5-HT and Kyn/Trp (%) in the small intestine of female *Ldlr*$^{-/-}$mice supplemented or not with indole derivatives (IAA, IPA, and tryptamine) (n=10 mice/group). **C.** flow cytometry analysis of CD45+, CD64+, CD4+, CD8+, and CD19+ cells (count) in the lamina propria of the small intestines of female *Ldlr*$^{-/-}$mice supplemented or not with indole derivatives (IAA, IPA, and tryptamine) (*Ldlr*$^{-/-}$ Vehicle n=7 mice, *Ldlr*$^{-/-}$ Indole n=6 mice). Individual data are presented as scattered dot plots, with the mean and s.e.m. The p values were determined using the two-tailed Mann-Whitney test. Source data are provided as a Source Data file.

A

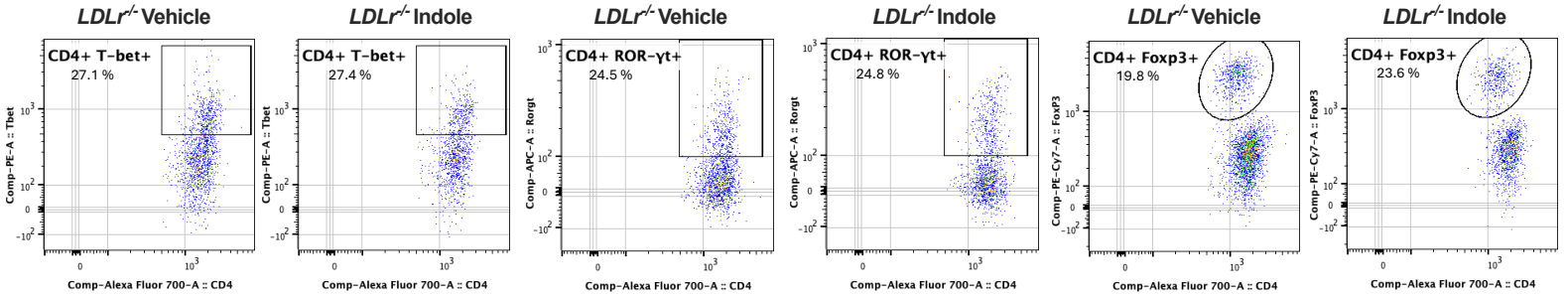
LDLr-/- Vehicle
CD4+ T-bet+
27.1 %
LDLr-/- Indole
CD4+ T-bet+
27.4 %
LDLr-/- Vehicle
CD4+ ROR-γt+
24.5 %
LDLr-/- Indole
CD4+ ROR-γt+
24.8 %
LDLr-/- Vehicle
CD4+ Foxp3+
19.8 %
LDLr-/- Indole
CD4+ Foxp3+
23.6 %
Comp-PE-A :: Tbet
Comp-APC-A :: Rorgt
Comp-PE-Cy7-A :: FoxP3
Comp-Alexa Fluor 700-A :: CD4

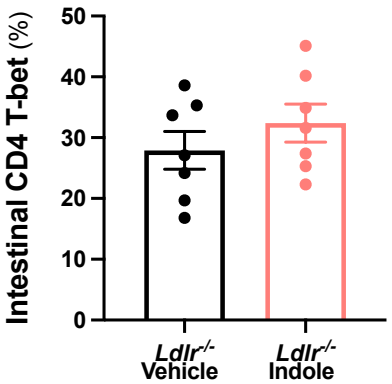
Intestinal CD4 T-bet (%)
Ldlr-/- Vehicle
Ldlr-/- Indole

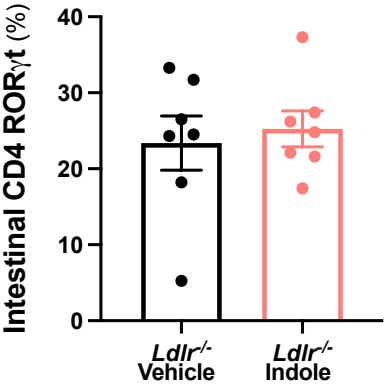
Intestinal CD4 RORγt (%)
Ldlr-/- Vehicle
Ldlr-/- Indole

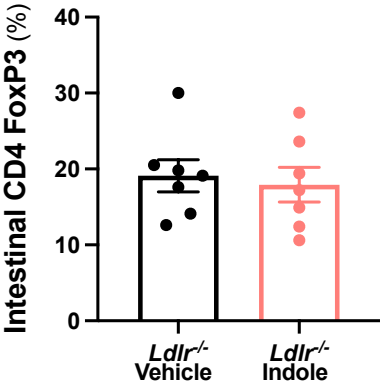
Intestinal CD4 FoxP3 (%)
Ldlr-/- Vehicle
Ldlr-/- Indole

B

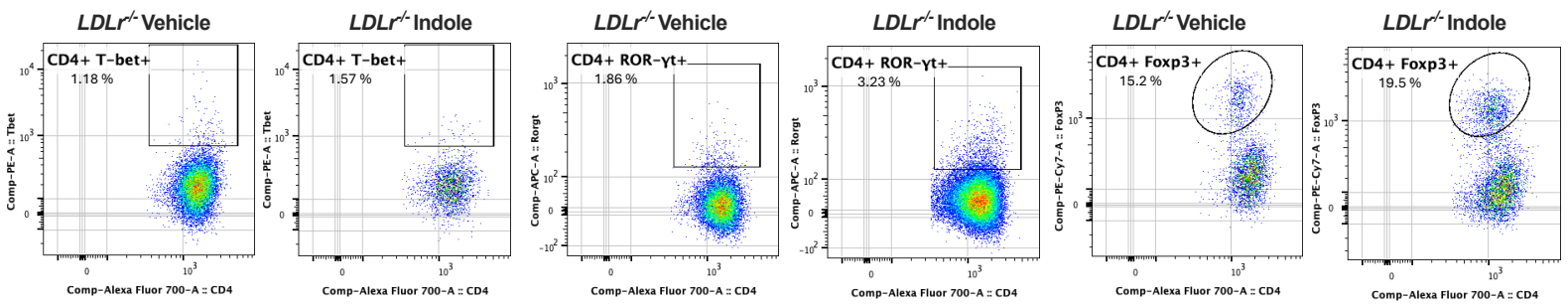
LDLr-/- Vehicle
CD4+ T-bet+
1.18 %
LDLr-/- Indole
CD4+ T-bet+
1.57 %
LDLr-/- Vehicle
CD4+ ROR-γt+
1.86 %
LDLr-/- Indole
CD4+ ROR-γt+
3.23 %
LDLr-/- Vehicle
CD4+ Foxp3+
15.2 %
LDLr-/- Indole
CD4+ Foxp3+
19.5 %
Comp-PE-A :: Tbet
Comp-APC-A :: Rorgt
Comp-PE-Cy7-A :: FoxP3
Comp-Alexa Fluor 700-A :: CD4

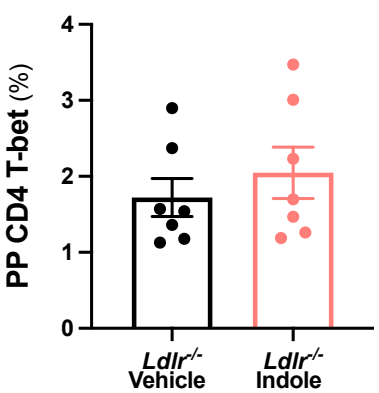
PP CD4 T-bet (%)
Ldlr-/- Vehicle
Ldlr-/- Indole

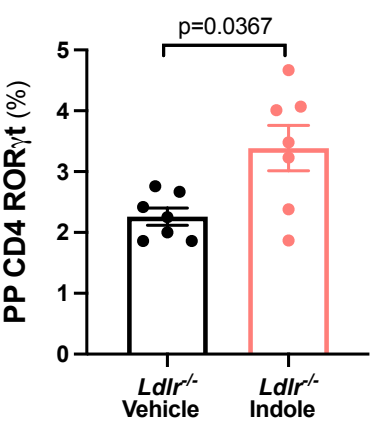
p=0.0367
PP CD4 RORγt (%)
Ldlr-/- Vehicle
Ldlr-/- Indole

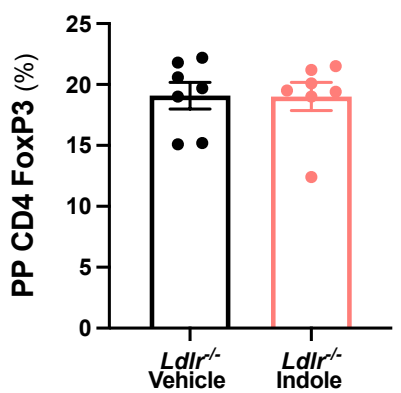
PP CD4 FoxP3 (%)
Ldlr-/- Vehicle
Ldlr-/- Indole

Supplementary Fig. 14: characterization of effects of indole supplementation on Th subsets by flow cytometry in small intestines and PPs. Representative plots and flow cytometry analysis of Th subset (as % of CD4+). The different T cell subsets were identified according to the T-bet, RORγt and FoxP3 expression in the lamina propria of small intestines **(A)** and Peyer's Patches (PP) **(B**), of female *Ldlr*$^{-/-}$mice supplemented or not with indole derivatives (IAA, IPA, and tryptamine) (n=7 mice/group). Individual data are presented as scattered dot plots, with the mean and s.e.m. The p values were determined using the two-tailed Mann-Whitney test. Source data are provided as a Source Data file.

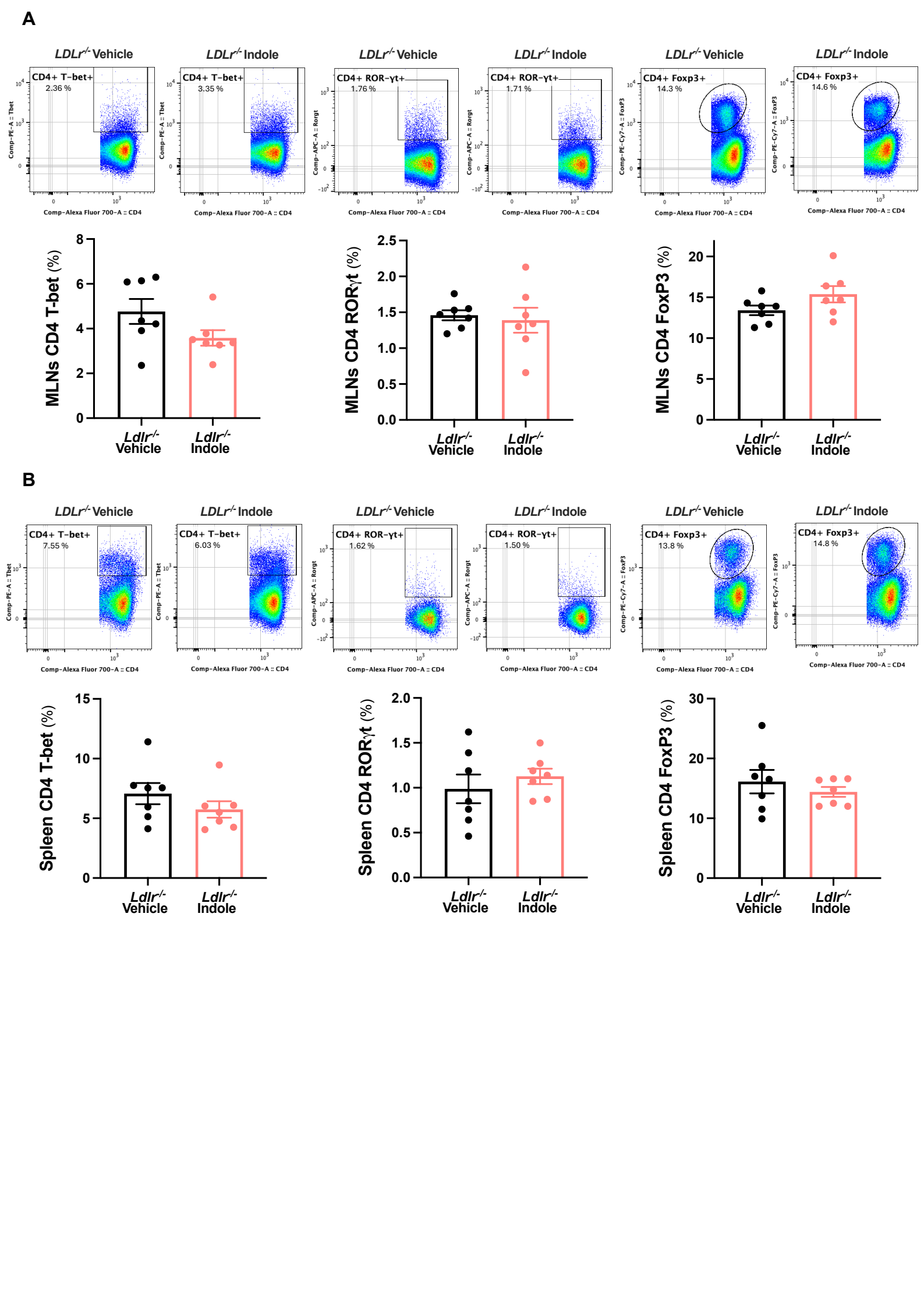
A
LDLr-/- Vehicle
LDLr-/- Indole
LDLr-/- Vehicle
LDLr-/- Indole
LDLr-/- Vehicle
LDLr-/- Indole
CD4+ T-bet+
2.36 %
CD4+ T-bet+
3.35 %
CD4+ RORγt+
1.76 %
CD4+ RORγt+
1.71 %
CD4+ Foxp3+
14.3 %
CD4+ Foxp3+
14.6 %
Comp-PE-A :: Tbet
Comp-APC-A :: Rorgt
Comp-PE-Cy7-A :: FoxP3
Comp-Alexa Fluor 700-A :: CD4
MLNs CD4 T-bet (%)
MLNs CD4 RORγt (%)
MLNs CD4 FoxP3 (%)
Ldlr-/- Vehicle
Ldlr-/- Indole
B
LDLr-/- Vehicle
LDLr-/- Indole
LDLr-/- Vehicle
LDLr-/- Indole
LDLr-/- Vehicle
LDLr-/- Indole
CD4+ T-bet+
7.55 %
CD4+ T-bet+
6.03 %
CD4+ RORγt+
1.62 %
CD4+ RORγt+
1.50 %
CD4+ Foxp3+
13.8 %
CD4+ Foxp3+
14.8 %
Comp-PE-A :: Tbet
Comp-APC-A :: Rorgt
Comp-PE-Cy7-A :: FoxP3
Comp-Alexa Fluor 700-A :: CD4
Spleen CD4 T-bet (%)
Spleen CD4 RORγt (%)
Spleen CD4 FoxP3 (%)
Ldlr-/- Vehicle
Ldlr-/- Indole

Supplementary Fig. 15: characterization of effects of indole supplementation on Th subsets by flow cytometry in MLNs and spleens. Representative plots and flow cytometry analysis of Th subset (as % of CD4+). The different T cell subsets were identified according to the T-bet, RORγt and FoxP3 expression in the lamina propria of Mesenteric Lymph Nodes (MLNs) **(A)**, and spleens (**B**) of female *Ldlr*$^{-/-}$mice supplemented or not with indole derivatives (IAA, IPA, and tryptamine) (n=7 mice/group). Individual data are presented as scattered dot plots, with the mean and s.e.m. Source data are provided as a Source Data file.